High performance polymer and polymer/inorganic thermoelectric materials

Ioannis Petsagkourakis

université de BORDEAUX

THÈSE

présentée pour obtenir le Grade de

DOCTEUR

DE L'UNIVERSITÉ BORDEAUX

ÉCOLE DOCTORALE DES SCIENCES CHIMIQUES

SPÉCIALITÉ: POLYMÈRES

par

IOANNIS PETSAGKOURAKIS

HIGH PERFORMANCE POLYMER AND POLYMER/INORGANIC THERMOELECTRIC MATERIALS

Sous la direction de : **Prof. Georges HADZIIOANNOU**
(co-directeur : **Prof. Stefan DILHAIRE**)

Soutenue le 8 Décembre 2016
Devant la commission d'examen formée de:

Prof. Jean OBERLÉ, Université Bordeaux, France	President
Prof. Xavier CRISPIN, Linköpings Universitet, Sweden	Rapporteur
Dr. Sylvie HEBERT, Université de Caen, France	Rapporteur
Prof. George MALLIARAS, MINES Saint-Etienne, France	Examinateur
Prof. Natalie STINGELIN, Georgia Institute of Technology, USA	Examinateur
Dr. Guillaume FLEURY, Université Bordeaux, France	Invité
Dr. Eleni PAVLOPOULOU, Université Bordeaux, France	Invité

université de BORDEAUX

THESIS

submitted to the

UNIVERSITY OF BORDEAUX

DOCTORAL SCHOOL OF CHEMICAL SCIENCES

by

IOANNIS PETSAGKOURAKIS

in partial fulfillment for the Degree of

DOCTOR OF PHILOSOPHY

in POLYMER SCIENCE

HIGH PERFORMANCE POLYMER AND POLYMER/INORGANIC THERMOELECTRIC MATERIALS

Defense date: 8 December 2016
Review committee :

Prof. Jean OBERLÉ, University of Bordeaux, France	President
Prof. Xavier CRISPIN, Linkoping University, Sweden	Rapporteur
Dr. Sylvie HEBERT, University of Caen, France	Rapporteur
Prof. George MALLIARAS, MINES, Saint-Etienne, France	Examinator
Prof. Natalie STINGELIN, Georgia Institute of Technology, USA	Examinator
Dr. Guillaume FLEURY, University of Bordeaux, France	Invited
Dr. Eleni PAVLOPOULOU, University of Bordeaux, France	Invited
Prof. Georges HADZIIOANNOU, University of Bordeaux, France	Thesis Director
Prof. Stefan DILHAIRE, University of Bordeaux, France	Thesis Director

In the name of the best within you, do not sacrifice this world to those who are its worst. In the name of the values that keep you alive, do not let your vision of man be distorted by the ugly, the cowardly, the mindless in those who have never achieved his title. Do not lose your knowledge that man's proper estate is an upright posture, an intransigent mind and a step that travels unlimited roads. Do not let your fire go out, spark by irreplaceable spark, in the hopeless swamps of the approximate, the not-quite, the not-yet, the not-at-all. Do not let the hero in your soul perish, in lonely frustration for the life you deserved, but have never been able to reach. Check your road and the nature of your battle. The world you desired can be won, it exists, it is real, it is possible, it's yours.

Ayn Rand

To my family

Acknowledgements

Once, I was asked, how do I see myself in the future and how do I want other people to look at me. My answer to that was, that I want to actually inspire the change in people; motivate them towards their best self. Following a career in academia would end up putting me in a position that I could actually achieve this goal; that of a Professor - as many university Professors act as role models for most of their students. On top of that, having an insatiable curiosity about the university (which I believe that I have, for better or for worse) actually helps reaching an academic/research position and makes it fun. Thus, I started a PhD in Bordeaux at 2013. I would like to thank Prof. Georges Hadziioannou and Prof. Stefan Dilhaire for giving me the opportunity to work with such a interesting and promising subject; that of Thermoelectric Polymers. Throughout the thesis I had the rare chance to approach the field of organic electronics from various different aspects, which was extremely frutiful for acquiring a more solid understanding over the properties of those unique materials. However, this work wouldn't happen if not, for two people. I would like to thank Dr. Eleni Pavlopoulou, for the countless scientific discussions that we had over time, on the structural and electrical characterizations of the material. Without her detail-oriented advices and solid scientific expertise, this thesis would not come to exist. Our discussions didn't only help me evolve as scientist, but also as an individual. and I am grateful for that. I was truly honoured to work with her. Of course, at this point it would be a crime if I wouldn't acknowledge Dr. Guillaume Fleury. The numerous discussions that we had during my thesis were crucial to solidify the results presented herein. Thanks to him, I also had the rare opportunity to prove the repeatability of my materials between different laboratories (since repeatability in the research community is extremely important). His rigorous corrections on the writing of the thesis were important lessons for me and my future as a researcher. Additionally, I would like to thank also Dr. Bryan Kuropatwa and Dr. Jon Maiz with whom I had collaborated for my project. Particularly, with Bryan we were working together since day 1 of my thesis and he was the one that firstly introduced me to the world of thermoelectrics; a fact that I am grateful of. For the realization of this thesis I had the chance to collaborate with other laboratories too. I would like to acknowledge Prof. Magnus Berggren, Prof. Xavier Crispin, and Dr. Zia Ullah Khan, from the university of Linkoping for the numerous discussions on the thermoelectric properties of polymers. From the same university (LiU), I would also like to acknowledge Prof. Mats Falhman and Dr. Xjianjie Liu for the UPS characterizations. From Bordeaux, I would like to thank the theoriticians from ISM, Dr. Luca Muccioli and my good friend and brother-in-science Mr. Manoj Gali for the countless discussions on the charge transport mechanisms of polymers. Finally I would like to thank Dr. Lional Hirsch, Dr.Mamatimin Abbas, Dr.Damien Thuau and Dr. Yan Fang Chen from IMS for assisting in setting up a transistor characterization setup and for allowing me to use their low-temperature electrical conductivity measurement. I would like to acknowledge also Ms. Aude Manson and Ms. Dominique Gouzerh, the secretaries of the group in LCPO. Especially, I am really greatful to Aude for all her assistance in administrative stuff during all these years that I spent working in the lab.

During my time in Bordeaux, I took invalueable life lessons - both on a scientific and on a personal level. By observing my bosses, not only I learnt how to manage several situations inside a work environment, but I also observed how to actually guide, lead and motivate people; a lesson that would be important in the future of my career. However, those weren't the most important things that I was taught. Through my various experiences inside the lab-life I learnt a really essential lesson; as long as you know where you stand, not only it doesn't matter what people think or say about you, but also that there is nothing and no-one to be afraid of. Prof. Hadziioannou taught me this lesson personally, and I am grateful to him for that, as true self-confidence is an crucial trait both for a scientist and for a (future) leader - in a laboratory or a company. And usually, this kind of 'self knowledge' doesn't come easy.

Finally, I would like to thank all my friends - multinational and Greek- inside and outside LCPO. If I had to name each and every one of you, I would have to write a second thesis; and a third, bigger one, would be to describe the precious time that I shared with you. Being in a university that gathers people from various nationalities, I was lucky to forge friendships with people from all the edges of the world. And with this, I realized that it is important to draw wisdom from many places. If we take it from only one place, it becomes rigid ad stale. But, interacting and understanding the other cultures can help you become whole as a person. (likewise having different point of views in a scientific field, can get a better understanding of the field) My time in Bordeaux wasn't for sure easy (especially when you arrive and you don't speak french) and to be sincere I also had faced a certsin degree of discrimination (inside and outside the lab), for coming from a theoritical background, for not speaking french and for being greek. However, the presence of all of you made it a truly wonderful experience. Also, I would like to thank my family. During the period of my thesis I had lost my maternal grandfather and paternal grandmother, so it wasn't an easy time, neither for me in Bordeaux, nor for my family in Greece. Thus, I dedicate this thesis to my family. And of course, I want to thank my parents and my brother for their non-stop support all these years.

Cheers to everyone,
Merci beaucoup pour tout,

Yiannis

Contents

Foreword.

The field of polymer electronics was given birth by the discovery of Shirakawa, Mac Diarmid and Heeger in 1977, that oxidized conjugated polymers could behave electrically as a metal.[1,2] Since then, those (semi)conducting polymers have been used in the fabrication of flexible organic solar cells,[3] flexible organic light emitting diodes,[4] or flexible sensors.[5] The thermoelectric properties of conducting polymers have gained the attention of the scientific community in the recent years, due to promising thermoelectric efficiencies with respect to their inorganic counterparts.[6] Although the effect of the oxidation level to the thermoelectric and electrical properties has been thoroughly studied in the litterature,[7-9] the influence of other structural (crystallinity) and electronic (charge carrier mobility) parameters on the efficiency of thermoelectric devices needs to be better apprehended.

Consequently the aim of this Ph.D. is to provide alternative approaches for the enhancement of thermoelectric properties and to relate the increase of thermoelectric efficiency to the electronic and structural properties of the polymer material. Several optimization routes have been investigated in this study, either by a fine tuning of the synthetic parameters leading to the thermoelectric material or by associating organic and inorganic materials in a thermoelectric composite.

The manuscript is organized in six chapters covering the various studies on thin films of poly(3,4-ethylenedioxythiophene) (PEDOT) derivatives doped with *p*-toluenesulfonate (Tos) molecules with one underlying theme related to a deeper understanding on the structure/properties relationships. The first chapter provides some highlights from the literature with a focus on the state-of-the-art studies in the field of polymer thermoelectrics.

The aim of this chapter is to briefly summarize the existing knowledge and understanding on the thermoelectric properties of polymers. The following chapters describe the works and studies realized during this Ph.D. and are presented under the form of manuscript submitted or to be submitted in order to highlight the main results. Some redundancies are thus presented throughout the manuscript (mainly in the introduction of each chapters). Finally, at the end of this manuscript, three appendices provide some insights on the thermoelectricity theoretical background, the experimental procedures and other studies on polymer thermoelectrics, respectively.

Chapter 1: State of the art and literature highlights.

1.1 Early studies on thermoelectric polymers and p-type thermoelectric polymers:

The first Seebeck measurements on semiconducting polymers were conducted in polyacetylene, as a means to understand its behavior with respect to the conduction mechanism. Particularly, Heeger *and coll*. have varied the carrier doping of polyacetylene showing that the Seebeck coefficient decreases for high carrier concentrations, following the behavior of typical inorganic semiconductors (**Figure 1a**). [10-12]

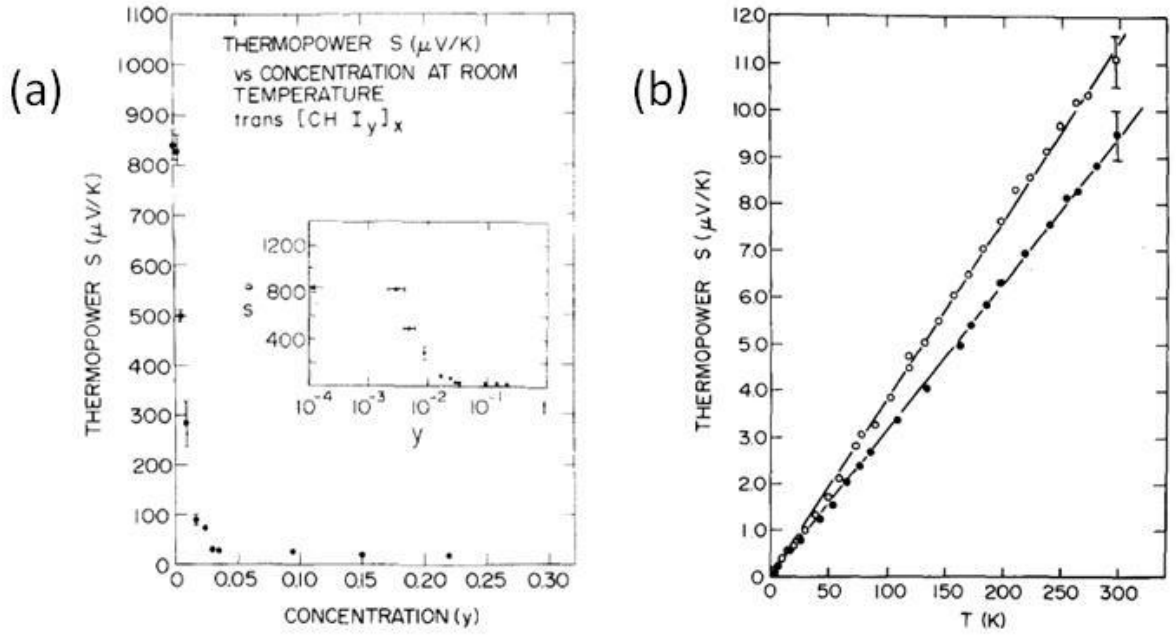

Figure 1: (a) The Thermopower (Seebeck coefficient) versus the concentration of the iodine dopant for polyacetylene,[11] (b) the Seebeck coefficient plotted against temperature for non-oriented (filled) and oriented (hollow) heavily doped polyacetylene.[10]

Additionally, low temperature Seebeck measurements were performed in order to investigate the metallic behavior of conducting polymer materials. A material with a typical metallic behavior has a linear Seebeck dependence with the temperature, as it can be observed in **Figure 1b** for polyacetylene. Nevertheless, due to its metallic nature, the measured Seebeck coefficient of highly conductive films was relatively low (< 20 μV/K), and the scientific community did not consider at this time conducting polymers for thermoelectric applications.[10-14]

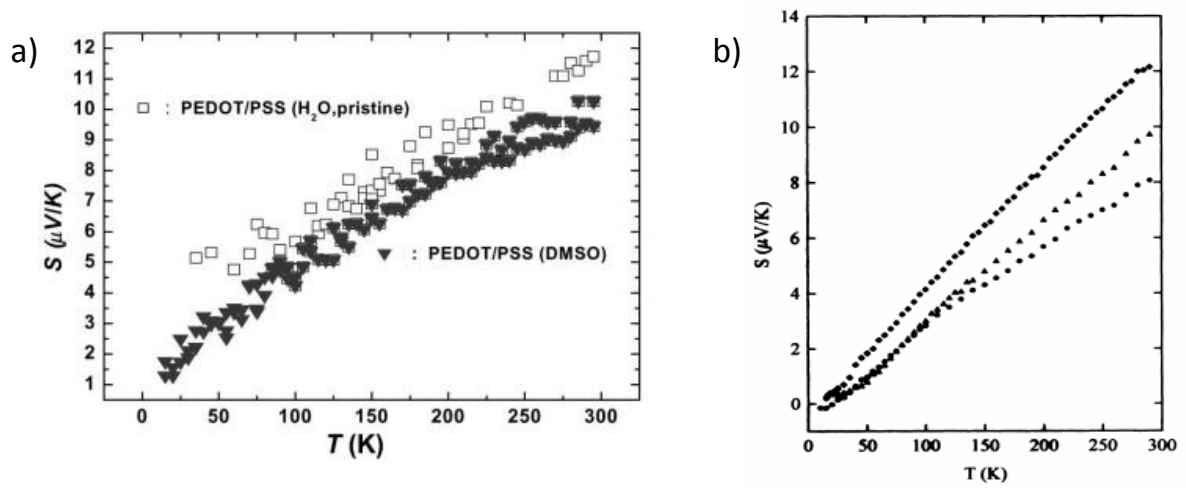

Figure 2: Seebeck coefficient versus Temperature for (a) PEDOT:PSS[15] and (b) Polyaniline.[16]

In the later years, Seebeck measurements were conducted on other conducting polymers as a means to elucidate their conduction behavior. Heeger *and coll*. and Kaiser *and coll*. have reported measurements on polyaniline[16] and polypyrrole[17], and retrieved as well a linear behavior of the Seebeck coefficient as regards to the temperature associated to relatively low values. Additionally, Kim *et al*. have conducted Seebeck measurements on poly(3,4-ethylenedioxythiophene) : poly(styrenesulfonate) (PEDOT:PSS) in order to understand the conductive properties of this newly discovered conductive ink (**Figure 2**).[15] The measured Seebeck coefficient of the PEDOT:PSS and its behavior against temperature

were reminiscent of that of a heavily doped semiconductor in the metallic regime of the Mott's transition. [18]

One of the first attempts to systematically focus on the thermoelectric properties of conducting polymers for application in thermoelectric devices, was reported from Leclerc *and coll*. in the 2000's.[19,20] The authors investigated the effect of the chemical structure of polycarbazoles on the conducting and thermoelectric properties. Although these polymers exhibited low thermoelectric efficiencies, with electrical conductivities in the order of magnitude of 10^{-2} S/cm, the Seebeck coefficient was around 400-500 μV/K, highlighting the potential of semi-conducting polymers for thermoelectric applications.[19,20]

This potential was strengthened through the studies of Jiang *et al*. on PEDOT:PSS.[21] In comparison with other conducting polymers, PEDOT:PSS is relatively stable in ambient conditions, and can be printed in films showing a high electrical conductivity (> 100 S/cm), making it a prospective candidate for any investigations in thermoelectrics. Kim *and coll*. discovered that the addition of a high boiling point solvent improved the figure of merit of the conducting polymer due to an enhanced electrical conductivity.[21]

Another systematic study on the thermoelectric properties of conducting polymers with regards to its optimization for thermoelectric applications was reported by Crispin *and coll*.[22] In this study the authors focused on the thermoelectric properties of the semiconducting poly(3-hexylthiophene) (P3HT). Solid state formalisms were applied on the measured properties in order to understand the thermoelectric behavior. This work was among the first registered attempts to optimize the thermoelectric properties of a polymer material by tuning its carrier concentration (**Figure 3**). Through this optimization, the P3HT Power Factor was increased by more than four decades but was still lower than the one of inorganic thermoelectric materials. However, this study highlighted that the relatively low

thermoelectric efficiencies of semi-conducting polymers can be further enhanced by a proper tuning of the electronic properties.[22]

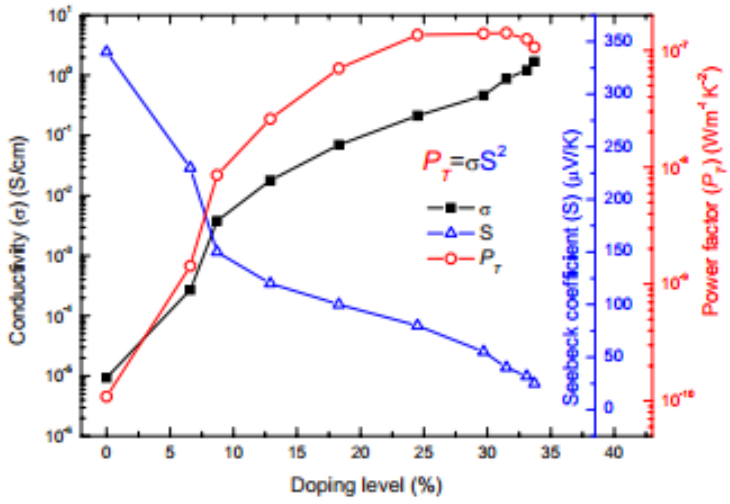

Figure 3: Electrical conductivity and Seebeck coefficient plotted against the doping levels for the P3HT.[22]

In 2011, Bubnova *et al*. published a study on poly(3,4-ethylenedioxythiophene) (PEDOT) derivatives doped with *p*-toluenesulfonate (Tos) molecules (PEDOT:Tos) and its thermoelectric optimization by reductive vapors.[8] The authors had synthesized conductive and insoluble PEDOT:Tos films through in-situ oxidative polymerization, and then optimized their thermoelectric properties by exposing the films to tetrakis-dimethylaminoethylene (TDAE) reductive vapors. By reducing the material, the Seebeck coefficient increased while the electrical conductivity decreased, following a behavior similar to the one observed in inorganic materials (**Figure 4**). However, in comparison to inorganic thermoelectric materials, the PEDOT:Tos films exhibited a relatively low thermal conductivity of 0.2-0.25 W/mK. As a result, the Power Factor was optimized from 38 to 324 $\mu W/mK^2$, which was the highest reported for conducting polymers. In this study the figure of merit, *ZT*, was calculated to 0.25, a record for a polymer material. This study was the first to really highlight the strong potential

of conducting polymers for thermoelectric applications and subsequently inspires many studies on the thermoelectric properties of conducting polymers.[6,8]

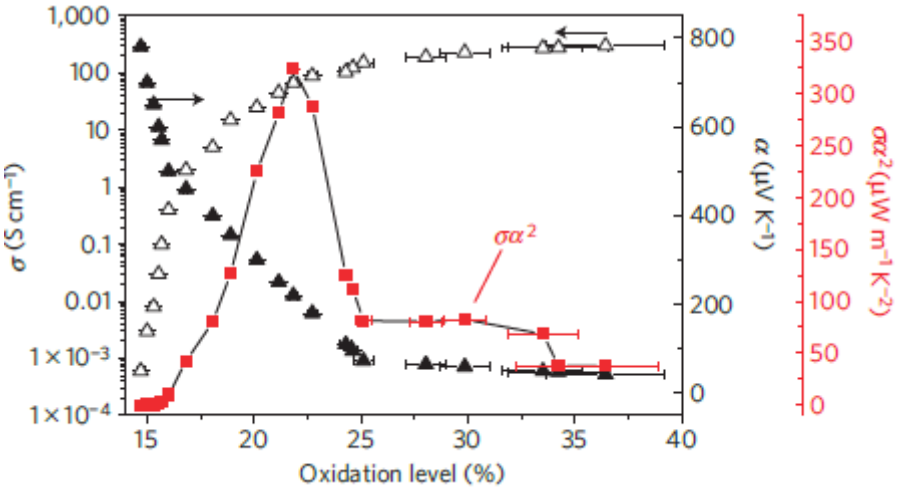

Figure 4: The electrical conductivity, σ, the Seebeck coefficient, α, and the Power Factor, $\sigma\alpha^2$, versus the oxidation levels of the PEDOT:Tos films.[8]

Following the breakthrough of Bubnova *et al*,[8] Park *et al*. published a report on PEDOT:Tos synthesized with in-situ polymerization with the presence of a block-copolymer surfactant.[23] The authors argued that the introduction of a block-copolymer assisted the structuration of the PEDOT:Tos films, resulting in a high electrical conductivities of 1355 S/cm. Furthermore, cyclic voltammetry was used as a means to reduce the material - in a similar manner as Bubnova *et al*.[7,8] Using this methodology, they managed to optimize the thermoelectric efficiency of PEDOT:Tos films to a record Power Factor of 1270 μW/mK^2 (**Figure 5**).[23]

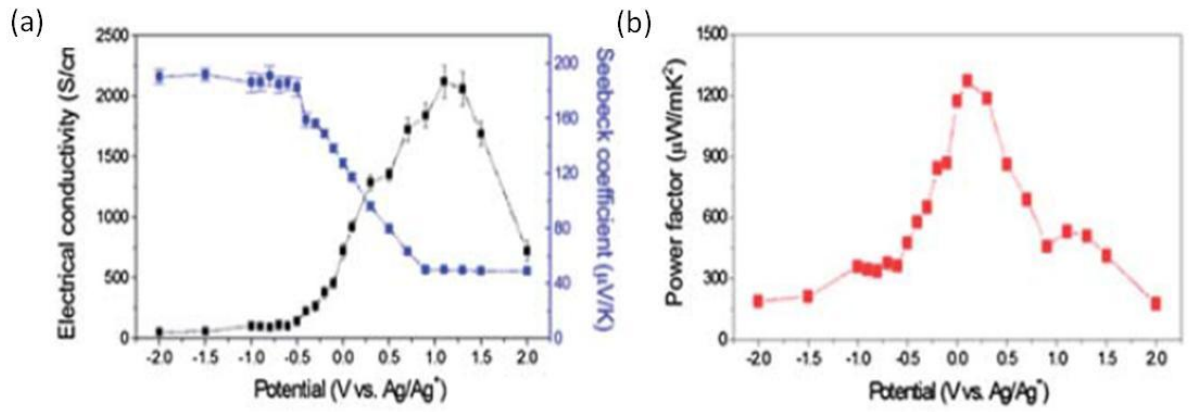

Figure 5: (a) Electrical conductivity, Seebeck coefficient and (b) Power Factor versus the applied potential for the electrochemical dedoping of the PEDOT:Tos films.[23]

The next record value for the *ZT* of a conducting polymers was reported in 2013 by Kim *et al*.[24] The authors optimized the thermoelectric and electrical properties of PEDOT:PSS by using solvent additives and post-treatments, such as dimethylsulfoxide (DMSO) and ethylene glycol (EG). At first they introduced these small molecules into the conductive ink, where they acted as plasticizers for the PEDOT chains during the thin film deposition. After bathing the PEDOT:PSS films in DMSO and EG to remove any excess of insulating PSS, they managed to enhance the polymer Power Factor to 469 μW/mK^2.[24] Combined with a relatively low thermal conductivity of 0.42 W/mK, the figure of merit reached 0.42 (**Figure 6**).

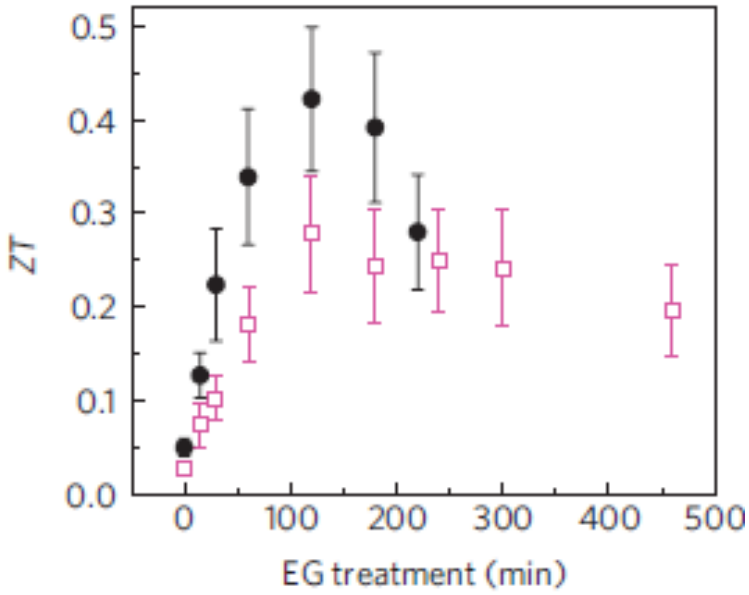

Figure 6: The figure of merit *ZT* versus the EG post-treatment time for PEDOT:PSS films deposited with the addition of EG (open squares) or DMSO (filled circles).[24]

Palumbiny *et al*. later demonstrated that this kind of treatment enhances the thin film crystallinity, highlighting the importance of the structure on the electrical properties of the PEDOT:PSS (**Figure 7**).[25,26]

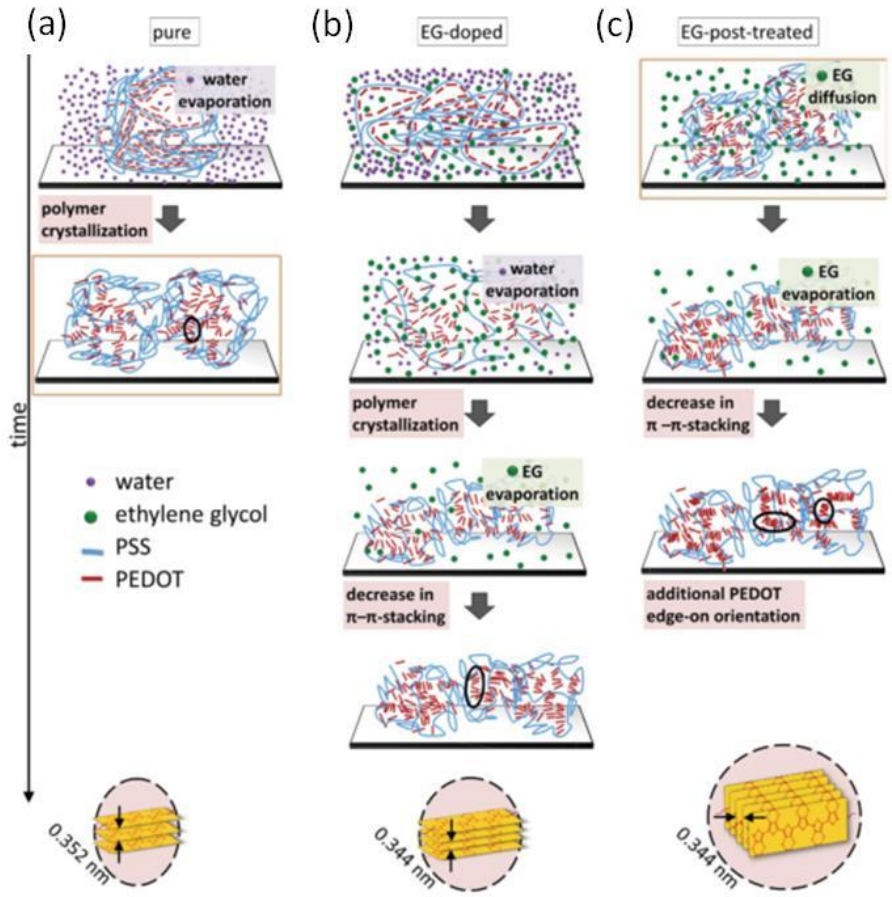

Figure 7: The effect of plasticizing agents like EG on the PEDOT:PSS structure. When EG is added to the PEDOT:PSS material (b), the crystallization process is slowed down resulting in better stacked chains, in comparison to the pure (a) material. When the thin films are further treated with a EG bath, the system recrystallizes and shift from an face-on to an edge-on configuration.[25]

Nevertheless, the origin of these interesting thermoelectric properties was still unclear. A first explanation was provided by Bubnova *et al*. in 2013.[27] The authors showed that conductive polymers with increased crystallinity can behave as semimetals, thus exhibiting both a high electrical conductivity and a high Seebeck coefficient (**Figure 8**). Additionally, a correlation between the enhanced thermoelectric properties and a broad band edge near the chemical potential was demonstrated. In PEDOT systems of high crystallinity, the π-orbitals of the PEDOT units recombine into a wider π-system, which broadens all the π-orbitals of the

polymer, thus increasing the slope at the Density of States and the Seebeck coefficient (See **Appendix A** for the theoretical background related to this assertion).

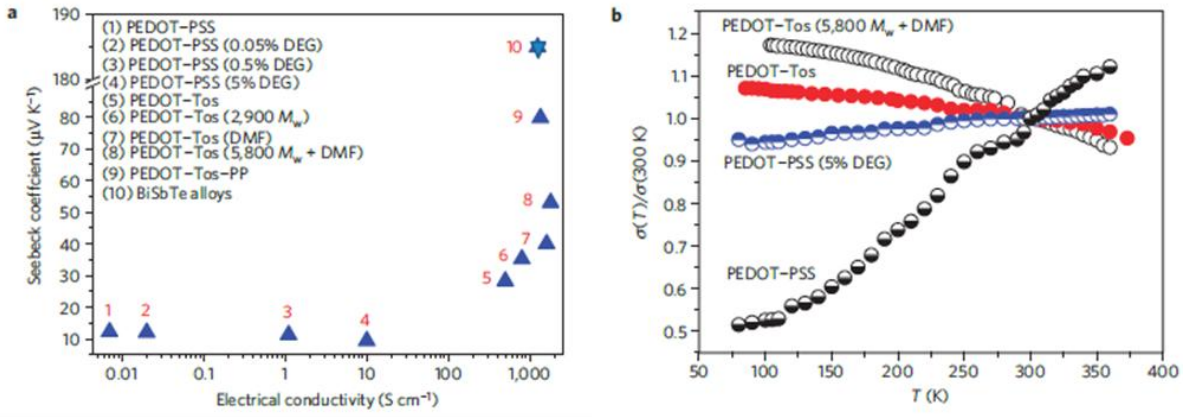

Figure 8: (a) the Seebeck coefficient versus the electrical conductivity, (b) the normalized electrical conductivity versus temperature for the various PEDOT species for various PEDOT based systems.[27]

This kind of extended π-system obtained for systems of high crystallinity was referred by the authors as a bipolaron network since the majority of the charge carriers are bipolarons. As a result, vapor phase polymerized PEDOT:Tos films exhibit Power Factors as high as 454 μW/mK^2.[27]

With the rising interest for polymer thermoelectric materials, the accuracy of the thermoelectric measurements in a thin film configuration was also discussed by Kemerink *and coll*. They demonstrated that a rigorous device geometry is needed for an accurate Seebeck measurement.[28] In particular, the length of the gold electrodes, L_e, should not be larger than the channel length between the two electrodes, L_c , in order to obtain an accurate thermovoltage signal (**Figure 9**).[28]

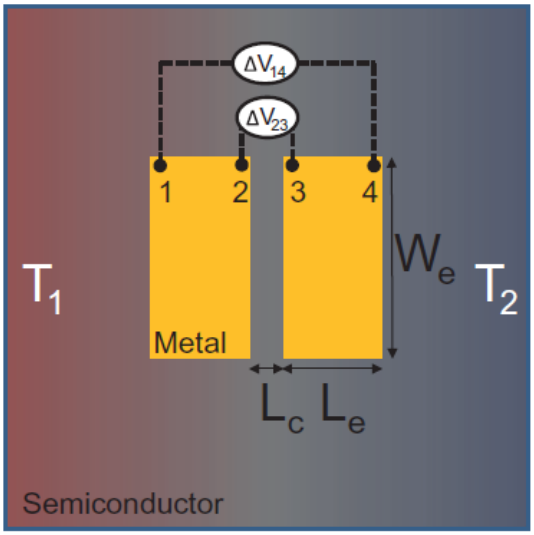

Figure 9: The typical device for the thermoelectric measurement. The various geometrical parameters have to be optimized in order to accurately determine the Seebeck coefficient.[28]

Nevertheless, the main challenge in order to evaluate the thermoelectric performance appears to be the measurement of the thermal conductivity, κ.[6,29] Most reports provided the Power Factor in the in-plane direction, *i.e.*, along the thin film substrate. The in-plane thermal conductivity has consequently to be determined in order to calculate the overall thermoelectric efficiency. Segalmann *and coll*. used time-domain thermoreflectance in combination with measurements of elastic constants to track down the in-plane thermal conductivity of PEDOT:PSS films evaluated to 1W/mK.[30] Wei *et al*. determined the in-plane thermal conductivity of PEDOT:PSS films by measuring the thermal diffusivity of the material, extracting a value of 0.8 W/mK for PEDOT:PSS.[31,32] Meanwhile, Weathers *et al*. measured the in-plane thermal conductivity of PEDOT:Tos films fabricated from various synthetic routes, in order to extract a relationship between in-plane κ and σ. The thermal conductivity was obtained with a 4-point measurement microdevice.[33,34] They found that the two parameters follow a linear relationship, highlighting that κ is also a parameter to be considered in the thermoelectric optimization of polymers. Highly crystalline and highly

doped conductive materials with a semi-metallic behavior are expected to exhibit a high thermal conductivity (around 1 W/mK). Nevertheless, this value is still relatively low with respect to the one of inorganic thermoelectric materials.[33]

Another lever to modulate the thermoelectric properties of conducting materials was reported by Wei *et al.* [35] and Crispin *and coll.*[36] The effect of the humidity on the thermoelectric properties of PEDOT:PSS was studied as such kind of materials are expected to absorb a significant amount of water. The swelling of the PEDOT:PSS films did not significantly affected the electrical properties (**Figure 10**). However, the Seebeck coefficient benefits from such treatment, increasing from 10 to 215 µV/K. The origin of this effect is related to the diffusion of ions due to the applied temperature difference. Hence, this novel thermo-ionic effect opens a new window of opportunity to enhance the thermoelectric properties of polymers for energy harvesting.[36]

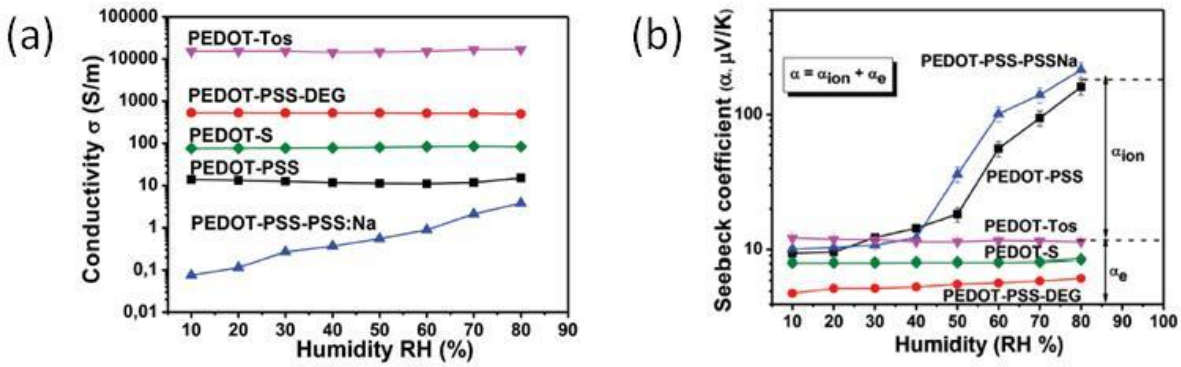

Figure 10: (a) Electrical conductivity and (b) Seebeck coefficient plotted against humidity.[36]

1.2 N-type thermoelectric polymers:

All the aforementioned reports referred to p-type polymer materials. For a thermoelectric generator both a p- and n- type materials are required. However, n-type polymers are usually unstable since they are oxidized in the atmosphere. Besides most reported systems lack in electrical conductivity, in comparison to their p-type equivalents.[37,38] Consequently doped fullerene or TTF:TCNQ salts were used as n-type organic thermoelectrics instead of polymers until the 2010's.[8,39-41] The first step towards efficient and stable n-type polymers were reported by Zhu *and coll.* in 2012 with the synthesis of metal coordination polymers such as poly(Ni-1,1,2,2-ethenetetrathiolate) depicted in **Figure 11**.[42]

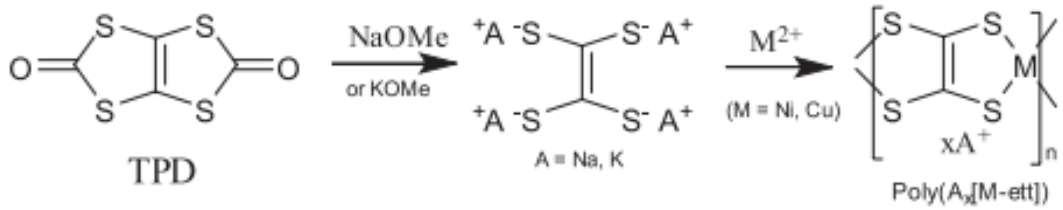

Figure 11: The synthetic route for the metal coordination polymers that Zhu and col. reported.[42]

In the metal coordination polymers, a metal is linked to organic ligands inside the polymer repetitive unit. By changing the metal and the ligands of the organic repetitive unit, various p- and n-type polymers can be synthesized for thermoelectric applications. Concerning the n-type compartment, the poly(Ni-1,1,2,2-ethenetetrathiolate) was stable in ambient conditions and exhibited a Power Factor of 66 μW/mK^2.[42]

Soluble n-type polymers were subsequently reported by Chabinyc *and coll.*[43] and Segalman *and coll.* in 2014.[44] These naphthalene derivatives (**Figure 12**) exhibited a low Power Factor of 1.4 μW/mK^2, due to an intrinsically low electrical conductivity (0.5 S/cm).

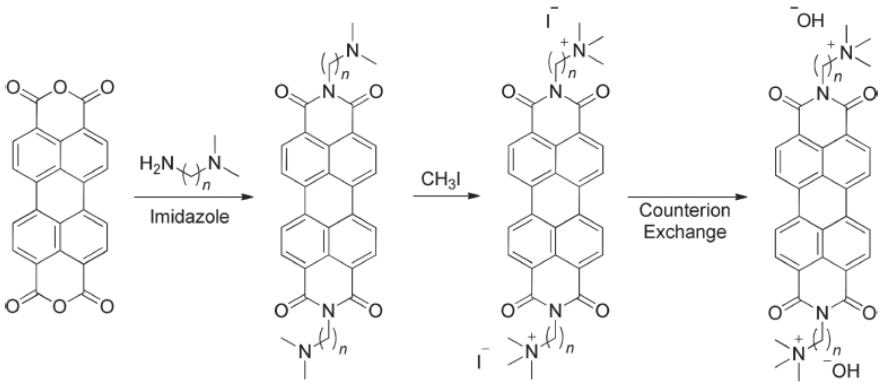

Figure 12: The naphthalene derivatives reported by Segalman and col. [44]

However, the Seebeck values of such n-type polymers are in the order of magnitude of 200 μV/K, making these materials quite appealing for thermoelectric applications.[44] Shi *et al.* reported in 2015 a family of soluble n-type Benzodifurandione Paraphenylenevinylidene BDPPV derivatives with electrical conductivities as high as 14 S/cm and a Power Factor of 28 $\mu W/mK^2$. [45] These authors highlighted the importance of the backbone structure on the electrical and thermoelectric properties, as the introduction of halogen groups to the polymer backbone proved to be detrimental for the thermoelectric behavior of the material.[45]

1.3 Thermoelectric polymer nanocomposites:

In the recent years, a large number of studies on thermoelectric properties of polymers were focused on the fabrication of polymer/inorganic nanocomposites. By introducing an inorganic material in a polymer matrix, a (nano)composite material can be obtained and benefits from the different properties of the two materials.[46] For example, the intrinsically high Seebeck coefficient of an inorganic material can be associated with an electrically conductive and thermally insulating polymer matrix.[46-50] Promising studies on nanocomposites formed from the association of carbon nanotubes with PEDOT:PSS[49] or polyaniline[50] were published in 2010, where the nanocomposites showed Power Factors as high as 20 and 25 $\mu W/mK^2$, respectively. At the same time, a study on PEDOT:PSS / bismuth telluride nanocomposites was also published and a promising Power Factor of 48 $\mu W/mK^2$ was obtained depending of the amount of the inorganic charges introduced in the polymer matrix.[51]

In all these approaches, the importance of the concentration of the inorganic charges and the interface between the polymer and the inorganic materials was pinpointed. The effect of the interface on the nanocomposite properties was systematically studied by Segalman *and coll.* who published work on nanocomposites of PEDOT:PSS with tellurium nanowires (**Figure 13**), exhibiting Power Factor close to $100\mu W/mK^2$.[47] [48] Particularly, these authors investigated the interfacial influence from a solid state physics approach, in order to elucidate the origin of the nanocomposite properties, hence highlighting the importance of the interface between polymer and inorganic material, for a high performance thermoelectric nanocomposite. Particularly, they showed that the charge carrier transport in such nanocomposites is occuring in the interface of the conducting polymer/inorganic material.[46,47]

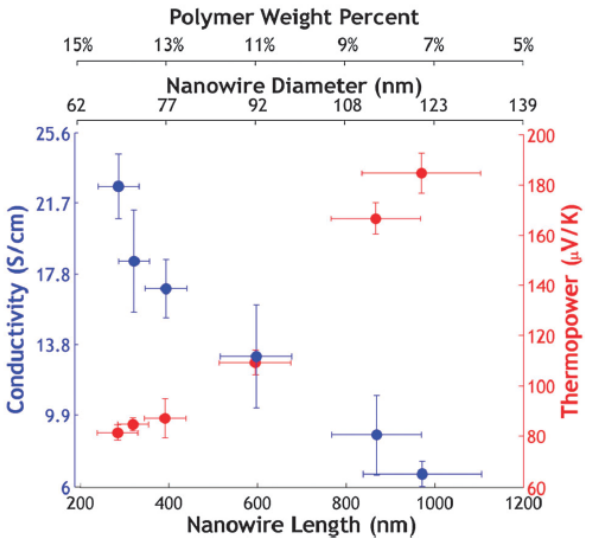

Figure 13: Electrical conductivity and Thermopower (Seebeck coefficient) versus the nanowire length, diameter and polymer weight percent.[48]

However, the former approaches only involved p-type materials. An study for a n-type thermoelectric nanocomposite was published by Ireland *et al*. in 2016.[52] The authors introduced $SnCl_2$ in a pyrromellitic diimide polymer matrix and observed a gradual increase of the thermoelectric properties with the concentration of the inorganic charge (**Figure 14**).

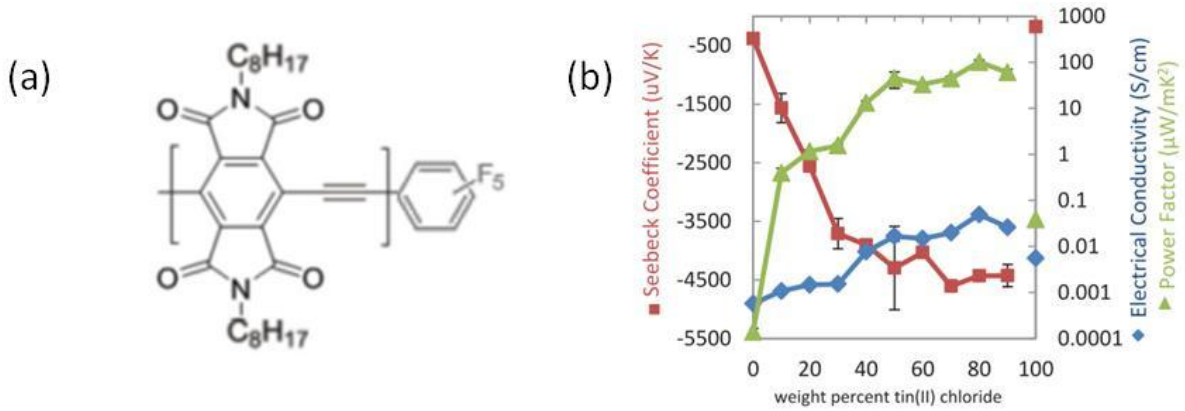

Figure 14: (a) The pyromellitic polymer used by Ireland *et al*. (b) the resulting Seebeck coefficient, electrical conductivity and Power Factor versus the $SnCl_2$ weight percent.[52]

As a result, the nanocomposite reached a Power Factor of 100 μW/mK^2. Using Ultraviolet Photoelectron Spectroscopy (UPS) measurements, the authors observed that the nanocomposite shows a modified electronic structure with additional states near the band edge (**Figure 15**). These extra electronic bands originate from the interfacial charge transfers between the two materials which eventually contribute to the tuning of the thermoelectric properties of the nanocomposite.[52]

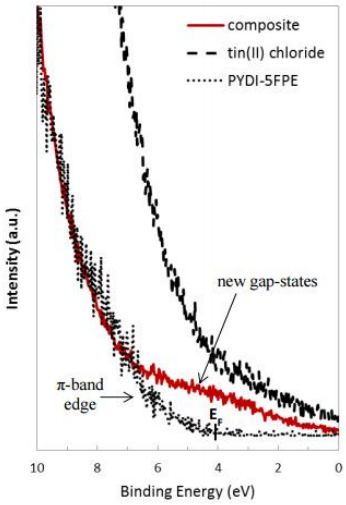

Figure 15: The UPS spectra at low binding energies for the polymer (dotted line), tin(II) chloride (dashed line), and the nanocomposite (red line).[52]

Muller *and coll.* published in 2016 an interesting approach based on the blending of P3HT with p- and n-type carbon nanotubes (**Figure 16**).[53] The low thermal conductivity (0.29 W/mK) and the high Seebeck coefficient (1000 μV/K) of P3HT was combined with the high electrical conductivity of the carbon nanotubes. The main accomplishment reported in this study was the observed shift on the sign of the thermovoltage from p- to n-type obtained by the UV irradiation of the nanocomposite. This behavior was correlated with the tuning of the doping levels of the polymer matrix under such treatments. Using this methodology to

fabricate p- and n-type legs, a 5 nA output current at 5 mV thermovoltage was obtained from a printed thermoelectric generator under a 35°C temperature gradient (**Figure 17**).[53]

Figure 17: One possible configuration of the thermoelectric generator composed of the p- and n- legs from P3HT / carbon nanotubes nanocomposites. Each leg has a 5mm width and they are arranged in a wristband in order to harvest the thermal energy of the human body.[53]

The introduction of a n-type charge in a p-type matrix was also reported by Wang *et al*, using PEDOT:Tos as a matrix.[54] The authors synthesized in-situ polymerized PEDOT:Tos containing n-type. When the PEDOT:Tos had an oxidation level of 34% - typical for as-cast PEDOT:Tos films -, the nanocomposite behaves as a p-type conductor. However, upon reduction, the nanocomposite exhibited an n-type behavior, with a thermovoltage in the order of magnitude of a few mVs, as the contribution of the n-type carbon nanotubes dominates the intrinsic p-type behavior of the PEDOT:Tos matrix (**Figure 18**). With this treatment, the nanocomposite Power Factor reached a value of 1050μW/mK^2.[54]

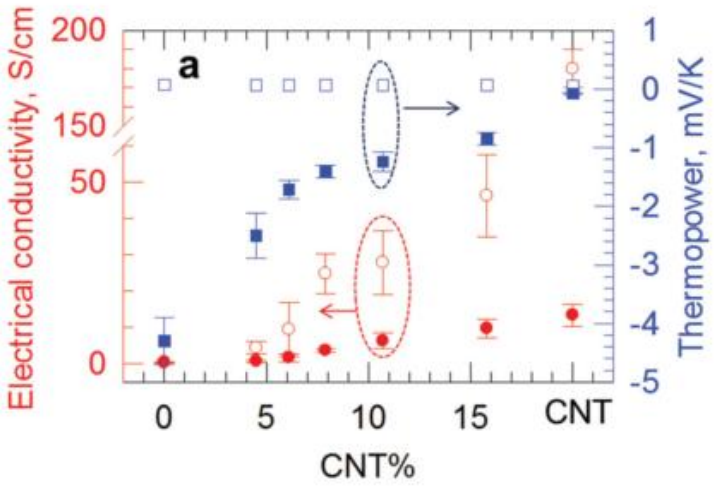

Figure 18: The electrical conductivity and thermopower (Seebeck coefficient) for the carbon nanotubes / PEDOT:Tos nanocomposites before (hollow) and after (filled) the chemical reduction of PEDOT:Tos for various carbon nanotube concentrations.[54]

1.4 Conclusions & Ph.D. scope:

The field of thermoelectric polymers can still be considered in its infancy as regards to other "organics electronics" fields. Most reported studies involved p-type materials and the optimization of their thermoelectric properties. To become competitive in the energy recovery landscape, additional breakthroughs are needed. Following the works led by the group Linkoping University, the thermoelectric behavior of p-type conducting polymers is rather well-understood even if some important challenges remain to be tackled, in particular on the polymer structure / thermoelectric relationships. On the other hand, for a fully functional thermoelectric generator, an n-type material is also needed. Due to the limited thermoelectric performance of n-type polymers, inorganic / organic nanocomposites constitute an interesting alternative and have already shown a high potential in order to modulate the thermoelectric behavior from p- to n-type. Besides such developments are also needed for the fabrication of fully operational thermoelectric generators. The evaluation of the power output delivered by such devices is crucial to evaluate the "organic thermoelectrics" technology.

Consequently my Ph.D. had two main objectives :

i. The development of efficient thermoelectric materials based on conducting polymers with a particular emphasis on the relationships between the polymer structure and the thermoelectric properties. This study was associated to the development of the characterization means needed to properly evaluate the thermoelectric efficiency of the materials which were nonexistent at my arrival in Bordeaux (in particular the Seebeck coefficient set-up). During these studies, a strong emphasis was given to the characterization of the structural features (crystallinity, chain orientation) as regards to the synthetic routes used to design the materials.

ii. The development of a n-type thermoelectric polymer material which we first envisioned as a composite material between a n-type charge and a polymer matrix following the literature review. This study had to result in the fabrication of organic thermogenerators for the evaluation of thermoelectric devices based on organic materials.

The different chapters of this Ph.D. manuscript reflect these two objectives. In the first four chapters, PEDOT:Tos thin films were synthetized from various formulations in order to better apprehend the relationships between crystallinity and thermoelectric / electrical properties. Eventually a correlation between the PEDOT:Tos electronic structure and the Seebeck coefficient was established as regards to the structural features exhibited by the PEDOT:Tos thin films. Finally the anisotropic electronic and thermal properties of the PEDOT:Tos thin films were investigated leading to an experimental correlation between the thermoelectric Figure of Merit and the charge carrier mobility. The last chapter of this manuscript is dedicated to the design of n-type materials through a novel methodology consisting of the fabrication of a "junction" between a n-type substrate and a PEDOT:Tos film. Such stack provides an elegant way to modulate the Seebeck coefficient through the variation of the PEDOT:Tos thin film thickness. As a result, novel hybrid thermoelectric generators were fabricated.

At the end of the manuscript, three extended appendices provide some insights on the theoretical background used throughout the manuscript, the experimental procedures (detailed characterization methodologies, experimental set-up) and studies on the synthesis of PEDOT:Tos and the application of hydroxymethylated PEDOT:Tos as p-type thermoelectric polymer.

1.5 References:

1 Geoghegan, M. & Hadziioannou, G. *Polymer Electronics*. (OUP Oxford, 2013).

2 Heeger, A. J. Nobel Lecture: Semiconducting and metallic polymers: The fourth generation of polymeric materials. *Reviews of Modern Physics* **73**, 681-700 (2001).

3 Hofmann, A. I. *et al.* An Alternative Anionic Polyelectrolyte for Aqueous PEDOT Dispersions: Toward Printable Transparent Electrodes. *Angew Chem Int Ed Engl* **54**, 8506-8510, doi:10.1002/anie.201503024 (2015).

4 Kuik, M. *et al.* 25th anniversary article: charge transport and recombination in polymer light-emitting diodes. *Adv Mater* **26**, 512-531, doi:10.1002/adma.201303393 (2014).

5 Persson, K. M. *et al.* Electronic Control over Detachment of a Self-Doped Water-Soluble Conjugated Polyelectrolyte. *Langmuir* **30**, 6257-6266, doi:10.1021/la500693d (2014).

6 Bubnova, O. & Crispin, X. Towards polymer-based organic thermoelectric generators. *Energy & Environmental Science* **5**, 9345, doi:10.1039/c2ee22777k (2012).

7 Bubnova, O., Berggren, M. & Crispin, X. Tuning the thermoelectric properties of conducting polymers in an electrochemical transistor. *J Am Chem Soc* **134**, 16456-16459, doi:10.1021/ja305188r (2012).

8 Bubnova, O. *et al.* Optimization of the thermoelectric figure of merit in the conducting polymer poly(3,4-ethylenedioxythiophene). *Nat Mater* **10**, 429-433, doi:10.1038/nmat3012 (2011).

9 Khan, Z. U. *et al.* Acido-basic control of the thermoelectric properties of poly(3,4-ethylenedioxythiophene)tosylate (PEDOT-Tos) thin films. *J. Mater. Chem. C* **3**, 10616-10623, doi:10.1039/c5tc01952d (2015).

10 Park, Y. W., Heeger, A. J., Druy, M. A. & MacDiarmid, A. G. Electrical transport in doped polyacetylene. *The Journal of Chemical Physics* **73**, 946, doi:10.1063/1.440214 (1980).

11 Park, Y. W., Denenstein, A., Chiang, C. K., Heeger, A. J. & MacDiarmid, A. G. Semiconductor-metal transition in doped (CH)x: Thermoelectric power. *Solid State Communications* **29**, 747-751, doi:http://dx.doi.org/10.1016/0038-1098(79)90153-4 (1979).

12 Moses, D. *et al.* Inter-soliton electron hopping transport in trans-(CH)x. *Solid State Communications* **40**, 1007-1010, doi:http://dx.doi.org/10.1016/0038-1098(81)90055-7 (1981).

13 Park, Y. W. *et al.* Proceedings of the International Conference on Science and Technology of Synthetic Metals Conductivity and thermoelectric power of the newly processed polyacetylene. *Synthetic Metals* **28**, D27-D34, doi:http://dx.doi.org/10.1016/0379-6779(89)90670-X (1989).

14 Zuzok, R., Kaiser, A. B., Pukacki, W. & Roth, S. Thermoelectric power and conductivity of iodine-doped ‘‘new’’ polyacetylene. *The Journal of Chemical Physics* **95**, 1270, doi:10.1063/1.461107 (1991).

15 Kim, J. Y., Jung, J. H., Lee, D. E. & Joo, J. Enhancement of electrical conductivity of poly(3,4-ethylenedioxythiophene)/poly(4-styrenesulfonate) by a change of solvents. *Synthetic Metals* **126**, 311-316, doi:http://dx.doi.org/10.1016/S0379-6779(01)00576-8 (2002).

16 Yoon, C. O., Reghu, M., Moses, D., Heeger, A. J. & Cao, Y. Counterion-induced processibility of polyaniline: Thermoelectric power. *Physical Review B* **48**, 14080-14084, doi:10.1103/PhysRevB.48.14080 (1993).

17 Kemp, N. T. *et al.* Thermoelectric power and conductivity of different types of polypyrrole. *Journal of Polymer Science Part B: Polymer Physics* **37**, 953-960, doi:10.1002/(SICI)1099-0488(19990501)37:9<953::AID-POLB7>3.0.CO;2-L (1999).

18 Mott, N. F. & Davis, E. A. *Electronic Processes in Non-Crystalline Materials*. (OUP Oxford, 2012).

19 Lévesque, I. *et al.* Highly soluble poly(2,7-carbazolenevinylene) for thermoelectrical applications: From theory to experiment. *Reactive and Functional Polymers* **65**, 23-36, doi:10.1016/j.reactfunctpolym.2004.11.008 (2005).
20 Lévesque, I. *et al.* Synthesis and Thermoelectric Properties of Polycarbazole, Polyindolocarbazole, and Polydiindolocarbazole Derivatives. *Chemistry of Materials* **19**, 2128-2138, doi:10.1021/cm070063h (2007).
21 Jiang, F.-X. *et al.* Thermoelectric Performance of Poly(3,4-ethylenedioxythiophene): Poly(styrenesulfonate). *Chinese Physics Letters* **25**, 2202 (2008).
22 Xuan, Y. *et al.* Thermoelectric properties of conducting polymers: The case of poly(3-hexylthiophene). *Physical Review B* **82**, doi:10.1103/PhysRevB.82.115454 (2010).
23 Park, T., Park, C., Kim, B., Shin, H. & Kim, E. Flexible PEDOT electrodes with large thermoelectric power factors to generate electricity by the touch of fingertips. *Energy & Environmental Science* **6**, 788-792, doi:10.1039/C3EE23729J (2013).
24 Kim, G. H., Shao, L., Zhang, K. & Pipe, K. P. Engineered doping of organic semiconductors for enhanced thermoelectric efficiency. *Nat Mater* **12**, 719-723, doi:10.1038/nmat3635 (2013).
25 Palumbiny, C. M. *et al.* The Crystallization of PEDOT:PSS Polymeric Electrodes Probed In Situ during Printing. *Adv Mater* **27**, 3391-3397, doi:10.1002/adma.201500315 (2015).
26 Palumbiny, C. M. *et al.* Molecular Reorientation and Structural Changes in Cosolvent-Treated Highly Conductive PEDOT:PSS Electrodes for Flexible Indium Tin Oxide-Free Organic Electronics. *The Journal of Physical Chemistry C* **118**, 13598-13606, doi:10.1021/jp501540y (2014).
27 Bubnova, O. *et al.* Semi-metallic polymers. *Nat Mater* **13**, 190-194, doi:10.1038/nmat3824 (2014).
28 Reenen, S. v. & Kemerink, M. Correcting for contact geometry in Seebeck coefficient measurements of thin film devices. *Organic Electronics* **15**, 2250-2255, doi:http://dx.doi.org/10.1016/j.orgel.2014.06.018 (2014).
29 He, M., Qiu, F. & Lin, Z. Towards high-performance polymer-based thermoelectric materials. *Energy & Environmental Science* **6**, 1352, doi:10.1039/c3ee24193a (2013).
30 Liu, J. *et al.* Thermal Conductivity and Elastic Constants of PEDOT:PSS with High Electrical Conductivity. *Macromolecules* **48**, 585-591, doi:10.1021/ma502099t (2015).
31 Wei, Q., Mukaida, M., Kirihara, K. & Ishida, T. Experimental Studies on the Anisotropic Thermoelectric Properties of Conducting Polymer Films. *ACS Macro Letters* **3**, 948-952, doi:10.1021/mz500446z (2014).
32 Wei, Q., Uehara, C., Mukaida, M., Kirihara, K. & Ishida, T. Measurement of in-plane thermal conductivity in polymer films. *AIP Advances* **6**, 045315, doi:doi:http://dx.doi.org/10.1063/1.4948447 (2016).
33 Weathers, A. *et al.* Significant electronic thermal transport in the conducting polymer poly(3,4-ethylenedioxythiophene). *Adv Mater* **27**, 2101-2106, doi:10.1002/adma.201404738 (2015).
34 Mavrokefalos, A., Pettes, M. T., Zhou, F. & Shi, L. Four-probe measurements of the in-plane thermoelectric properties of nanofilms. *Review of Scientific Instruments* **78**, 034901, doi:doi:http://dx.doi.org/10.1063/1.2712894 (2007).
35 Wei, Q., Mukaida, M., Kirihara, K., Naitoh, Y. & Ishida, T. Thermoelectric power enhancement of PEDOT:PSS in high-humidity conditions. *Applied Physics Express* **7**, 031601, doi:10.7567/apex.7.031601 (2014).
36 Wang, H., Ail, U., Gabrielsson, R., Berggren, M. & Crispin, X. Ionic Seebeck Effect in Conducting Polymers. *Advanced Energy Materials* **5**, n/a-n/a, doi:10.1002/aenm.201500044 (2015).
37 Katz, H. E. *et al.* A soluble and air-stable organic semiconductor with high electron mobility. *Nature* **404**, 478-481 (2000).

38 See, K. C., Landis, C., Sarjeant, A. & Katz, H. E. Easily Synthesized Naphthalene Tetracarboxylic Diimide Semiconductors with High Electron Mobility in Air. *Chemistry of Materials* **20**, 3609-3616, doi:10.1021/cm7032614 (2008).
39 Sumino, M. *et al.* Thermoelectric properties of n-type C60 thin films and their application in organic thermovoltaic devices. *Applied Physics Letters* **99**, 093308, doi:doi:http://dx.doi.org/10.1063/1.3631633 (2011).
40 Inabe, T. *et al.* Electronic structure of alkali metal doped ${\mathrm{C}}_{60}$ derived from thermoelectric power measurements. *Physical Review Letters* **69**, 3797-3799 (1992).
41 Yu, C., Murali, A., Choi, K. & Ryu, Y. Air-stable fabric thermoelectric modules made of N- and P-type carbon nanotubes. *Energy & Environmental Science* **5**, 9481, doi:10.1039/c2ee22838f (2012).
42 Sun, Y. *et al.* Organic thermoelectric materials and devices based on p- and n-type poly(metal 1,1,2,2-ethenetetrathiolate)s. *Adv Mater* **24**, 932-937, doi:10.1002/adma.201104305 (2012).
43 Schlitz, R. A. *et al.* Solubility-limited extrinsic n-type doping of a high electron mobility polymer for thermoelectric applications. *Adv Mater* **26**, 2825-2830, doi:10.1002/adma.201304866 (2014).
44 Russ, B. *et al.* Power factor enhancement in solution-processed organic n-type thermoelectrics through molecular design. *Adv Mater* **26**, 3473-3477, doi:10.1002/adma.201306116 (2014).
45 Shi, K. *et al.* Toward High Performance n-Type Thermoelectric Materials by Rational Modification of BDPPV Backbones. *J Am Chem Soc* **137**, 6979-6982, doi:10.1021/jacs.5b00945 (2015).
46 Malen, J. A., Yee, S. K., Majumdar, A. & Segalman, R. A. Fundamentals of energy transport, energy conversion, and thermal properties in organic–inorganic heterojunctions. *Chemical Physics Letters* **491**, 109-122, doi:10.1016/j.cplett.2010.03.028 (2010).
47 Coates, N. E. *et al.* Effect of interfacial properties on polymer-nanocrystal thermoelectric transport. *Adv Mater* **25**, 1629-1633, doi:10.1002/adma.201203915 (2013).
48 Yee, S. K., Coates, N. E., Majumdar, A., Urban, J. J. & Segalman, R. A. Thermoelectric power factor optimization in PEDOT:PSS tellurium nanowire hybrid composites. *Phys Chem Chem Phys* **15**, 4024-4032, doi:10.1039/c3cp44558e (2013).
49 Kim, D., Kim, Y., Choi, K., Grunlan, J. C. & Yu, C. Improved Thermoelectric Behavior of Nanotube-Filled Polymer Composites with Poly(3,4-ethylenedioxythiophene) Poly(styrenesulfonate). *ACS Nano* **4**, 513-523, doi:10.1021/nn9013577 (2010).
50 Yao, Q., Chen, L., Zhang, W., Liufu, S. & Chen, X. Enhanced Thermoelectric Performance of Single-Walled Carbon Nanotubes/Polyaniline Hybrid Nanocomposites. *ACS Nano* **4**, 2445-2451, doi:10.1021/nn1002562 (2010).
51 Zhang, B., Sun, J., Katz, H. E., Fang, F. & Opila, R. L. Promising Thermoelectric Properties of Commercial PEDOT:PSS Materials and Their Bi2Te3Powder Composites. *ACS Applied Materials & Interfaces* **2**, 3170-3178, doi:10.1021/am100654p (2010).
52 Ireland, R. M. *et al.* ZT > 0.1 Electron-Carrying Polymer Thermoelectric Composites with In Situ SnCl2Microstructure Growth. *Advanced Science* **2**, n/a-n/a, doi:10.1002/advs.201500015 (2015).
53 Dorling, B. *et al.* Photoinduced p- to n-type Switching in Thermoelectric Polymer-Carbon Nanotube Composites. *Adv Mater* **28**, 2782-2789, doi:10.1002/adma.201505521 (2016).
54 Wang, H. *et al.* Thermally Driven Large N-Type Voltage Responses from Hybrids of Carbon Nanotubes and Poly(3,4-ethylenedioxythiophene) with Tetrakis(dimethylamino)ethylene. *Adv Mater* **27**, 6855-6861, doi:10.1002/adma.201502950 (2015).

Chapter 2: Structurally-driven enhancement of the thermoelectric properties of PEDOT:Tos thin films.

Preface:

In this chapter the structural properties of PEDOT:Tos thin films are tailored by adding a high boiling point additive to the oxidant formulation. Molecules like Dimethylsulfoxide or Dimethylformamide have a plasticizing effect on the PEDOT chains during the annealing step of the synthesis, resulting in PEDOT:Tos thin films of higher degree of crystallinity with a major population of edge-on oriented crystallites. The Seebeck coefficient of the resulted PEDOT:Tos films was not significantly affected by these treatments. However an important increase of the electrical conductivity was noticed and was correlated to an increase of the hole mobility of the PEDOT:Tos thin films. In order to investigate the effect of the structural modifications to the electronic properties of the material, the product of the relative crystallinity with the edge-on orientation fraction of the films was plotted against the in-plane hole mobility. As a result, a correlation was found between the in-plane mobility and the amount of edge-on crystallites. Thus, these structural modifications leads to an enhancement of the PEDOT:Tos Power Factor from 25 to 78.5 W/mK^2. This chapter transposes the results published in *Scientific Reports* in the article entitled "Structurally driven enhancement of thermoelectric properties within Poly(3,4-ethylenedioxythiophene) thin films".[1]

2.1 Introduction:

Thermoelectric (TE) materials have the potential to convert vast amounts of waste heat directly into electricity, therefore reducing the dependence on fossil fuel.[2] Combined with the rising need for clean energy, efficient thermoelectric materials are a subject of great interest.[3,4] In thermoelectrics, the concept of a phonon glass/electron crystal (PGEC) is often used to describe an ideal thermoelectric material. According to PGEC, a good TE material should inhibit the conduction of phonons (thus having a low thermal conductivity) while efficiently conducting electronic charge carriers. In order to quantify the efficiency of TE systems, the figure of merit, *ZT*, is used as a measure of performance. It is defined as $ZT = S^2\sigma T/\kappa$, where S is the Seebeck coefficient, σ is the electrical conductivity, T is the temperature and κ the thermal conductivity.[2] Materials engineering is offering unprecedented routes towards optimizing *ZT* by tuning the electronic and thermal properties, e.g. by introducing thermal boundaries and/or structural discontinuities at the nanoscale that effectively scatter phonons. Thus, values of *ZT* up to 2.2 have since been achieved with SnSe crystals over the last decade.[5] Alternatively, conducting polymers have recently gained momentum in the TE community for applications at room temperature.[5-8] Their great advantage is an intrinsically low thermal conductivity at room temperature (0.2-0.6 W/mK) that is complemented by their easy processability and their low cost. Thin films of poly(3,4-ethylenedioxythiophene) (PEDOT) derivatives doped with *p*-toluenesulfonate (Tos) molecules can exhibit a *ZT* as high as 0.25 at room temperature,[7] which is only 4 times lower than that of conventional Bi_2Te_3 at room temperature,[3-5] thus underlining the high potential of such systems for future applications.

For a given thermal conductivity, the figure of merit downscales to the Power Factor, $S^2\sigma$, at a constant temperature leading to a valid method of materials comparison. The

electrical conductivity can be further broken down for metals and doped semiconductors using $\sigma = eN\mu$, with N being the carrier concentration, μ the carrier mobility and e the electron charge.[9] For the PEDOT:Tos system, most efforts to optimize the Power Factor have been focused on tuning N.[7,10] Note that S decreases with N, while σ increases at the same time,[7] rendering this optimization quite challenging. An alternative strategy is the enhancement of mobility while maintaining a constant N.

Transport properties of semiconducting polymers are driven by the polymer structure in the active layer.[11-13] For example, higher polymer crystallinity results in higher carrier mobility.[14] Several methodologies have been proposed in the literature for enhancing the degree of crystallinity for semiconducting polymers.[15] As far as the PEDOT-based systems are concerned, it was proved that the addition of dimethylsulfoxide (DMSO) in the dispersion delays the crystallization kinetics of PEDOT, thus resulting in an increased degree of crystallinity and a higher electrical conductivity.[14,16] Several other additives have been studied with respect to poly(3,4-ethylenedioxythiophene):poly(styrene sulfonate) (PEDOT:PSS), like ethylene glycol[5] (EG) and dimethylformamide (DMF).[17] For thermoelectric applications, PEDOT:Tos shows a higher potential since it exhibits a higher Seebeck coefficient with respect to PEDOT:PSS.[6] In this work we present, an thorough study of the effect of several solvent additives on the thermoelectric properties of PEDOT:Tos thin films. The additives were selected based on gradual increase of their boiling point temperatures, T_b. Additives with a high boiling point are expected to reside in the film for longer time during film processing, acting as a plasticizer and promoting crystallization. A comprehensive characterization of these films has been performed, with respect to their thermoelectric, electrical and structural properties.

2.2 Results and discussion: Effect of high boiling point additives on the properties of PEDOT:Tos films

In order to investigate the effect of solvent additives (see **Table 1**) on the thermoelectric properties, the Seebeck coefficient, *S*, was first measured and the results presented in **Figure 1**. The processing of the PEDOT:Tos thin films with these additives was found not to significantly affect the resulting Seebeck coefficients, which has a constant value of 34 ± 5 μV/K. The electrical conductivity was also measured for the various films and, as apparent in **Figure 1**, σ follows a bell-shaped curve with respect to the additive boiling point, exhibiting a maximum value of approximately 640 S/cm for DMF. Since *S* is constant, the Power Factor, $S^2\sigma$, displays a similar bell-shaped trend as the electrical conductivity, with a maximum value at 78.5 μW/mK^2 for DMF.

Additive	Tb (°C)	σ (S/cm)	S (μV/K)	μ(x10^{-4}cm^2/Vs)
No additive (Pristine)	-	230 ± 10	32 ± 5	2.4 ± 0.1
Acetonitrile (ACN)	82	275 ± 10	32 ± 5	-
Toluene (Tol)	110	300 ± 10	33 ± 5	3.2 ± 0.3
Chlorobenzene (CB)	137	310 ± 10	35 ± 5	-
Dimethylformamide (DMF)	153	640 ± 10	35 ± 5	6.6± 0.4
Dimethylsulfoxide (DMSO)	189	605 ± 15	32 ± 5	6.5 ± 0.5
Ethylene Glycol (EG)	197	355 ± 10	32 ± 5	3.6 ± 0.2
Propylene Carbonate (PC)	242	165 ± 10	35 ± 5	-

Table 1. Solvent additives and their respective boiling points, T_b. The electrical conductivity, σ, the Seebeck coefficient, S, and the in-plane moblility, μ, of the corresponding PEDOT:Tos films are also reported.

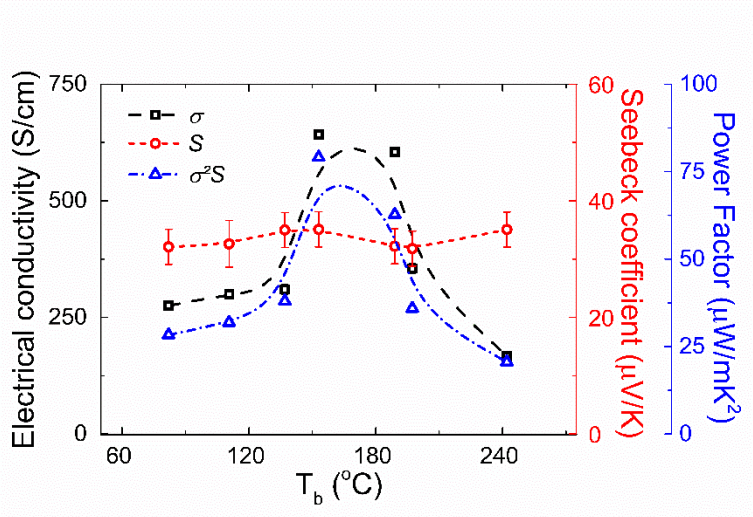

Figure 1. Thermopower data. S, σ, and the corresponding $S^2\sigma$ obtained for PEDOT:Tos thin films prepared with the various Tb additives.

To understand the physical origin of this behavior, the dependence of σ with regards to N and μ has to be examined. In semiconducting polymers like the PEDOT-based ones, N is correlated to the oxidation level, since doping is achieved by oxidizing the polymer chain.[7,18] Oxidized sulfur atoms are subsequently stabilized by the anion of the tosylate counter-ion.[19] Holes act as the charge carrier of the system as proven by the positive Seebeck coefficients. Since σ can be tuned by either tuning N through doping and/or μ, probing the oxidation level of PEDOT:Tos thin films is an indirect way to investigate any modifications of the carrier concentration. X-ray photoelectron spectroscopy was used to determine the oxidation level of each sample. The PEDOT:Tos material has two different sulfur atoms; one in the tosylate counter-ion molecule (S_a) and the other in the thiophene unit (S_b). These two sulfur atoms have different chemical environments, therefore showing two distinct XPS signatures. S_a resides in a highly electronegative environment due to the presence of three surrounding oxygen atoms, yielding a signal measured at higher binding energies (168-170 eV), while the signal at low binding energies (163-166 eV) corresponds to the doublet of S_b.[7,20] XPS spectra for sulfur S(2p) for three PEDOT:Tos distinct samples are presented in **Figure 2**. For clarity

we have chosen to present only the spectra acquired for the pristine PEDOT:Tos film (no additive used) and those treated with toluene and DMF; exhibiting conductivities of 230 S/cm, 300 S/cm and 640 S/cm, respectively. A perfect overlap of the three S(2p) spectra is observed, suggesting that there is no significant change in the oxidation level induced by treatment process. Quantification of the oxidation level was determined *via* the ratio of the S_b doublet area with respect to the S_a doublet area. An oxidation level of 33% was calculated for all PEDOT:Tos thin films, which is in accordance with that previously reported in the literature for PEDOT:Tos.[7] It can therefore be concluded that the carrier concentration, *N*, of the system remains constant throughout. This implies that the measured changes in electrical conductivity are due to the mobility.

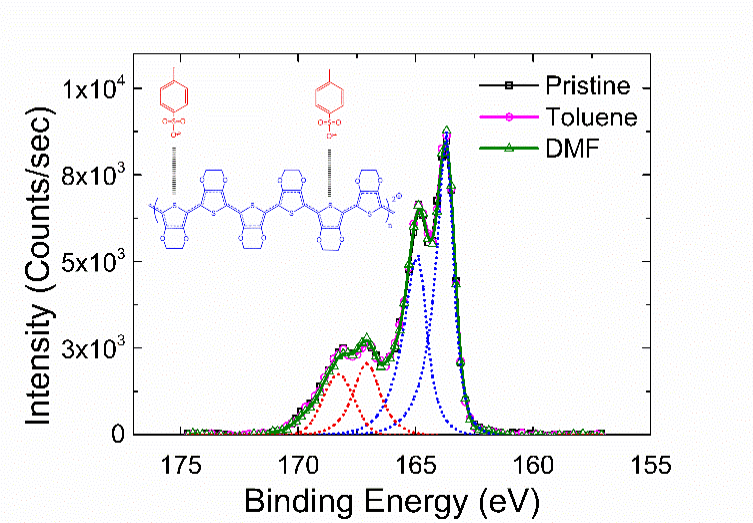

Figure 2. S(2p) XPS spectra of the reference PEDOT:Tos film (black curve) and those treated with toluene (magenta) and DMF (green). The red and blue dashed lines represent the fitted doublets for the Tos and EDOT units, respectively. Inset: chemical structure of PEDOT:Tos.

PEDOT-based polymers are heavily doped semiconductors due to their high carrier density.[14] Therefore, conventional transistors are not appropriate for the determination of the mobility of such polymers owing to the screening of the applied electric field by the charge

carriers. For this reason, electrolyte gated transistors have been proposed in the literature as an alternative for the measurement of transport properties.[14,21,22] These transistors incorporate an ion gel as the dielectric layer, which modifies the density of charge carriers and allows the observation of field effects. The capacitive properties of the gate electrode and the bulk dedoping of the PEDOT system were also taken into consideration for the device fabrication and the calculation of charge carrier mobility.[23-25] Details on device fabrication, measurements of the transistor output characteristics and mobility calculation are provided in **Appendix B**. The output characteristics of the transistors and the conductance versus the gate voltage plot are presented for the pristine and DMF added PEDOT:Tos thin films in **Figure 3 and 4**, respectively.

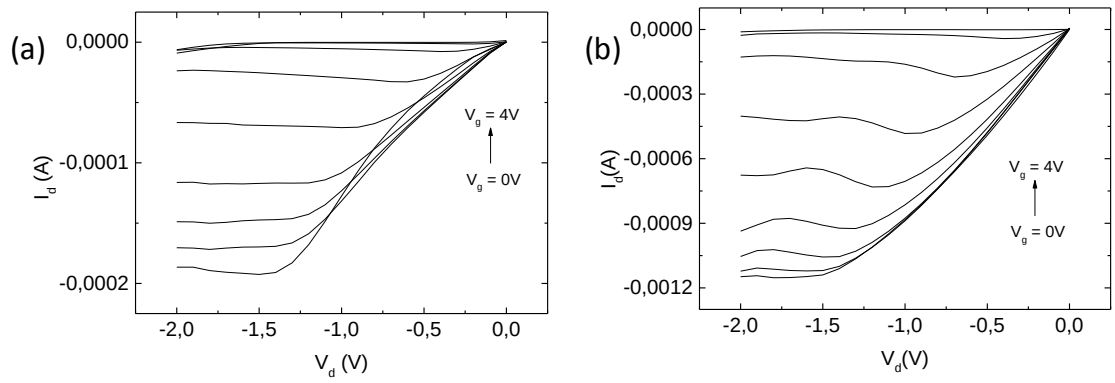

Figure 3. Output characteristics of the transistors. (a) for the pristine and (b) DMF added PEDOT:Tos films.

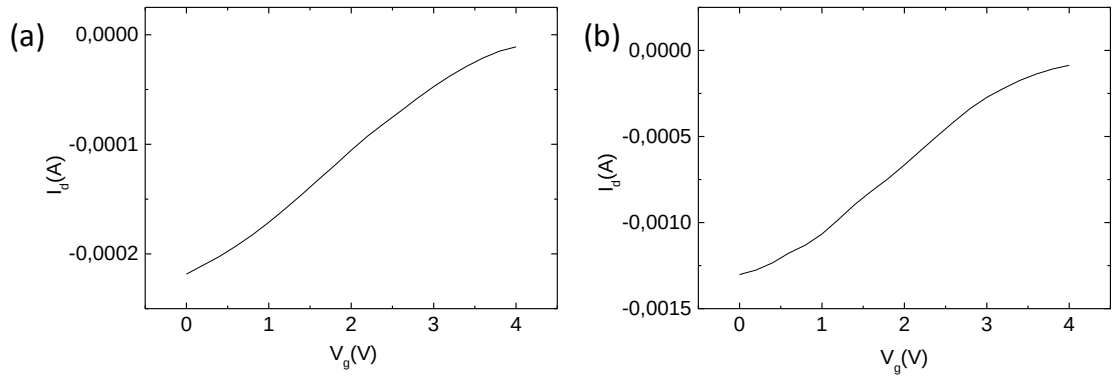

Figure 4. Conductance versus the gate voltage. (a) for the pristine and (b) DMF added PEDOT:Tos films.

The higher drain current for the DMF treated samples in both **Figure 3** and **4** is indicative of a higher charge carrier mobility for that material. The in-plane mobility was retrieved from the transfer characteristics using a capacitance of $7.5 \times 10^{-6} \pm 0.8 \times 10^{-6}$ F for the PEDOT:Tos films obtained from the *I-V* curve (**Figure 5**) at a constant voltage rate of 0.01V/s ($I = C \cdot dV/dt$).

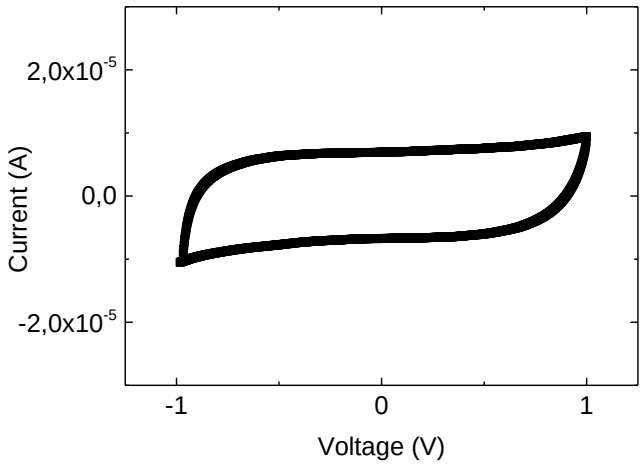

Figure 5: The Current vs Voltage curve for the devices at a voltage rate 0.01V/s. The capacitance o the polymer film is extracted from the two plateaus.

The results of the in-plane mobility of the selected films are summarized in **Table 1**. Logically, the in-plane mobility *versus* the additive boiling point plot (See **Figure 6**) presents a similar bell-shape as the one reported in **Figure 1** for conductivity. This underlines the direct influence of the mobility on the electrical conductivity behavior.

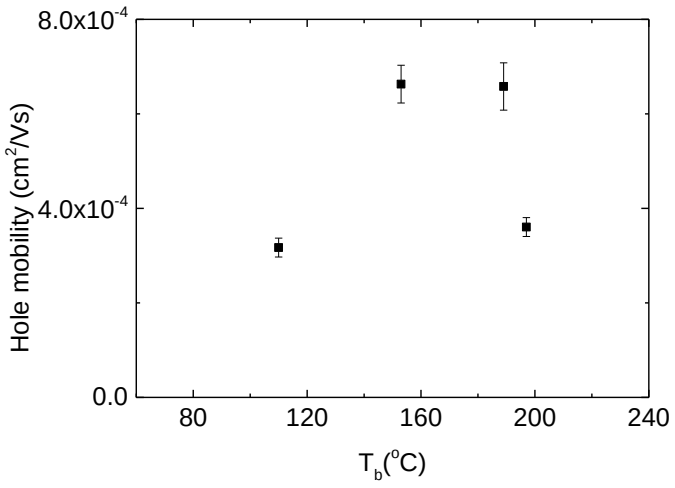

Figure 6. In-plane mobility of the PEDOT:Tos films plotted with respect to the boiling point of the various processed additives.

To further assert the correlation between the measured σ and μ, the electrical conductivity versus the in-plane mobility was plotted in **Figure 7** for the systems under investigation. A linear dependence of the electrical conductivity with respect to hole mobility was observed, which is in accordance with the solid state equation $\sigma = eN\mu$.[9] An estimation of the carrier concentration, *N*, was obtained from the slope of the linear fit. A value of 5.8 x 10^{24} carriers/cm^3, in accordance with those reported in literature for heavily doped semiconductors ($\approx 10^{21}$ - 10^{24} carriers/cm^3), was calculated.[14]

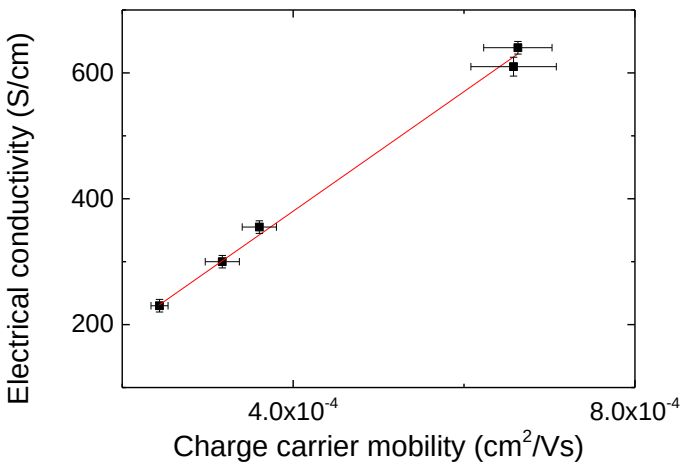

Figure 7. Plot of σ vs. μ for a series of PEDOT:Tos with additives. In accordance with the conductivity expression for doped semiconducting, σ is directly proportional to μ.

Transport properties of organic semiconductors are strongly related to their thin film morphology.[11-13,15,16,26-29] In order to understand the nature of the additive effect on mobility, the structural properties of the PEDOT:Tos thin films were probed by GIWAXS. The (q_r, q_z) 2D scattering pattern recorded for the pristine PEDOT:Tos film as well as those recorded for the toluene-treated and DMF-treated films are presented in **Figure 8a**. We opt to present these data because there is a gradual increase in conductivity, from 230 S/cm for the pristine film, to 300 S/cm for toluene, to 640 S/cm for DMF. Clearly these films scatter anisotropically, with the majority of scattered intensity along the near out-of-plane axis ($q_r \approx 0$), that is, perpendicular to the substrate. This is indicative of preferential orientation of PEDOT crystallites in the film which will be addressed in the next section. In **Figure 8b**, the radially averaged scattered intensity is plotted with respect to the scattering vector q. Note that in all cases, the scattered intensity is presented after normalization for film thickness and background subtraction, to allow for quantitative comparison between samples. For all the PEDOT:Tos thin films, the strong peak at 0.44 $Å^{-1}$ and the following at 0.88 $Å^{-1}$ are attributed

to the (100) and (200) reflections, in accordance to the assignment proposed by Aasmundtveit *et al.*.[30] The resultant repeat distance is 14.28 Å and corresponds to the unit cell length along the *a* axis that is the EDOT direction, perpendicular to the polymer chain axis *c*. A schematic of the unit cell showing the directions of the *a*, *b* and *c* axes is provided in **Figure 9**. A third peak is observed at around 1.3 $Å^{-1}$ that can be assigned to the (300) reflection. However the very low intensity of this peak suggests a limited long-range order along the *a*-axis, indicating a material with paracrystalline distortions. At 1.77 $Å^{-1}$ a broad and intense peak is observed that is assigned to the (020) reflection and corresponds to the π-π stacking direction.[30]

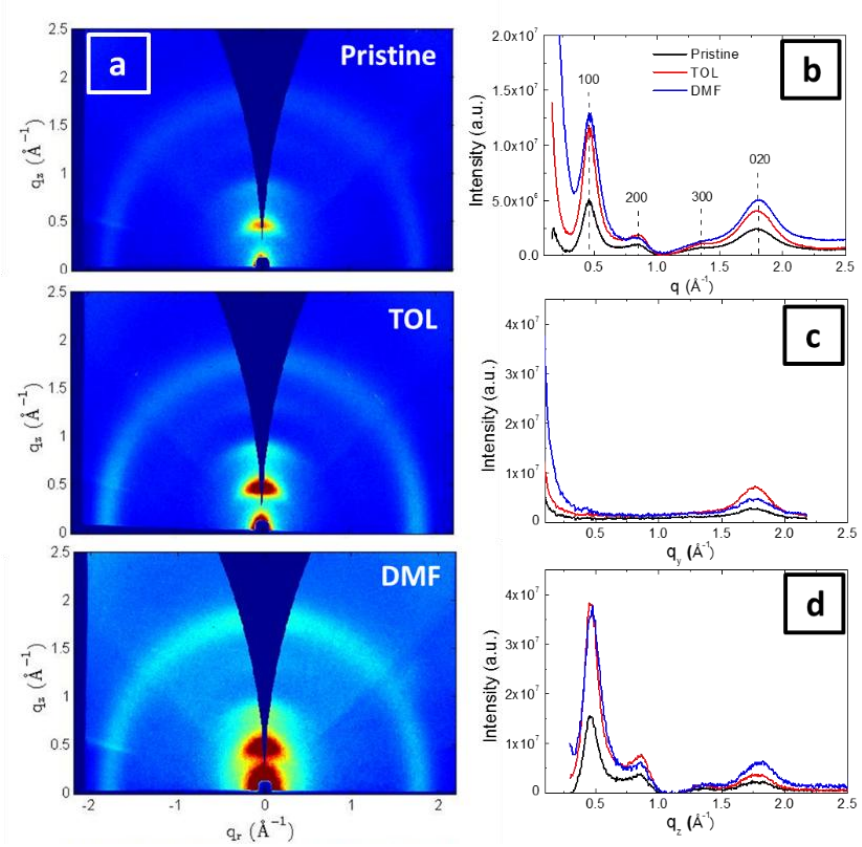

Figure 8. GIWAXS characterization of PEDOT:Tos thin films with additives. (a) 2D GIWAXS images recorded for the pristine PEDOT:Tos and those treated with toluene and DMF. The corresponding 1D scattering patterns: (b) the radially averaged intensity with respect to the scattering vector *q*, (c) the in-plane intensity line-cut and (d) the near out-of-plane intensity line-cut. In all cases the scattering intensity was normalized by film thickness and the substrate scattering was subtracted.

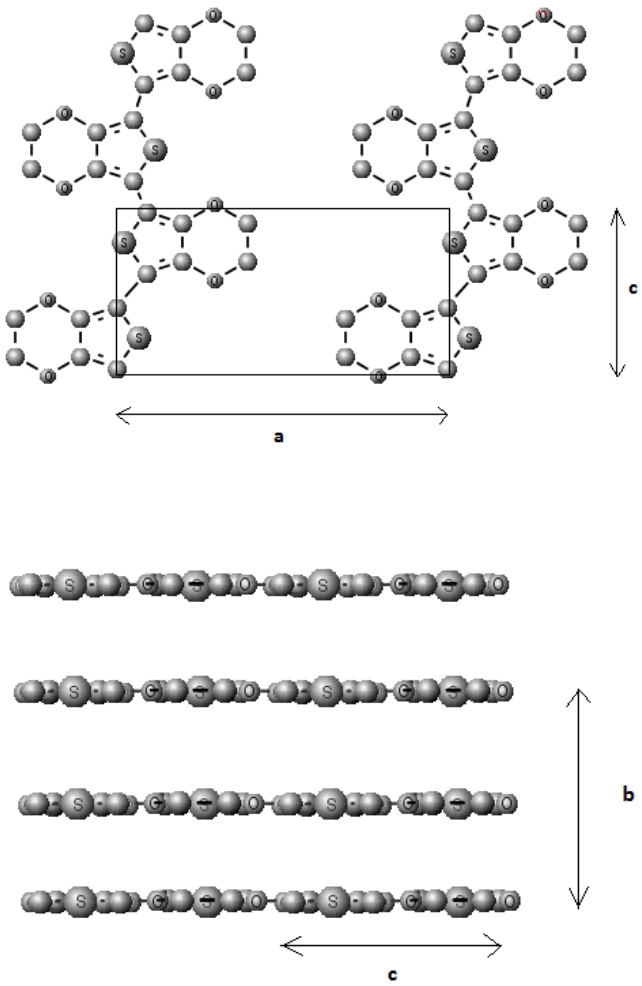

Figure 9. PEDOT:Tos structure with its orthorhombic unit cell (Adapted by Aasmundtveit *et al*.[30]) The *b*-axis is along the substrate. The unit cell dimensions are *a* = 14 Å, *b* = 6.8 Å, *c* = 7.8 Å.

Besides, an increase of the scattered intensity, particularly apparent for the (100) and (020) peaks, was observed when the PEDOT:Tos thin films were processed with the additives. Given the fact that the area below the scattering peaks is indicative of the degree of crystallinity - the higher crystallinity resulting in higher intensities - the pristine PEDOT:Tos film is less crystalline than those prepared with additives. Even if the area of the (100) peaks can lead to a measure of the relative crystallinity, a more rigorous analysis involves the $I(\chi)$ polar plots, χ being the polar angle defined with respect to the normal direction.[31] The area of the $I(\chi)\times sin(\chi)$ *vs* χ plots for the (100) peak (see **Figure 10**) was subsequently used as a

measure of the relative crystallinity considering the PEDOT films as "in-plane powders" (i.e. isotropic in-plane orientation of the crystallites)[31] and the results normalized with respect to the most crystalline sample are presented in **Figure 11**.

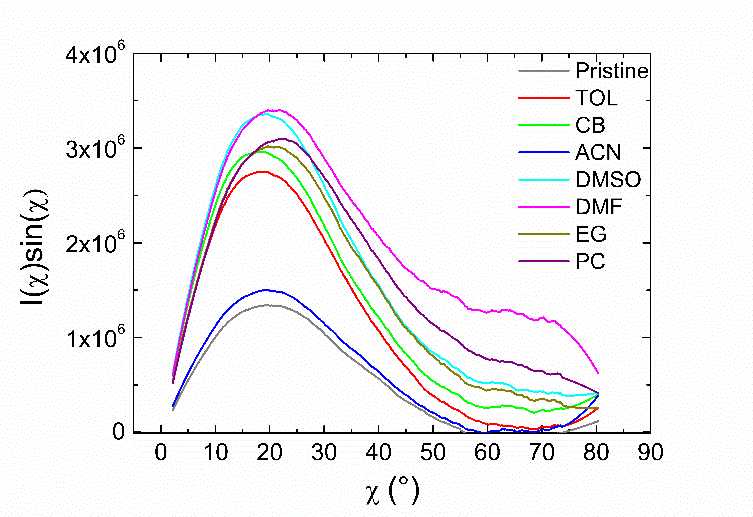

Figure 10. *I(χ)×sin(χ) vs χ* plots for the (100) peak of the various PEDOT:Tos thin films. The area of the *I(χ)•sin(χ) vs χ* plots for the (100) peak was subsequently used as a measure of the relative crystallinity considering the PEDOT films as "in-plane powders" (i.e. isotropic in-plane orientation of the crystallites). Additionally an estimation of the edge-on fraction is possible through this plot. Given that *I(χ)×sin(χ)* plot represents the orientation distribution function of the (100) crystallites and considering that edge-on crystallites are oriented with a *χ* between 0° and 45°, the fraction of edge-on oriented crystallites can be estimated from the ratio between the *I(χ)×sin(χ)* vs *χ* integral from 0° to 45° and the one from 0° to 90°.

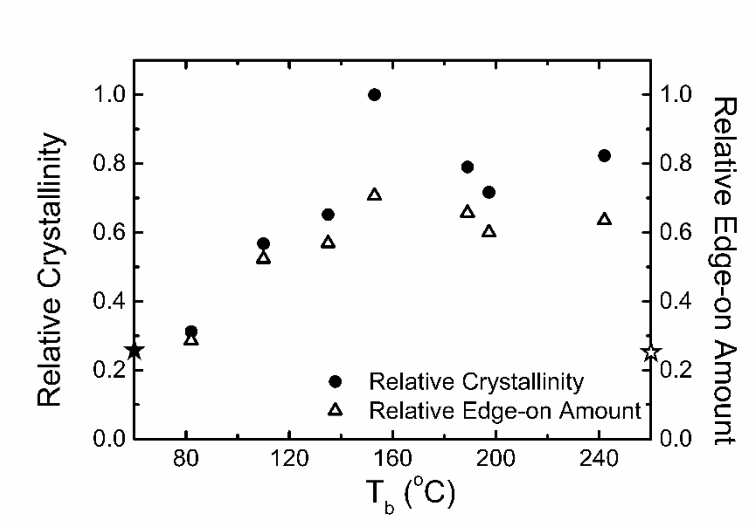

Figure 11. Relative crystallinity and relative amount of edge-on oriented crystallites as a function of the boiling point of the various additives. The star symbols on both axes correspond to the respective data obtained for the pristine PEDOT:Tos films. Crystallinity data were normalized by the value obtained for the most crystalline one.

The relative crystallinity increases with respect to the boiling temperature of the additive until a maximum for DMF followed by a lower plateau for the higher boiling point additives. This behavior supports our initial hypothesis that using additives with various boiling points can favorably alter the crystallization properties of the PEDOT:Tos films. Given that the main solvent of our dispersion (1-butanol) has T_b = 115°C, introducing a higher boiling point additive, such as DMF or DMSO, would slow the evaporation rate of the solvents, delay the crystallization kinetics of the polymer chains and allow further crystallization. These observations are in agreement with other reports in the field of organic electronics.[14,16,28]

In order to examine the anisotropic nature of the 2D images, the in-plane and near out-of-plane line-cuts are presented in **Figure 8c-8d**. In the near out-of-plane pattern ($I(q_z)$ vs q_z, **Figure 8d**), we observe the (h00) group and the (020) reflection, similarly to the $I(q)$ vs q

pattern, while in the in-plane pattern ($I(q_y)$ vs q_y, **Figure 8c**) the (h00) reflections are absent and only the broad (020) reflection at 1.77 $Å^{-1}$ is observed. The absence of the (h00) group from the in-plane pattern allows one to conclude that there is a preferential orientation of the crystallites in the film with respect to the substrate. It further indicates that the PEDOT chains are mainly oriented in an edge-on configuration, *i.e.* the thiophene rings of EDOT are preferentially aligned with their planes normal to the substrate. However crystallites oriented with face-on, *i.e.* with the thiophene ring parallel to the film plane, should still be present, since the (020) peak corresponding to π-π stacking is apparent in both line-cuts. Quantitative information on the crystallite orientation can be extracted from the $I(\chi)\times sin(\chi)$ vs χ plots (see **Figure 10**). In particular the fraction of edge-on oriented crystallites can be estimated from the ratio between the $I(\chi)\times sin(\chi)$ vs χ integral from 0° to 45° and the one from 0° to 90°. For all PEDOT:Tos thin films, the majority of the crystallites (between 0.75 and 0.9) are oriented edge-on which is consistent with the absence of the (100) peak in the in-plane line-cut (**Figure 8c**).

For crystalline semiconducting polymers, both thin film crystallinity[6,12,14] and chain/crystallite orientation[13,27,32] influence the charge transport properties. In order to take into account both parameters, the product between the relative crystallinity with the edge-on fraction was calculated. This product has in fact a physical meaning, as it represents the amount of edge-on crystallites in the PEDOT:Tos thin films. **Figure 11** shows that the relative edge-on amount follows clearly the crystallinity progression. Since relative crystallinity has been taken into account, using this product as a structural parameter allows for direct comparison between different samples. Interestingly, a clear correlation exists between the mobility and the relative amount of edge-on crystallites, as shown in **Figure 12**.

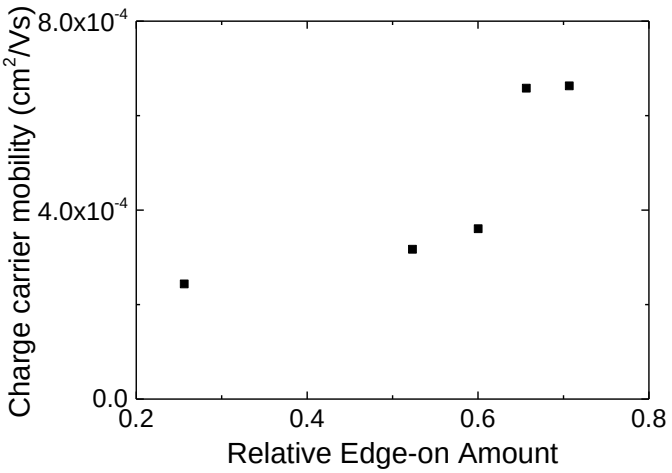

Figure 12. In-plane mobility of the PEDOT:Tos thin films with various high boiling point additives with respect to the amount of edge-on oriented crystallites.

The increase in the in-plane mobility with the quantity of edge-on crystallites is in agreement with the current understanding of efficient charge transport in semiconducting polymers, where the main transport mechanism occurs by hopping between doped conjugated chains.[13] For conducting polymers like PEDOT, it is also accepted that charge transport is anisotropic, and is dictated by the presence of highly conducting crystalline "metallic" islands that are embedded in a less conducting amorphous polymer matrix.[33] Thus, systems with higher crystallinity are expected to exhibit higher mobility and therefore electrical conductivity. Furthermore, it has been shown by Sirringhaus *et al.*[13] and Crossland *et al.*[27] that charge mobility depends on the orientation of the crystalline lamellae of semiconducting polymers with respect to the measurement plane. In fact, reported mobilities of crystalline semiconducting polymers are three times higher along the polymer backbone (*c*-axis) with respect to that measured along the π-π stacking direction (*b*-axis), while that measured along the *a*-axis direction is a hundred times lower than that measured along the *b*-*c* plane. Therefore, in order to achieve high in-plane mobility, an edge-on orientation is necessary,

where the chains are π-stacked along this plane and, thus, interchain and intrachain hopping transport along the backbone are promoted. Thus, a combination of the aforementioned structural parameters (i.e. edge-on orientation and crystallinity) is pivotal for polymer films with high carrier in-plane mobility. This is confirmed with the results displayed in **Figure 12**; the films that contain the highest amounts of edge-on crystallites exhibit the highest mobility. To the best of our knowledge, this study is one of the very few reports regarding a quantitative correlation between transport properties and structural characteristics in polymer semiconductors[11,28] and the only one concerning PEDOT-based materials.

2.3 Conclusion:

High boiling point additives were used as a tool for tuning the structural, electrical and thermoelectric properties of PEDOT:Tos thin films. It was observed that processing PEDOT:Tos with such additives can result in more crystalline films, leading to a threefold maximum increase in conductivity, with respect to the pristine film. The Seebeck coefficient remained unaffected and the Power Factor therefore increases with the electrical conductivity. In order to examine the origin of the improvement, XPS measurements proved that carrier density is not affected, implying that conductivity should be driven solely by mobility changes. Indeed, in-plane mobility measurements confirmed the tight relation with conductivity. Lastly, we demonstrated that the behavior of mobility is dictated by the structural properties of the PEDOT:Tos films, and specifically by the thin film crystallinity combined to the preferential edge-on orientation of the PEDOT crystallites. This study underlines the substantial importance of structural fine-tuning through processing methods. Enhanced charge transport and improved thermoelectric performance are proven by an increase of the Power Factor from 25 to 78.5 $\mu W/mK^2$ and can be readily obtained for PEDOT:Tos thin films following this methodology.

2.4 References:

1 Petsagkourakis, I. *et al.* Structurally-driven Enhancement of Thermoelectric Properties within Poly(3,4-ethylenedioxythiophene) thin Films. *Scientific Reports* **6**, 30501, doi:10.1038/srep30501 (2016)

2 Goldsmid, H. J. *Recent Trends in Thermoelectric Materials, Semiconductors and Semimetals* Vol. 69 (2000).

3 Venkatasubramanian, R., Siivola, E., Colpitts, T. & O'Quinn, B. Thin-film thermoelectric devices with high room-temperature figures of merit. *Nature* **413**, 597-602 (2001).

4 Snyder, G. J. & Toberer, E. S. Complex thermoelectric materials. *Nat Mater* **7**, 105-114 (2008).

5 Zhao, L. D. Ultrahigh power factor and thermoelectric performance in hole-doped single-crystal SnSe. *Science* **351**, 141-144 (2016).

6 Bubnova, O. *et al.* Semi-metallic polymers. *Nat Mater* **13**, 190-194, doi:10.1038/nmat3824 (2014).

7 Bubnova, O. *et al.* Optimization of the thermoelectric figure of merit in the conducting polymer poly(3,4-ethylenedioxythiophene). *Nat Mater* **10**, 429-433, doi:10.1038/nmat3012 (2011).

8 Weathers, A. *et al.* Significant electronic thermal transport in the conducting polymer poly(3,4-ethylenedioxythiophene). *Adv Mater* **27**, 2101-2106, doi:10.1002/adma.201404738 (2015).

9 Charles, K. *Introduction to Solid State Physics*. 7 edn, (Wiley, 1995).

10 Khan, Z. U. *et al.* Acido-basic control of the thermoelectric properties of poly(3,4-ethylenedioxythiophene)tosylate (PEDOT-Tos) thin films. *J. Mater. Chem. C* **3**, 10616-10623, doi:10.1039/c5tc01952d (2015).

11 Woo, C. H., Piliego, C., Holcombe, T. W., Toney, M. F. & Fréchet, J. M. J. A Quantitative Correlation between the Mobility and Crystallinity of Photo-Cross-Linkable P3HT. *Macromolecules* **45**, 3057-3062, doi:10.1021/ma202203z (2012).

12 Goh, C., Kline, R. J., McGehee, M. D., Kadnikova, E. N. & Fréchet, J. M. J. Molecular-weight-dependent mobilities in regioregular poly(3-hexyl-thiophene) diodes. *Applied Physics Letters* **86**, 122110, doi:10.1063/1.1891301 (2005).

13 Sirringhaus, H. *et al.* Two-dimensional charge transport in self-organized, high-mobility conjugated polymers. *Nature* **401**, 685-688 (1999).

14 Wei, Q., Mukaida, M., Naitoh, Y. & Ishida, T. Morphological change and mobility enhancement in PEDOT:PSS by adding co-solvents. *Adv Mater* **25**, 2831-2836, doi:10.1002/adma.201205158 (2013).

15 Rogers, J. T., Schmidt, K., Toney, M. F., Bazan, G. C. & Kramer, E. J. Time-resolved structural evolution of additive-processed bulk heterojunction solar cells. *J Am Chem Soc* **134**, 2884-2887, doi:10.1021/ja2104747 (2012).

16 Palumbiny, C. M. *et al.* The Crystallization of PEDOT:PSS Polymeric Electrodes Probed In Situ during Printing. *Adv Mater* **27**, 3391-3397, doi:10.1002/adma.201500315 (2015).

17 Ouyang, J. "Secondary doping" methods to significantly enhance the conductivity of PEDOT:PSS for its application as transparent electrode of optoelectronic devices. *Displays* **34**, 423-436, doi:10.1016/j.displa.2013.08.007 (2013).

18 Bubnova, O. & Crispin, X. Towards polymer-based organic thermoelectric generators. *Energy & Environmental Science* **5**, 9345, doi:10.1039/c2ee22777k (2012).

19 Groenendaal, L., Jonas, F., Freitag, D., Pielartzik, H. & Reynolds, J. R. Poly(3,4-ethylenedioxythiophene) and Its Derivatives: Past, Present, and Future. *Advanced Materials*

12, 481-494, doi:10.1002/(SICI)1521-4095(200004)12:7<481::AID-ADMA481>3.0.CO;2-C (2000).

20 K.Z. Xing , M. F., X.W. Chen , O. Inganas, W.R. Salaneck The electronic structure of poly(3,4-ethylene-dioxythiophene)": studied by XPS and UPS. *Synthetic metals* **89**, 161-165 (1997).

21 Massonnet, N., Carella, A., de Geyer, A., Faure-Vincent, J. & Simonato, J.-P. Metallic behaviour of acid doped highly conductive polymers. *Chem. Sci.* **6**, 412-417, doi:10.1039/c4sc02463j (2015).

22 Zhang, K. *et al.* Effect of host-mobility dependent carrier scattering on thermoelectric power factors of polymer composites. *Nano Energy* **19**, 128-137, doi:10.1016/j.nanoen.2015.11.005 (2016).

23 Andersson, P., Forchheimer, R., Tehrani, P. & Berggren, M. Printable All-Organic Electrochromic Active-Matrix Displays. *Advanced Functional Materials* **17**, 3074-3082, doi:10.1002/adfm.200601241 (2007).

24 Herlogsson, L., Crispin, X., Tierney, S. & Berggren, M. Polyelectrolyte-Gated Organic Complementary Circuits Operating at Low Power and Voltage. *Advanced Materials* **23**, 4684-4689, doi:10.1002/adma.201101757 (2011).

25 Larsson, O., Laiho, A., Schmickler, W., Berggren, M. & Crispin, X. Controlling the Dimensionality of Charge Transport in an Organic Electrochemical Transistor by Capacitive Coupling. *Advanced Materials* **23**, 4764-4769, doi:10.1002/adma.201103131 (2011).

26 Deribew, D. *et al.* Crystallization-Driven Enhancement in Photovoltaic Performance through Block Copolymer Incorporation into P3HT:PCBM Blends. *Macromolecules* **46**, 3015-3024, doi:10.1021/ma302128h (2013).

27 Crossland, E. J. W. *et al.* Anisotropic Charge Transport in Spherulitic Poly(3-hexylthiophene) Films. *Advanced Materials* **24**, 839-844, doi:10.1002/adma.201104284 (2012).

28 Boudouris, B. W. *et al.* Real-Time Observation of Poly(3-alkylthiophene) Crystallization and Correlation with Transient Optoelectronic Properties. *Macromolecules* **44**, 6653-6658, doi:10.1021/ma201316a (2011).

29 Shen, X., Duzhko, V. V. & Russell, T. P. A Study on the Correlation Between Structure and Hole Transport in Semi-Crystalline Regioregular P3HT. *Advanced Energy Materials* **3**, 263-270, doi:10.1002/aenm.201200509 (2013).

30 Aasmundtveit, K. E. *et al.* Structure of thin films of poly(3,4-ethylenedioxythiophene). *Synthetic Metals* **101**, 561-564, doi:http://dx.doi.org/10.1016/S0379-6779(98)00315-4 (1999).

31 Rivnay, J., Mannsfeld, S. C. B., Miller, C. E., Salleo, A. & Toney, M. F. Quantitative Determination of Organic Semiconductor Microstructure from the Molecular to Device Scale. *Chemical Reviews* **112**, 5488-5519, doi:10.1021/cr3001109 (2012).

32 Jimison, L. H., Toney, M. F., McCulloch, I., Heeney, M. & Salleo, A. Charge-Transport Anisotropy Due to Grain Boundaries in Directionally Crystallized Thin Films of Regioregular Poly(3-hexylthiophene). *Advanced Materials* **21**, 1568-1572, doi:10.1002/adma.200802722 (2009).

33 Kaiser, A. B. & Skakalova, V. Electronic conduction in polymers, carbon nanotubes and graphene. *Chem Soc Rev* **40**, 3786-3801, doi:10.1039/c0cs00103a (2011).

Chapter 3: Formulation and Structural engineering of PEDOT:Tos thins films for efficient thermoelectric material.

Preface:

As a follow-up to the previous chapter, an alternative way is proposed in order to enhance the thin film crystallinity and electronic/thermoelectric properties of the PEDOT:Tos material. The synergy between organic bases and plasticizers added in PEDOT formulations is examined as a novel engineering route to further improve the thermoelectric properties of PEDOT:Tos thin films. The methodology lies on the control of the polymerization kinetics achieved by introducing organic bases that complements the control of crystallinity induced by plasticizers. The crystallographic and electronic structure optimization leads to enhanced thermoelectric properties with respect to the pristine films.

3.1 Introduction:

Organic thermoelectric materials based on poly(3,4-ethylenedioxythiophene) (PEDOT) conducting derivatives appear as a promising alternative for the development of low-cost printed thermo-generators for near room temperature applications. As opposed to their inorganic counterparts, conducting polymers exhibit several advantages such as solution processability, material abundance and an inherent low thermal conductivity.[1,2] The energy conversion efficiency for thermoelectric materials can be defined using the figure of merit, $ZT = (S^2\sigma T)/\kappa$, where S is the Seebeck coefficient, σ, the electrical conductivity, and κ the thermal conductivity at a given temperature T.[2] The optimization of the thermoelectric properties for such materials mainly focuses on the improvement of the Power Factor, $S^2\sigma$, as their low and mostly constant thermal conductivity (0.2-0.4 W/mK) already constitutes a strong asset.[1,3-5] As the Seebeck coefficient and electrical conductivity follow an antagonistic behaviour with respect to the carrier concentration of the system, a proper tuning of the PEDOT doping level was shown to be crucial for enhanced thermoelectric properties.[2,3] Alternatively, a suitable engineering of the PEDOT crystalline structure was demonstrated to be highly beneficial to the thermoelectric efficiency due to a noticeable increase of the charge carrier mobility.[6] Additional effects of the structural optimization on the thermoelectric properties can be retrieved by examining the electronic band structure of the material, notably the Fermi level position as well as the shape and filling of the density of states (DoS).[4,7] In particular, the Seebeck coefficient, S, is proportional to the DoS slope at the Fermi position in Mott's formalism – i.e. a steeper slope leading to a higher Seebeck coefficient.[8] Thus an appropriate tailoring of the DoS is essential for improved thermoelectric properties. Enhancing PEDOT crystallinity has been shown to strongly affect the electronic structure of PEDOT derivatives, by assisting carrier delocalization along the conjugation axis as well as by improving the π-orbital overlapping along the π-stacking direction.[9-11] As a consequence, the electronic

transition from a Fermi glass to a semi-metallic behaviour has been reported for PEDOT:Tos and the corresponding electronic structure was referred as a bipolaron network band structure by Crispin and co-workers.[4] Both electrical conductivity and Seebeck coefficient were positively affected by this band structure modification.

The crystallinity of semi-conducting polymer thin films is strongly dependent on the synthetic and processing parameters.[12-15] For instance, the addition of Dimethylsulfoxide (DMSO) or Ethylene Glycol (EG) in PEDOT formulations results in thin films of higher crystallinity.[6,14,16] It is commonly accepted that these additives act as plasticizers for the PEDOT chains during the in-situ polymerization leading to enhanced crystallinity as confirmed by grazing incidence X-ray scattering experiments.[6] Increasing the conjugated polymer molecular weight is a second lever which can lead to enhanced crystallinity,[17-19] and, as a result, to improved electronic properties.[20,21] Consequently the control of the oxidative PEDOT polymerization is essential for optimal electronic and structural properties as the release of free protons during the process induces an acceleration of the polymerization kinetics which is detrimental for chain length control.[22] The introduction of organic bases in the PEDOT formulations, such as pyridine or imidazole, limits this auto-catalyzed mechanism leading to higher molecular weight PEDOT chains with larger orbital delocalization.[21,23]

Recently, the optimization of the Power Factor of in-situ polymerized PEDOT:Tos thin films, where Tos is the doping p-toluenesulfonate counter-anion, was reported by using DMSO or dimethylformamide (DMF) as additives.[6] This processing methodology leads to an increase of the thin film crystallinity, which translates into enhanced electrical conductivity and carrier mobility at a constant carrier concentration. Interestingly the Seebeck coefficient was not significantly affected by the introduction of additives. In this report, the synergy between organic bases and plasticizers added in the EDOT formulations is examined as a novel engineering route to further improve the thermoelectric properties. The methodology

we propose herein lies on the control of the polymerization kinetics achieved by introducing organic bases that complements the beneficial effect of plasticizers on the crystallinity. The structural, electronic and thermoelectric properties are affected in a way that a 10-fold increase of the thermoelectric power with respect to pristine films is achieved.

3.2 Results and Discussion: Proton scavenging additives for the tuning of thermoelectric properties of PEDOT:Tos

The thermoelectric properties of PEDOT:Tos thin films were enhanced via tuning the polymerization kinetics and crystallisation degree. PEDOT:Tos thin films were prepared by thermally activated in-situ solution oxidative polymerization of EDOT monomers in the presence of $Fe(Tos)_3$.[6,24,25] By adding an organic base to the EDOT/$Fe(Tos)_3$ formulation, the polymerization process was retarded resulting in higher molecular weight polymer chains.[21,23-25] Polymerization kinetics were followed by UV-Vis spectroscopy in formulations with and without pyridine (Pyr), respectively. Throughout the polymerization, similar shaped absorbance curves were recorded and **Figure 1** highlights the influence of the organic base on the kinetics by plotting the absorbance at 1600 nm (corresponding to the bipolaron signature) versus the polymerization time.

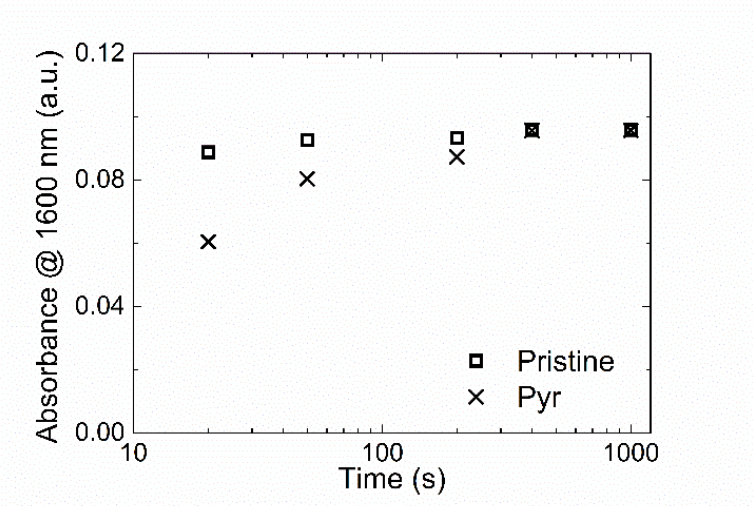

Figure 1: Absorbance at 1600 nm versus polymerization time for the pristine and the pyridine formulations.

For the pristine formulation, the bipolaron shoulder developed quickly and remained almost constant for polymerization time higher than 20 s. This is a clear indication of a fast polymerization process originated from the oxidative polymerization mechanism.[24,25] As opposed, the polymerization is retarded in the presence of pyridine as the asymptotic behaviour related to the maximum conversion of the EDOT monomers is only observed after 200 s. The reaction rate of the oxidative EDOT polymerization (see **Equation 1**) can be expressed by taking into account the rate-determining oxidation by Fe(III) of EDOT to the EDOT radical cation including a second term inherent to the accelerating influence of protons:[24]

$$r = k_1 C_{EDOT}^2 C_{Fe(III)}^2 + k_2 C_{H^+} C_{EDOT} C_{Fe(III)} \quad (1)$$

where r is the reaction rate, k_1 and k_2 the rate constants for the oxidation of EDOT by the catalyst and the accelerating influence of protons, respectively, and C_x the concentration of the different species.

Accordingly capture of protons by an organic base during the polymerization[22,24] or formation of complexes between the organic base and the iron catalyst[21] can result in a severe reduction of the polymerization rate. Those effects lead to the production of higher molecular weight PEDOT chains as already reported in literature.[23]

For conjugated polymers, the electronic properties are improved for chains with larger π-orbital delocalization.[18,26] Hole mobilities of the different systems were subsequently determined by fabricating electrolyte-gated transistors which allow us to retrieve the hole mobility of such highly doped systems.[27,28] The capacitive effect of the gate electrode and the dedoping of the PEDOT:Tos films in the bulk channel of the transistor (instead of the surface

monolayer) that might lead into over-estimation of the charge carrier mobility were taken into consideration for the device fabrication.[29,30] **Figure 2** shows the current-voltage characteristics as well as the transconductance versus gate voltage for the systems under study. The different transistor output characteristics are consistent with the ones reported for high mobility PEDOT materials.[27,2831,32]

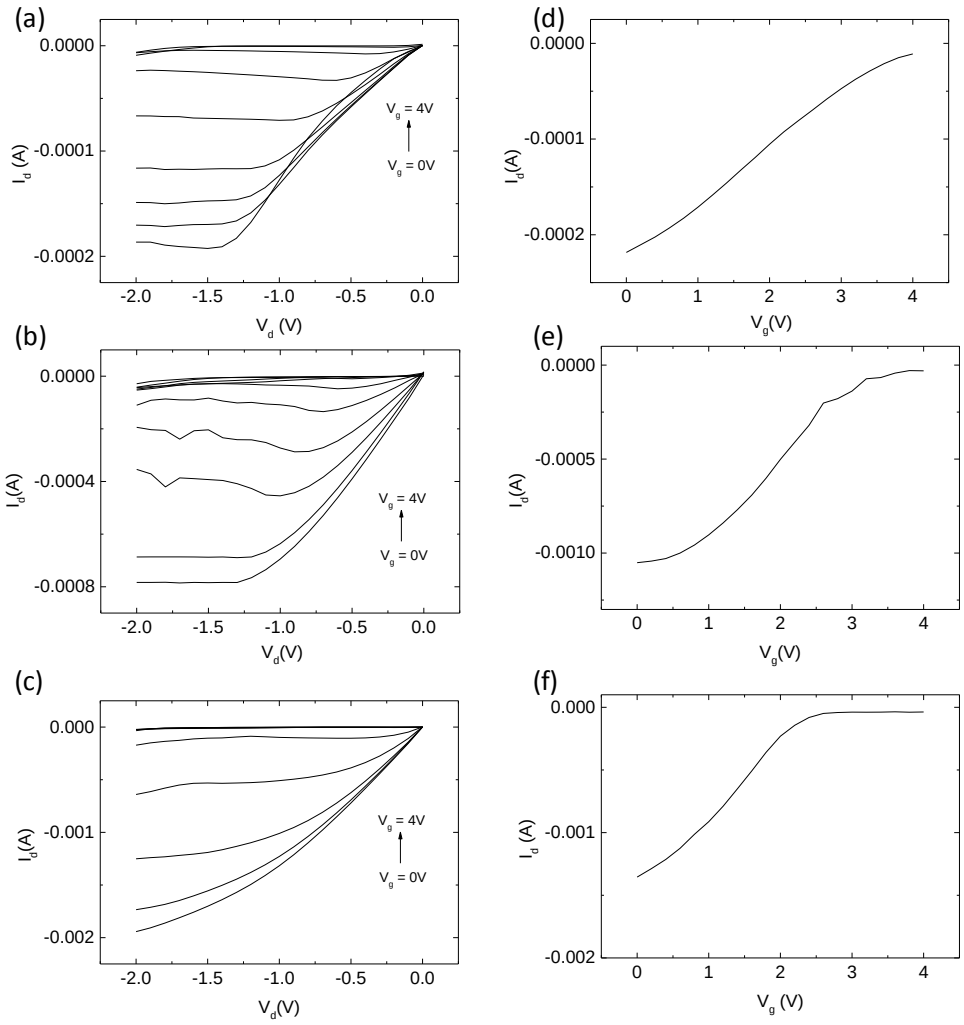

Figure 2: Output characteristics of the electrolyte-gated transistors and transfer curves (a, d) for the pristine, (b, e) Pyr formulated, (c, f) Pyr/DMSO formulated PEDOT:Tos films, respectively. The transfer curves were recorded for a Vd=2V.

The treatment with pyridine results in higher drain current, I_d (**Figure 2b**), in the output characteristics, while the transistors turn "off" faster; a feature evident in both the

output and transfer curves of the materials (**Figures 2a-2b, 2d-2e**). This characteristics are consistent with a higher charge carrier mobility for the pyridine treated PEDOT:Tos films. The mobility values were retrieved from the analysis of the transfer curves (see **Table 1** and calculation details in **Appendix B**). It is noteworthy that the treatment with pyridine induces a two fold increase of the mobility value which is coherent with larger π-orbital delocalization of PEDOT:Tos chains, subsequently leading to improved charge transport characteristics.[18] We further examined both systems by measuring the electrical conductivity and Seebeck coefficient in thin film configuration. The results are presented in **Table 1** and a drastic enhancement of the electrical conductivity was observed for the PEDOT film prepared from the formulation with pyridine.

Samples	σ (S/cm)	S (μV/K)	$S^2\sigma$ (μW/mK^2)	μ x10^{-4}(cm^2/Vs)
Pristine PEDOT	230 ± 10	33 ± 5	25 ± 8	2.4 ± 0.1
Pyr PEDOT	580 ± 20	40 ± 2	96 ± 12	6.9 ± 0.3
(Pyr/DMSO) PEDOT	1222 ± 32	44 ± 2	237 ± 27	12.4 ± 1.0

Table 1: Electrical, electronic and thermoelectric properties of the PEDOT:Tos films

As the oxidation level probed by XPS spectroscopy (**Figure 3**) is constant for the PEDOT:Tos films under study, this increase is directly related to the increase of charge carrier mobility (a carrier concentration of 5.8x10^{24} carriers/cm^3 was obtained from the slope of σ versus μ plot for the various films). PEDOT films prepared from the pyridine formulation also presented a mild enhancement of the Seebeck coefficient resulting on an overall 4-fold increase of the Power Factor, $S^2\sigma$.

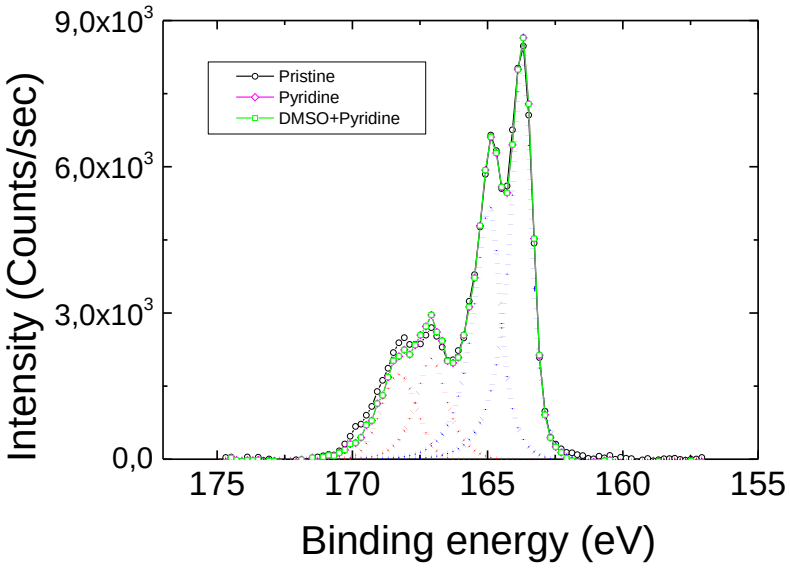

Figure 3: S(2p) XPS spectra of the reference PEDOT:Tos film (black curve) and those treated with pyridine (magenta) and Pyridine+DMSO (green). The red and blue dashed lines represent the fitted doublets for the Tos and EDOT units, respectively.

As exposed in the previous chapter, the introduction of DMSO allows an overall increase of crystallinity as well as an improvement of the thermoelectric properties for PEDOT:Tos thin films;[6] an evident follow-up consists to combine DMSO and pyridine in the same formulation in order to achieve a synergetic effect on the final thermoelectric properties. Such a synergy was indeed observed as both the electrical conductivity and the Seebeck coefficient increase with regards to the pristine material (from σ = 230 to σ = 1222 S/cm and from S = 33 to S = 44 µV/K) resulting to a Power Factor of 237 $\mu W.m^{-1}.K^{-2}$ without any modification of the oxidation level (i.e. 33% for all the PEDOT:Tos thin films under study, see **Figure 3**). This optimized value stems from an improved hole mobility (μ = $12.4x10^{-4} \pm 10^{-4}$ $cm^2.V^{-1}.s^{-1}$) as evidenced by the output and transfer characteristics of the electrolyte-gated transistors presented in **Figure 2c-2f**.

As transport properties of polymer semiconductors are strongly related to morphological features,[6,12,15,33,34] GIWAXS experiments were performed to elucidate the structural origin of the enhanced electronic and thermoelectric properties. The 2D scattering patterns for the various films are presented in **Figure 4** after being corrected for the flat field, polarization, solid angle and efficiency. They have also been normalized by the incident photon flux, the acquisition time (30 s) and the scattering volume, in order to allow for direct comparison between samples. A clear anisotropic signature can be observed on the patterns. As the majority of the scattered intensity is along the near out-of-plane q_z axis, a preferential orientation of the PEDOT crystallites perpendicular to the substrate is retrieved for all PEDOT thin films.[35] Additionally a large increase of the scattered intensity is apparent for PEDOT thin films prepared from the Pyr and Pyr/DMSO formulations. The radially averaged scattered intensity profiles, plotted in **Figure 4d**, are coherent with the PEDOT:Tos orthorhombic crystalline structure reported by Aasmundtveit *et al* and presented in Chapter 2.[35] Indeed three reflections that correspond to the (h00) peak family (q_{h00} = 0.44, 0.88, 1.3 Å) as well as a broader (020) peak at 1.77 Å are apparent. No modification of the unit cell related to the different formulations was observed. Furthermore the radially averaged scattered intensity depicted in **Figure 4d** allow us to relate the film crystallinity to the formulation process by comparing the area of the (100) peak. A gradual increase of crystallinity is evident from the pristine sample to the Pyr/DMSO sample.

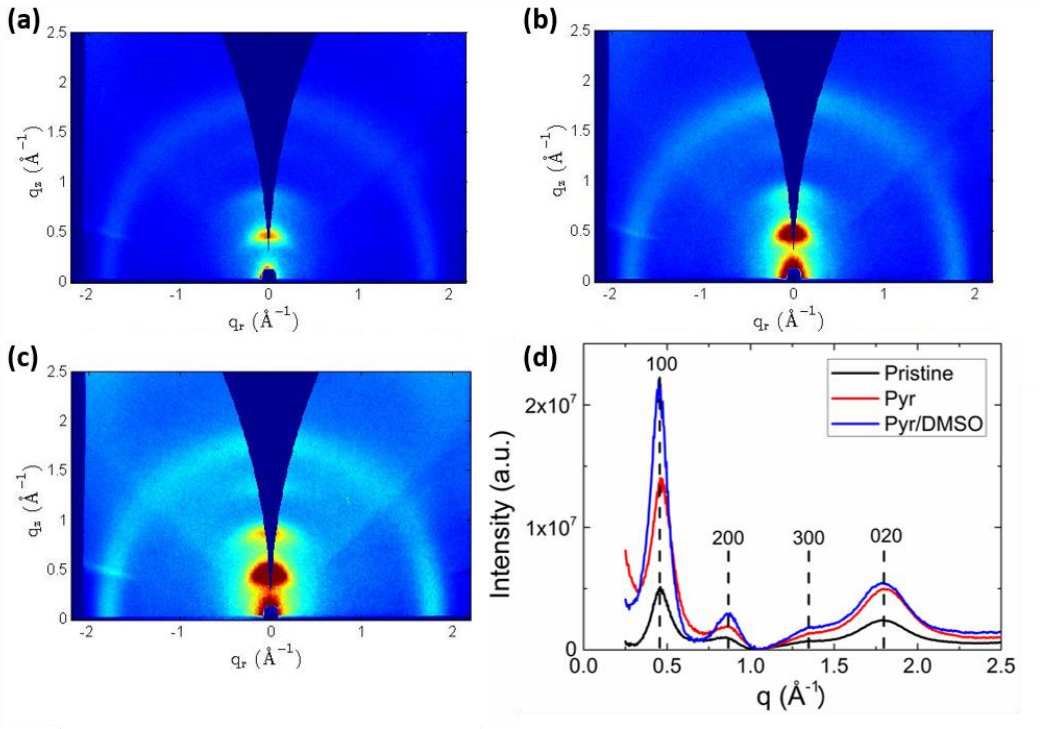

Figure 4: (a, b, c) The GIWAXS patterns for the pristine, Pyr and Pyr/DMSO formulated PEDOT:Tos films, (d) the radially averaged intensity plotted against the scattering vector *q*.

The addition of DMSO to PEDOT formulations was already shown to increase the crystallinity of PEDOT:Tos thin film due to a plasticization effect during the evaporation of the solvents.[6,14] Nevertheless the introduction of pyridine in the PEDOT formulation is acting on a different level; this increase of crystallinity is most probably related to the lower EDOT polymerization rate associated with the formation of higher molecular weight chains[19] (Note that pyridine is expected to evaporate concurrently to 1-butanol that is the main solvent of the formulation, due to their similar boiling points). Combining pyridine and DMSO leads to PEDOT:Tos thin films with the highest crystallinity as a synergetic effect occurs between the two additives.

According to the formalism developed by Crispin and co-workers,[4] the Seebeck coefficient of semi-crystalline π-conjugated materials benefits from an asymmetry of the DoS

near the Fermi level. For π-conjugated systems, this asymmetry can be achieved by proper doping, leading to bipolaron bands extending the valence and conduction bands. This asymmetry can be further assisted by the delocalization of the charge carriers to ultimately generate a bipolaron network. From a structural point of view, a higher charge carrier delocalization can originate from both a longer conjugation length of the doped chains and from an increased structural order.[1,4] In both cases, overlapping of the π-orbitals into a widened π-system is promoted leading to an asymmetry in the DoS. This can be true for polymers that exhibit a high crystallization degree and/or highly doped chains,[4] as it is the case for the highly crystalline PEDOT films under study.

Ultra-violet Photoelectron Spectroscopy (UPS) measurements were performed on the different PEDOT materials to enlighten their electronic structure and relate it to the enhanced electrical and thermoelectric properties observed upon the addition of pyridine and DMSO in the formulation. The normalized UPS spectra are presented in **Figure 5a** and are in accordance with previously reported PEDOT:Tos spectra.[4,36,37] The distinct signatures observed at 15.8, 9.5 and 6.1 eV correspond to the inelastic electron scattering at the film surface and σ states, respectively.[36] **Figure 5b** presents a magnified view at the lower binding energies, at which the band edge corresponding to deeper π-orbitals is localized. A broadening of the band edge is evident for the synergetic PEDOT:Tos sample which is related to a higher delocalization of the charge carriers in these deeper π-orbitals.[38,39] A similar broadening should extend to all π-bands (including the ones near the Fermi position) which would result in a more asymmetric DoS at the Fermi level.[38,39] This is further translated into an increase of the Seebeck coefficient for the Pyr/DMSO PEDOT:Tos material since the DoS slope is proportional to *S* through the Mott formula.[4]

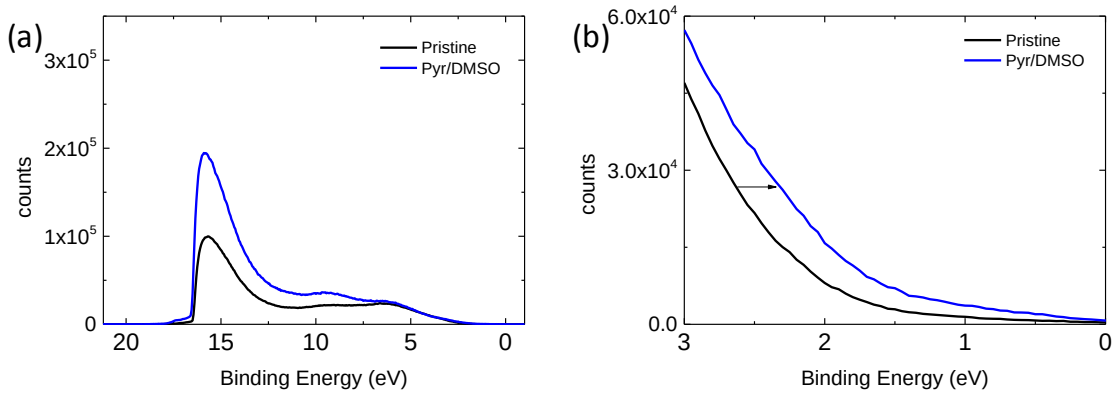

Figure 5: (a) UPS spectra of the pristine and Pyr/DMSO PEDOT:Tos thin films as well as (b) a magnified view of their respective band edge in the low binding energy region.

This extended overlapping of the π orbitals retrieved from the UPS analysis and intrinsic of the increased thin film crystallinity, is also beneficial for the electrical conductivity of the polymer film.[4] In conducting polymers, the main charge transport mechanism is hopping transport of the charge carriers between low-energy "metallic" islands inside the amorphous polymer matrix.[40] From an electronic point of view, these areas can be considered as the overlapping π orbitals of the crystalline doped conjugated chains.[41] Hence, the hopping of the carriers along these regions is assisted by decreasing the structural disorder of the PEDOT:Tos thin films. This macroscopically results in higher carrier mobility and thus higher σ, as observed for the Pyr/DMSO thin films (see **Table 1**).

With this structural engineering the thermoelectric Power Factor of the PEDOT:Tos was increased one order of magnitude from 25 to 237 μW/mK^2, with a constant oxidation level of 33%. An alternative strategy for the optimization of the thermoelectric Power Factor is the tuning of the doping levels of the material.[3] The Seebeck coefficient and the electrical conductivity follow an antagonistic behavior with respect to the oxidation levels of the material.[3] However, through proper tuning of the doping levels, the Power Factor can reach an

optimum value for the material. Bubnova *et al* reported an optimization of the PF of PEDOT:Tos by reducing the material with Tetrakisdimethylamino ethylene (TDAE) vapors.[3] Alternatively, Park *et al* used cyclic voltammetry in order to reduce the PEDOT:Tos and optimize its thermoelectric properties.[42] Electrochemical techniques like cyclic voltammetry or chronocoulometry can provide a quantitative and precise control of the oxidation levels of the polymer material.[42] Consequently, chronocoulometry was used for a rigorous control of the material redox state. By using chronocoulometry, charges are injected into the material at a constant voltage over a fixed time, allowing a controlled reduction of the system.[43]

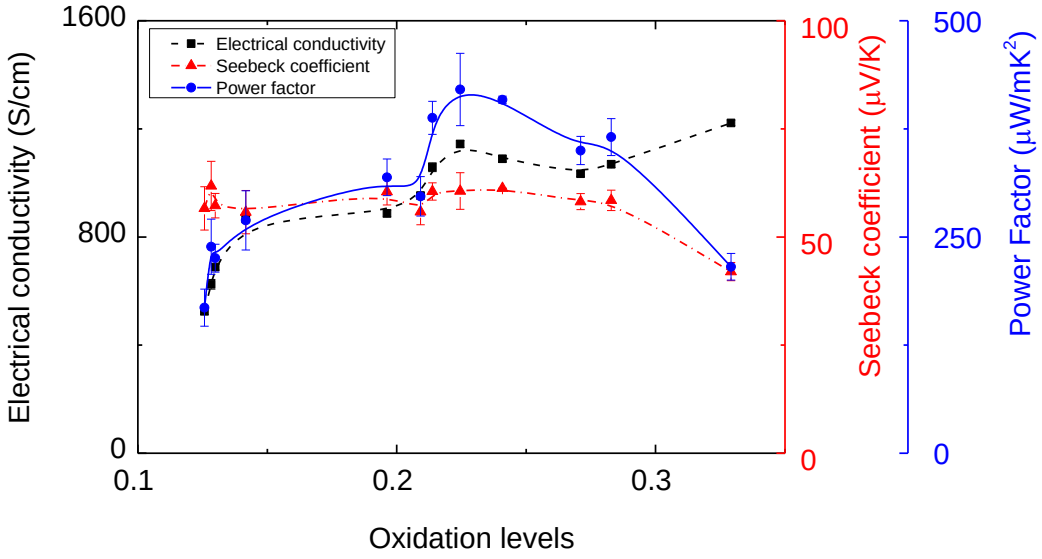

Figure 6: The electrical conductivity, Seebeck coefficient and Power Factor plotted against the oxidation levels of the PEDOT:Tos films.

In **Figure 6** are presented the electrical conductivity, Seebeck coefficient and Power Factor against the oxidation levels for the PEDOT:Tos (Pyr/DMSO) films. Electrical conductivity and Seebeck coefficient are following the expected antagonistic behavior with respect to the oxidation levels of the materials. Hence, the Power Factor reached an optimum value of 420±42 μW/mK^2 at an oxidation level of 21%, which was determined by XPS

spectra as shown in **Figure 7** for the precursor film and the optimized film. The optimized oxidation level of the PEDOT:Tos films is close to the one reported from Bubnova et al (22%) for the chemical reduction of PEDOT:Tos thin films.[3]

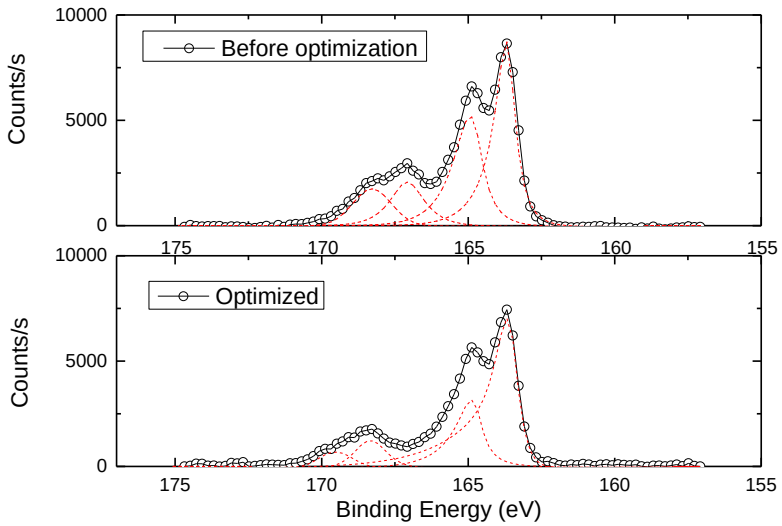

Figure 7: The S(2p) spectra of the PEDOT:Tos films before (upper) and after (down) optimization, respectively.

The optimized properties of the PEDOT:Tos films remained constant for a period of one week as presented in **Figure 8** under ambient conditions. After a period of one week the Seebeck coefficient starts to decrease and the electrical conductivity to increase, a behavior inherent to the oxidation of the material from the oxygen of the atmosphere.

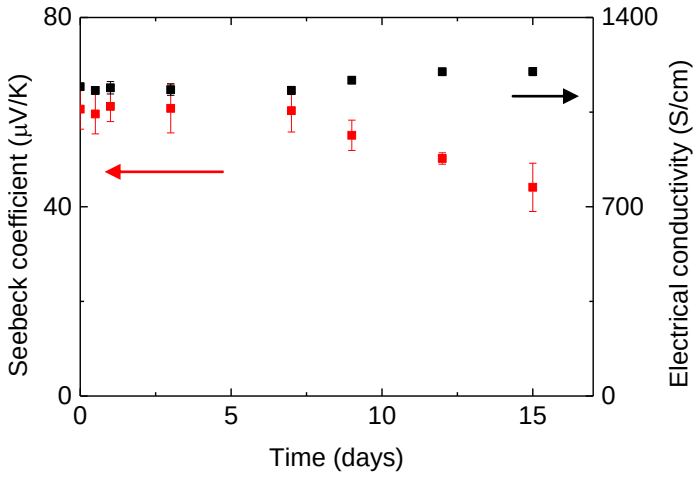

Figure 8: The Seebeck coefficient (red square, left axis) and electrical conductivity (black square, right axis) of the optimized PEDOT:Tos samples vs time.

3.3 Conclusions:

Tuning the polymerization kinetics of PEDOT:Tos thin films with pyridine leads to enhanced electric and thermoelectric properties as attested by both a mild increment of the Seebeck coefficient and a three-fold increase of the electrical conductivity. Processing these PEDOT:Tos thin films from formulation containing both pyridine and DMSO synergistically results in a Power Factor as high as 237 $\mu W/mK^2$ inherent to an increased charge carrier mobility and a higher degree of crystallinity. Origins of these effects have been traced by UPS to a band broadening near the Fermi level due to a more extended π-orbital system. These findings are consistent with the current understanding on the correlation between electronic and structural properties since PEDOT:Tos thin films with the highest crystallinity exhibits as well the most broadened band edge due to extended π-orbital overlapping, and thus, the higher thermoelectric efficiency. Eventually, the thermoelectric Power Factor was optimized (237 to 420 $\mu W/mK^2$) through an electrochemical tuning of the oxidation levels.

3.4 References:

1 Bubnova, O. & Crispin, X. Towards polymer-based organic thermoelectric generators. *Energy & Environmental Science* **5**, 9345, doi:10.1039/c2ee22777k (2012).

2 Snyder, G. J. & Toberer, E. S. Complex thermoelectric materials. *Nat Mater* **7**, 105-114 (2008).

3 Bubnova, O. *et al.* Optimization of the thermoelectric figure of merit in the conducting polymer poly(3,4-ethylenedioxythiophene). *Nat Mater* **10**, 429-433, doi:10.1038/nmat3012 (2011).

4 Bubnova, O. *et al.* Semi-metallic polymers. *Nat Mater* **13**, 190-194, doi:10.1038/nmat3824 (2014).

5 Kim, G. H., Shao, L., Zhang, K. & Pipe, K. P. Engineered doping of organic semiconductors for enhanced thermoelectric efficiency. *Nat Mater* **12**, 719-723, doi:10.1038/nmat3635 (2013).

6 Petsagkourakis, I. *et al.* Structurally-driven Enhancement of Thermoelectric Properties within Poly(3,4-ethylenedioxythiophene) thin Films. *Scientific Reports* **6**, 30501, doi:10.1038/srep30501

7 Ihnatsenka, S., Crispin, X. & Zozoulenko, I. V. Understanding hopping transport and thermoelectric properties of conducting polymers. *Physical Review B* **92**, doi:10.1103/PhysRevB.92.035201 (2015).

8 Cutler, M. & Mott, N. F. Observation of Anderson Localization in an Electron Gas. *Physical Review* **181**, 1336-1340, doi:10.1103/PhysRev.181.1336 (1969).

9 Kim, N. *et al.* Role of interchain coupling in the metallic state of conducting polymers. *Phys Rev Lett* **109**, 106405, doi:10.1103/PhysRevLett.109.106405 (2012).

10 Hsu, B. B. *et al.* The Density of States and the Transport Effective Mass in a Highly Oriented Semiconducting Polymer: Electronic Delocalization in 1D. *Adv Mater* **27**, 7759-7765, doi:10.1002/adma.201502820 (2015).

11 Sun, J. *et al.* Simultaneous Increase in Seebeck Coefficient and Conductivity in a Doped Poly(alkylthiophene) Blend with Defined Density of States. *Macromolecules* **43**, 2897-2903, doi:10.1021/ma902467k (2010).

12 Boudouris, B. W. *et al.* Real-Time Observation of Poly(3-alkylthiophene) Crystallization and Correlation with Transient Optoelectronic Properties. *Macromolecules* **44**, 6653-6658, doi:10.1021/ma201316a (2011).

13 Woo, C. H., Piliego, C., Holcombe, T. W., Toney, M. F. & Fréchet, J. M. J. A Quantitative Correlation between the Mobility and Crystallinity of Photo-Cross-Linkable P3HT. *Macromolecules* **45**, 3057-3062, doi:10.1021/ma202203z (2012).

14 Palumbiny, C. M. *et al.* The Crystallization of PEDOT:PSS Polymeric Electrodes Probed In Situ during Printing. *Adv Mater* **27**, 3391-3397, doi:10.1002/adma.201500315 (2015).

15 Rogers, J. T., Schmidt, K., Toney, M. F., Bazan, G. C. & Kramer, E. J. Time-resolved structural evolution of additive-processed bulk heterojunction solar cells. *J Am Chem Soc* **134**, 2884-2887, doi:10.1021/ja2104747 (2012).

16 Palumbiny, C. M. *et al.* Molecular Reorientation and Structural Changes in Cosolvent-Treated Highly Conductive PEDOT:PSS Electrodes for Flexible Indium Tin Oxide-Free Organic Electronics. *The Journal of Physical Chemistry C* **118**, 13598-13606, doi:10.1021/jp501540y (2014).

17 Endrődi, B., Mellár, J., Gingl, Z., Visy, C. & Janáky, C. Molecular and Supramolecular Parameters Dictating the Thermoelectric Performance of Conducting Polymers: A Case Study Using Poly(3-alkylthiophene)s. *The Journal of Physical Chemistry C* **119**, 8472-8479, doi:10.1021/acs.jpcc.5b00135 (2015).

18 Goh, C., Kline, R. J., McGehee, M. D., Kadnikova, E. N. & Fréchet, J. M. J. Molecular-weight-dependent mobilities in regioregular poly(3-hexyl-thiophene) diodes. *Applied Physics Letters* **86**, 122110, doi:10.1063/1.1891301 (2005).

19 Zen, A. *et al.* Effect of Molecular Weight on the Structure and Crystallinity of Poly(3-hexylthiophene). *Macromolecules* **39**, 2162-2171, doi:10.1021/ma0521349 (2006).
20 Juška, G., Genevičius, K., Arlauskas, K., Österbacka, R. & Stubb, H. Features of charge carrier concentration and mobility inπ-conjugated polymers. *Macromolecular Symposia* **212**, 209-218, doi:10.1002/masy.200450820 (2004).
21 Ha, Y. H. *et al.* Towards a Transparent, Highly Conductive Poly(3,4-ethylenedioxythiophene). *Advanced Functional Materials* **14**, 615-622, doi:10.1002/adfm.200305059 (2004).
22 Winther-Jensen, B., Breiby, D. W. & West, K. Base inhibited oxidative polymerization of 3,4-ethylenedioxythiophene with iron(III)tosylate. *Synthetic Metals* **152**, 1-4, doi:http://dx.doi.org/10.1016/j.synthmet.2005.07.085 (2005).
23 Huang, J.-H. & Chu, C.-W. Achieving efficient poly(3,4-ethylenedioxythiophene)-based supercapacitors by controlling the polymerization kinetics. *Electrochimica Acta* **56**, 7228-7234, doi:10.1016/j.electacta.2011.03.044 (2011).
24 Elschner, A., Kirchmeyer, S., Lovenich, W., Merker, U. & Reuter, K. *PEDOT: Principles and Applications of an Intrinsically Conductive Polymer*. (CRC Press, 2010).
25 Lövenich, W. PEDOT-properties and applications. *Polymer Science Series C* **56**, 135-143, doi:10.1134/s1811238214010068 (2014).
26 Crossland, E. J. W. *et al.* Anisotropic Charge Transport in Spherulitic Poly(3-hexylthiophene) Films. *Advanced Materials* **24**, 839-844, doi:10.1002/adma.201104284 (2012).
27 Massonnet, N., Carella, A., de Geyer, A., Faure-Vincent, J. & Simonato, J.-P. Metallic behaviour of acid doped highly conductive polymers. *Chem. Sci.* **6**, 412-417, doi:10.1039/c4sc02463j (2015).
28 Wei, Q., Mukaida, M., Naitoh, Y. & Ishida, T. Morphological change and mobility enhancement in PEDOT:PSS by adding co-solvents. *Adv Mater* **25**, 2831-2836, doi:10.1002/adma.201205158 (2013).
29 Herlogsson, L., Crispin, X., Tierney, S. & Berggren, M. Polyelectrolyte-Gated Organic Complementary Circuits Operating at Low Power and Voltage. *Advanced Materials* **23**, 4684-4689, doi:10.1002/adma.201101757 (2011).
30 Larsson, O., Laiho, A., Schmickler, W., Berggren, M. & Crispin, X. Controlling the Dimensionality of Charge Transport in an Organic Electrochemical Transistor by Capacitive Coupling. *Advanced Materials* **23**, 4764-4769, doi:10.1002/adma.201103131 (2011).
31 Lee, K. H. *et al.* "Cut and Stick" Rubbery Ion Gels as High Capacitance Gate Dielectrics. *Advanced Materials* **24**, 4457-4462, doi:10.1002/adma.201200950 (2012).
32 Kim, S. H. *et al.* Electrolyte-Gated Transistors for Organic and Printed Electronics. *Advanced Materials* **25**, 1822-1846, doi:10.1002/adma.201202790 (2013).
33 Jimison, L. H., Toney, M. F., McCulloch, I., Heeney, M. & Salleo, A. Charge-Transport Anisotropy Due to Grain Boundaries in Directionally Crystallized Thin Films of Regioregular Poly(3-hexylthiophene). *Advanced Materials* **21**, 1568-1572, doi:10.1002/adma.200802722 (2009).
34 Skrypnychuk, V. *et al.* Ultrahigh Mobility in an Organic Semiconductor by Vertical Chain Alignment. *Adv Mater*, doi:10.1002/adma.201503422 (2016).
35 Aasmundtveit, K. E. *et al.* Structure of thin films of poly(3,4-ethylenedioxythiophene). *Synthetic Metals* **101**, 561-564, doi:http://dx.doi.org/10.1016/S0379-6779(98)00315-4 (1999).
36 K.Z. Xing , M. F., X.W. Chen , O. Inganas, W.R. Salaneck The electronic structure of poly(3,4-ethylene-dioxythiophene)": studied by XPS and UPS. *Synthetic metals* **89**, 161-165 (1997).
37 Lindell, L. *et al.* Transparent, Plastic, Low-Work-Function Poly(3,4-ethylenedioxythiophene) Electrodes. *Chemistry of Materials* **18**, 4246-4252, doi:10.1021/cm061081m (2006).
38 Koller, G. *et al.* Intra- and Intermolecular Band Dispersion in an Organic Crystal. *Science* **317**, 351-355, doi:10.1126/science.1143239 (2007).

39 Crispin, X. *et al.* Electronic Delocalization in Discotic Liquid Crystals: A Joint Experimental and Theoretical Study. *Journal of the American Chemical Society* **126**, 11889-11899, doi:10.1021/ja048669j (2004).
40 Kaiser, A. B. & Skakalova, V. Electronic conduction in polymers, carbon nanotubes and graphene. *Chem Soc Rev* **40**, 3786-3801, doi:10.1039/c0cs00103a (2011).
41 Clark, J., Silva, C., Friend, R. H. & Spano, F. C. Role of intermolecular coupling in the photophysics of disordered organic semiconductors: aggregate emission in regioregular polythiophene. *Phys Rev Lett* **98**, 206406, doi:10.1103/PhysRevLett.98.206406 (2007).
42 Park, T., Park, C., Kim, B., Shin, H. & Kim, E. Flexible PEDOT electrodes with large thermoelectric power factors to generate electricity by the touch of fingertips. *Energy & Environmental Science* **6**, 788-792, doi:10.1039/C3EE23729J (2013).
43 Anson, F. C. & Osteryoung, R. A. Chronocoulometry: A convenient, rapid and reliable technique for detection and determination of adsorbed reactants. *Journal of Chemical Education* **60**, 293, doi:10.1021/ed060p293 (1983).

Chapter 4: Structure - Property correlations for conducting polymers for the design of efficient thermoelectric materials.

Preface:

The optimization of the thermoelectric properties of PEDOT:Tos thin films obtained in the previous chapters was traced to a mobility driven enhancement. This chapter acts as a follow-up to two previous chapters with an investigation on the correlation between the Seebeck coefficient and the charge carrier mobility for the various PEDOT films of constant carrier concentration. The origin of this coupling comes from the modifications of the electronic structure inherent to the increase of the thin film crystallinity. Furthermore, a link between the crystallographic and electronic structure with the charge transport mechanism is highlighted. Finally, a transition on the conductivity behavior was observed at low temperatures for the PEDOT:Tos films under study, while at higher temperatures the material behavior approaches that of a semimetal. The implications as regards to the thermoelectric properties of the various materials are subsequently discussed.

4.1 Introduction:

Conducting polymers are a category of heavily doped organic semiconductors that have gained the attention of the scientific community due to their a wide range of applications (e.g. hole injection layers in organic solar cells or organic light emitting diodes [1,2], transparent electrodes [1,3]). Recent highlights on conducting polymers have shown their high potential for the fabrication of thermoelectric converters[4-6] due to an encouraging figure of Merit, $zT = \frac{S^2\sigma T}{\kappa} \approx 0.4$ at room temperature, where S is the Seebeck coefficient, σ the electrical conductivity and κ the thermal conductivity, at a given temperature T.[7,8] Besides their inherent low thermal conductivity (0.5-1 W/mK) constitutes a strong asset with respect to their inorganic counterparts, which has led the scientific community to focus on the optimization of the Power Factor, $S^2\sigma$. Both parameters can be expressed as regards to intrinsic material transport characteristics. Firstly the electrical conductivity for such materials is expressed as:

$$\sigma = q \cdot N \cdot \mu \tag{1}$$

where q is the electric charge, N the carrier concentration and μ the charge carrier mobility.

The carrier concentration is correlated with the filling and shape of the Density of States (DoS) of the material,[9-11] while the charge carrier mobility is linked to the shape of the DoS for conducting polymers for which the dominant charge transport mechanism is hopping.[10,12,13] On the other hand, the Seebeck coefficient can be expressed as:

$$S(E,T) = \frac{\pi^2}{3} \cdot \frac{k^2 T}{q} \cdot \left(\frac{\partial ln(\sigma(E))}{\partial E}\right)_{E=E_f} \tag{2}$$

where k is the Bolzmann constant and E_f the Fermi Level (the chemical potential at 0 K).

Equation (2) is often referred as Mott's equation and implies that the Seebeck coefficient is analogous to the slope of the DoS at the Fermi Level.[14,15] Therefore, the Seebeck coefficient is particularly sensitive to the filling and shape of the DoS as well as the position of the Fermi level. These theoretical concepts were proven to be consistent for conducting polymers such as poly(3,4-ethylenedioxythiophene) (PEDOT).[8] Particularly a Power Factor optimization was readily associated to a careful tuning of the carrier concentration,[16-18] while it was described in a later report that polymer materials with a steeper DoS near the Fermi position exhibit higher S and σ.[8] From a molecular point of view, the broadening of the band edges (i.e. concurrent with a steeper DoS at the Fermi level) occurs due to an increased number of states near the chemical potential, as a consequence of the delocalization of charge carriers both at the intrachain and interchain levels. Practically, this interchain carrier delocalization is accomplished through the increase of the thin film crystallinity leading to an extended overlapping of π-orbitals.[4,8] On the other hand, a higher carrier delocalization at the intrachain is obtained for higher conjugation length polymer chains.[8]

As reported in the previous chapters, the electrical conductivity of PEDOT doped with toluenesulfonate small molecules (PEDOT:Tos) was enhanced, due to higher thin film crystallinity.[19] This was accomplished by using plasticizers, like dimethylesulfoxyde (DMSO), during the in-situ oxidative polymerization of the PEDOT:Tos thin films. Interestingly, the Seebeck coefficient was not significantly affected by these treatments. As opposed the incorporation of an organic base in the in-situ oxidative polymerization media has been shown to result in a concurrent increase of the electrical conductivity and Seebeck coefficient, which was translated in a ten-fold increase of the Power Factor of the PEDOT:Tos thin films (Chapter 3). It was shown in both cases that the electrical and thermoelectric behavior of the PEDOT:Tos thin films was mobility driven as the carrier concentration remained unaffected by the various treatments.[19] This allows to distinguish the influence of μ

and *N*, on *S*, enabling a rigorous investigation of the coupling between *S* and μ. Thus, in the present study we aim to systematically investigate the relationship between polymer structural and electronic properties, to the thermoelectric behavior of conducting polymers, providing an alternative way for thermoelectric optimization of polymer materials.

4.2 Results and Discussion: Relationships between mobility and Seebeck coefficient in PEDOT:Tos thin films

PEDOT:Tos thin films obtained from different oxidative polymerization formulations were selected to study the relationship between the charge carrier mobility and the Seebeck coefficient. **Table 1** listed the values of the Seebeck coefficient, *S*, the electrical mobility, σ, and the charge carrier mobility, μ, determined for the different PEDOT:Tos thin films. As already reported, the increase of the charge carrier mobility for the PEDOT:Tos thin films formulated with additives is related to an increase of the crystallinity of the system while XPS measurements demonstrated a constant charge carrier concentration notwithstanding the type of additives.[19] Accordingly, the enhanced charge carrier mobility leads to an increase of the electrical conductivity which is clearly evident from **Equation (1)**. Nevertheless a concurrent increase of the Seebeck coefficient was as well observed for the systems with the highest charge carrier mobility (i.e. the PEDOT:Tos thin films synthesized from a formulations containing pyridine) as shown in **Figure 1**.

Additives	σ (S/cm)	S (μV/K)	$\mu\ x10^{-4}$(cm^2/Vs)
No additive (Pristine)	230 ± 10	32.0 ± 5	2.4± 0.1
Toluene (Tol)	300 ± 10	32.6 ± 5	3.2± 0.3
Dimethylformamide (DMF)	640 ± 10	35.1 ± 5	6.6± 0.4
Dimethylsulfoxide (DMSO)	605 ± 15	32.2 ± 5	6.5± 0.5
Ethylene Glycol (EG)	355 ± 10	34.0 ± 5	3.6± 0.2
Pyridine	580 ± 20	40.0 ± 2	6.9± 0.3
Pyridine+Toluene	600 ± 20	40.5 ± 2	7.0± 0.3
Pyridine+DMSO	1220 ± 32	44.0 ± 2	12.4± 1.0
Pyridine+DMF	1225 ± 40	44.0 ± 3	12.8± 0.9
Pyridine+EG	890 ± 70	42.2 ± 5	9.8± 0.2

Table 1: The electrical conductivity σ, Seebeck coefficient *S* and charge carrier mobility μ, of the PEDOT:Tos films synthesized with the various additives.

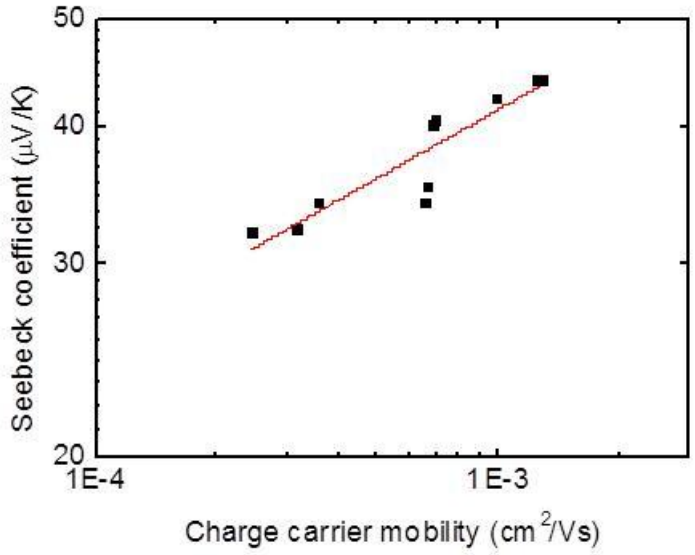

Figure 1: Seebeck coefficient *versus* carrier mobility for the PEDOT:Tos thin films in log-scale. The red line corresponds to the $S \sim \mu^{0.2}$ power law fit.

This coupling between S and μ is related to a co-dependence of both parameters with the DoS shape[8,12]. Taking into consideration the energy dependent electrical conductivity (valid in energies close to Fermi position),

$$\sigma(E) = qD(E)\mu(E) \tag{3}$$

where $D(E)$ is the density of states and $\mu(E)$ is the charge carrier mobility, the Mott's formalism on thermoelectricity (**Equation 2**) can be rewritten as:

$$S = \frac{\pi^2}{3}\frac{k^2T}{q}\left(\frac{1}{\mu}\frac{\partial\mu}{\partial E} + \frac{1}{D}\frac{\partial D}{\partial E}\right)_{Ef} \tag{4}$$

Equation (4) implies that the Seebeck coefficient is the sum of a mobility dependent term and a Density of States dependent term. In most thermoelectric studies, the first term is considered negligible due to the high dependence of Seebeck to the carrier concentration.[8,20,21] However, Sun *et al* recently proved that the mobility dependent Seebeck term becomes important in

inorganic systems with large temperature dependent charge carrier mobility,[20] providing an alternative way for thermoelectric optimization. For polymer materials, many studies reported a relationship between the Seebeck coefficient and the electronic properties of the material.[22-26] However, it is not trivial to decorrelate the effect of μ and N on the Seebeck coefficient, as any changes of N would affect both μ and S.[21,25,26] As a result, in most reports, the Seebeck coefficient is decreasing with the electrical conductivity, as an increased charge carrier concentration is detrimental for the thermoelectric behavior of the material.[17,21,25] Nonetheless, in 2013, Bubnova *et al*. proved that highly crystalline polymer systems with high electrical conductivity can also be thermoelectrically efficient, due to a wider DoS at the Fermi position.[8] In a highly crystalline conducting polymer, the π-orbitals of the conjugated chains overlapped forming an extended π-system. These broader π-bands are being translated into a sharper slope of the DoS at E_f , which benefits the thermoelectric behavior of the polymer material (*cf.* **Equation (2)**).[4,8,12]

It is commonly accepted that charge carrier mobility in conducting polymers is linked both to the thin film crystallinity of the system and the electronic structure of the material.[12,13,19,27,28] Specifically, thin films of higher degree of crystallinity would have higher charge carrier mobility, as the hopping transport between the conducting sites for the polymer is promoted.[19] Consequently, Seebeck coefficient and charge carrier mobility are interdependent to the thin film crystallinity of the conducting polymer, which implies that there should be a relationship between the two parameters. A first experimental investigation on the effect of charge carrier mobility on the thermoelectric properties of conducting materials was provided by Zhang *et al*. in 2016[12] who highlighted that the Seebeck coefficient of a conducting polymer is directly related to the PEDOT charge carrier mobility. These findings were based on the theoretical formalism that both Seebeck coefficient and charge carrier mobility are related to the shape of the Density of States.[8,12] The effect of thin film

crystallinity and charge carrier mobility is indeed apparent in **Equation (4)**. The first term, the mobility dependent Seebeck term, is related to the relaxation of the charge carriers in the conducting media and becomes important for temperature dependent charge carrier mobility semicrystalline systems.[20] On the other hand, the second term, $\left(\frac{1}{D}\frac{\partial D}{\partial E}\right)_{E_f}$, is proportional to the slope of the logarithm of DoS at E_f. For a conducting polymer, a high degree of crystallinity leads to an important slope of the DoS, inherent to broadened π-orbitals (See Chapter 3).[8] Thus, the polymer structure is indirectly related to the Seebeck coefficient. For the PEDOT:Tos thin films under study, the charge carrier concentration is constant. Consequently the observed increase of the Seebeck coefficient has to originate from the DoS slope or/and the mobility dependent term of **Equation (4)**. However, the high charge carrier density of these π-conjugated polymers would be detrimental for the second term of **Equation (4)**, hindering the effect of the thin film crystallinity.[19] Meanwhile, these systems follow a low-mobility hopping conduction[20,29] which would not favor the first term of **Equation (4)**, as proposed by Sun *et al*.[30] Consequently, a mild mobility dependency of the Seebeck coefficient has to be expected in agreement with the tendency observed in **Figure 1** ($S \sim \mu^{0.2}$). As both the Seebeck coefficient and the charge carrier mobility are related to the broadening of the DoS at the Fermi position, the electronic structure of the materials has to be investigated in order to elucidate the behavior observed in **Figure 1**.

Ultraviolet Photoelectron Spectroscopy (UPS) was performed on four key samples in order to characterize the electronic structure as regards to the PEDOT:Tos formulations of gradual increase in thin film crystallinity (i.e. pristine, formulated with DMSO, pyridine and DMSO + pyridine). The resulting UPS spectra are presented in **Figure 2** and are in good agreement with previous reports on PEDOT:Tos materials with a extracted work function value of 4.6-4.8 eV.[3,8] Three distinctive peaks - one at 15.8 eV related to the inelastic electron scattering due to the sample surface, and two at 9.5 and 6.1 eV which are σ states of the

systems, respectively - are retrieved from the UPS spectra.[27] Besides, as the thin film crystallinity increases, the intensity of the HOMOβ is increasing with respect to the intensity of HOMOα. This phenomenon is related to the distribution of the carriers over the different energy states and thin films of higher crystallinity exhibit more populated high energy states.

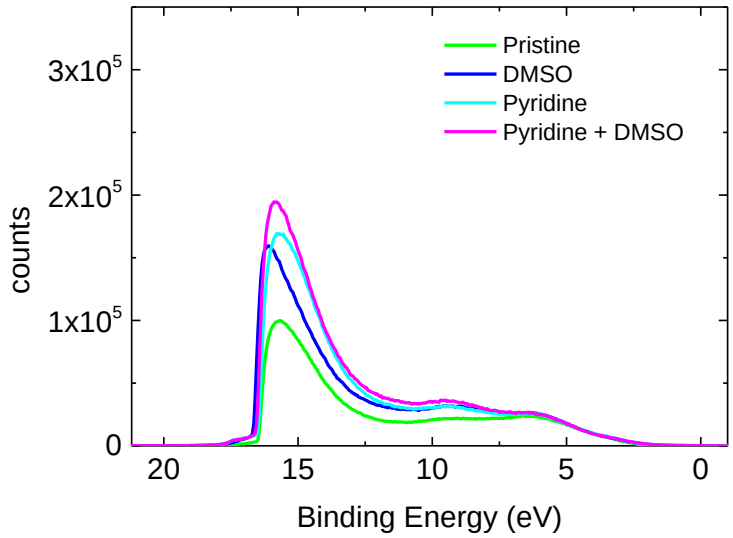

Figure 2: The UPS spectra for the various PEDOT:Tos samples.

By focusing on energies lower than 4.5 eV (**Figure 3**), deeper π-orbitals states can be examined which allow us to notice a broadening of the DoS for the most crystalline samples.[4,8,31,32] Indeed a higher degree of crystallinity is translated in conducting polymers to an extended overlapping of the π-orbitals.[4,8] This broadening of the band-edge is concurrent to enhanced charge carrier mobility and Seebeck coefficient (see **Figure 3**), highlighting the coupling between these parameters in the PEDOT:Tos films under study.

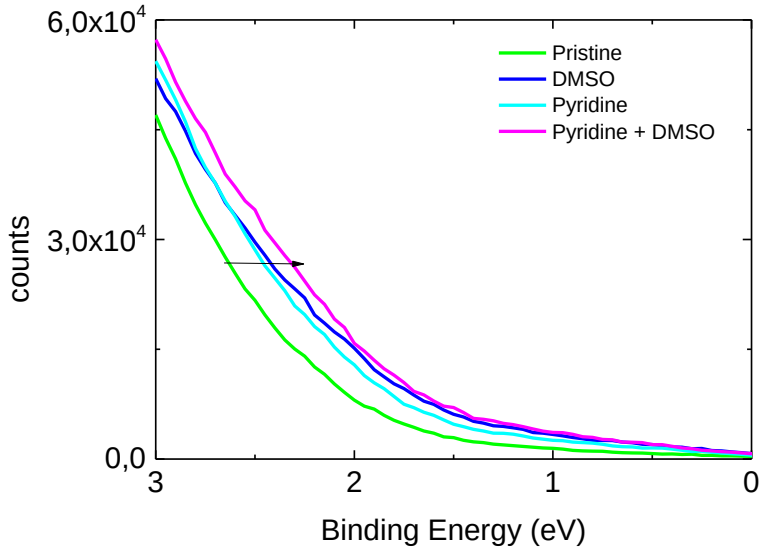

Figure 3: The UPS spectra for the four representative PEDOT:Tos thin films zoomed in the lower binding energies, were the band edge is apparent.

It is commonly accepted that this band broadening is transferred to all intermolecular π-bands, including the ones close to the Fermi position.[31,32] Consequently a higher slope of the DoS at the Fermi position is retrieved leading to higher Seebeck coefficient values for the most crystalline films. It is noteworthy that this formalism does not fully explain the dissimilar Seebeck coefficients observed for the DMSO treated and the pyridine treated PEDOT:Tos films, as their correspondent UPS spectra are overlapped (See **Figure 2 and 3**). One possible explanation is related to the macromolecular structure of the PEDOT chains obtained from pyridine formulation. As pyridine reduces the polymerization kinetics, the resulting PEDOT chains are expected to be of higher molecular weight. As a result, an intrachain hopping transport has to be considered and would heavily affect the overall charge transport behavior of the PEDOT:Tos material.[4,8] When an intrachain hopping transport is substantial (comparatively to the interchain hopping transport), the material would exhibit a semi-metallic behavior and, thus, enhanced thermoelectric efficiency.

Temperature-dependent electrical conductivity measurements were performed in order to track down these effects on the four key PEDOT:Tos systems.[8,28,29,33,34] The results are presented in **Figure 4**. The electrical conductivity of all PEDOT:Tos films was normalized with respect to their room temperature value.

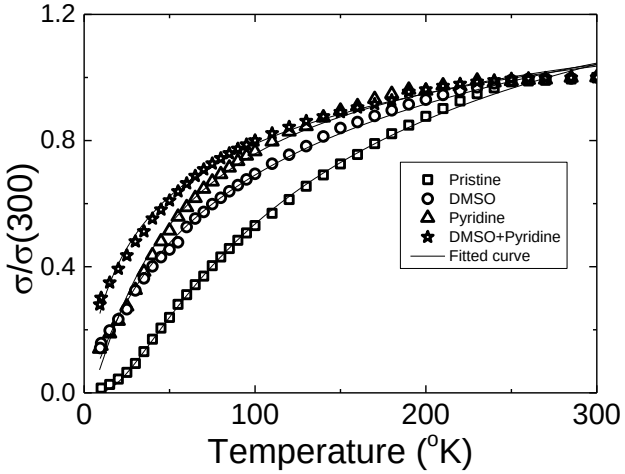

Figure 4. Normalized electrical conductivity (with respect to room temperature) *versus* temperature for PEDOT:Tos thin films. The full lines are the fitting curves according to the VRH model.

For all samples it appears that the electrical conductivity is thermally activated. For semi-crystalline conducting polymer systems, charge transport mainly occurs through hopping of the charge carriers between "metallic" islands (i.e. doped PEDOT:Tos crystallites) dispersed in an amorphous matrix.[29,34,35] Consequently the most crystalline PEDOT:Tos thin films have inherently a lower amount of thermally activated traps, favoring the charge carrier hopping between these "metallic" sites.[29,34-36] The Variable Range Hopping (VRH) model (**Equation (5)**) can be used to describe the hopping transport in such systems.[14,28,29]

$$\sigma = \sigma_o \cdot e^{-(\frac{T_o}{T})^p} \quad (5)$$

where the pre-factor σ_o has a negligible dependence over T, T_o is a hopping parameter related to the DoS at the Fermi level. The factor $p = \frac{1}{1+d}$ is related to the dimensionality, d, of the charge transport of the system, being 1-D, 2-D or 3-D for $p \approx 0.5$, 0.33 and 0.25, respectively. The VRH model satisfactorily fits the behavior of the different samples (see **Table 2** for the VRH parameters), as previously reported for similar PEDOT based materials.[28,33,37]

Additive	**σ (S/cm)**	**S (μV/K)**	**μ x10^{-4} (cm^2/Vs)**	**p**	**T_o(K)**	**$\sigma_{ratio(1/K)}$**
No additive (Pristine)	230 ± 10	32 ± 5	2.4 ± 0.1	0.66	170	0.11
Dimethylsulfoxide (DMSO)	605 ± 10	35 ± 5	6.5 ± 0.3	0.59	135	0.09
Pyridine	580 ± 20	40 ± 2	6.9 ± 0.3	0.33	68	0.10
Pyridine+DMSO	1222± 32	44 ± 2	12.4 ± 1.0	0.32	50	0.08

Table 2. The electrical and thermoelectric properties of the examined system. In the table are presented the electrical conductivity, σ, the Seebeck coefficient, S, the in-plane moblility, μ, the calculated VRH parameters p and T_o , and the calculated σ_{ratio}, $\frac{1}{\sigma} \cdot \frac{d\sigma}{dT}$, at T = 10 K for the PEDOT:Tos films.

A progression of p with respect to the degree of crystallinity of the sample is noticed, from p = 0.66 for the less crystalline sample to p = 0.33 for the most crystalline one. For conducting polymers, a value of p = 0.5 is often reported and corresponds to 1-D charge transport in the VRH formalism, even if such behavior is impractical for such disordered systems.[37-39] These systems are thus considered as effective 3-D systems in which charge transport mainly occurs along the π-stacking direction, hence the 1-D behavior.[37,38,40] Values close to p = 0.33 were also reported for PEDOT materials, although such systems cannot strictly be treated as 2-D due to the semicrystalline nature of the material.[28,40] Nevertheless, in the PEDOT:Tos thin films of higher degree of crystallinity, a quasi-2-D charge transport mechanism could be envisioned as hopping transport occurs along both the π-stacking direction and the chain backbone, resulting in a dominant 2-D hopping transport.

As reported by Sun *et al*,[20] a VRH dominated charge transport mechanism would hinder the effect of the first term of **Equation (4)** - the "mobility dependent" Seebeck term. According to this formalism, this particular term becomes important when $d\mu/dT > \mu$. For the heavily doped systems studied herein, the charge carrier concentration is constant, thus the ratio $\sigma_{ratio} = \frac{1}{\sigma} \cdot \frac{d\sigma}{dT}$ can be used as a qualitative means in order to compare μ with $d\mu/dT$ at a given temperature. Consequently, this ratio was calculated for the lowest measured temperature, 10 K, for all the PEDOT:Tos systems. As shown in **Table 2**, σ_{ratio} is much lower than 1 for all the samples. Consequently the $d\mu/dT < \mu$ and we can assume that the first term of **Equation (4)**, $\frac{1}{\mu}\frac{\partial \mu}{\partial E}$, is not significantly affecting the Seebeck coefficient.[20] The observed characteristics of **Figure 1** originate thus from a higher slope of the DoS at E_f..

However, the tendency observed in **Figure 4** does not correspond to the semi-metallic behavior expected for an efficient thermoelectric material,[8] while the measured Seebeck was representative of that of a semi-metallic polymer. This implies that a transition in the charge transport has to occur over the temperature range probed during the temperature-dependent electrical conductivity measurements. In order to gain further insights in the observed behaviors, the reduced activation energy, $W = \frac{\partial ln\sigma}{\partial lnT}$, was plotted *versus* the temperature (**Figure 5**) as it allows to discriminate between different conduction behaviors.[14,29,33,39,41] Depending of the value of the slope of *W*, a material belongs in the "metallic" (positive slope), "insulating" (negative slope) or "critical" regime of the Mott's Metal-Insulator Transition (MIT) (zero slope), respectively .[14,29,39] Most semi-conductors fall into the insulating regime,[14,29] while most semi-metals belong to the critical regime of the MIT.[14,29,42]

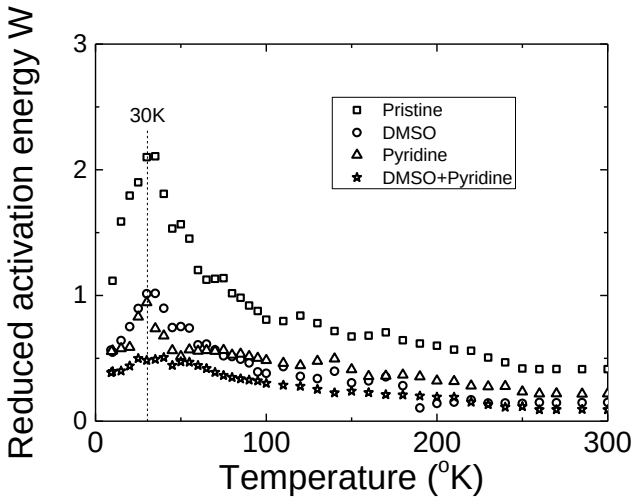

Figure 5: Reduced activation energy, W, *versus* temperature for PEDOT:Tos thin films.

For all the systems, a transition is observed around 30 K. As the slope of *W* is positive below 30 K, the systems fall into the metallic regime. Above 30 K, the slope of *W* is negative and tends at higher temperature towards a constant value (i.e. the MIT critical regime) for the highest crystallinity systems. This kind of behavior is typical of inorganic semi-conductors like Germanium,[43,44] but it is usually observed at a lower temperature (~10 K). Furthermore the sharpness of the transition at 30 K is clearly dependent of the PEDOT:Tos formulations with a rather feeble transition for the most crystalline thin films. This can be explained by the lower proportion of temperature activated charge traps which consequently have a limited contribution in the charge transport mechanism at all temperatures. Indeed, with increasing degree of crystallinity, the amount of temperature activated charge traps inherent to structural defects diminishes. The effect of those traps becomes more important in lower temperatures, as there are less phonons that could otherwise assist overcoming any vibrational barriers. As a result, any existent transitions in the hopping transport behavior ,which would be otherwise invisible, become evident in the low temperature range. Thus, in systems of high crystallinity, the phonon scattering is lower, leading to smoother transitions between the conduction

regimes in accordance with the behaviors observed in **Figure 5**. Additionally, the systems of **Figure 5** fall in the MIT critical regime at higher temperatures, which is in agreement with the ones obtained on a PEDOT:Tos system of higher crystallinity falling in the MIT critical regime over a large range of temperatures without any visible transition.[8]

4.3 Conclusion:

Through various processing modifications, the structural, electronic and thermoelectric properties of in situ polymerized PEDOT:Tos were tuned. It was found that samples with increased degree of thin film crystallinity would result in PEDOT of higher carrier mobility and higher Seebeck coefficient. A mild dependency of the S on the carrier mobility was found, $S \sim \mu^{0.2}$,which was correlated with the broadening of the π-orbitals near the band edge observed by UPS. In order to further investigate the dominant charge transport behavior, low temperature electrical conductivity measurements were conducted on the samples. All samples followed the Mott's Variable Range Hopping model, while a transition from 1-D to 2-D hopping transport was observed with the gradual increase of the thin film crystallinity. A transition from the metallic to the insulating regime was found at 30 K, whose intensity diminishes with the increase of the thin film crystallinity of the systems. Our findings highlight the coupling between structure to the electronic/thermoelectric properties and charge transport behavior of conducting polymers, providing an alternative road towards more efficient polymer thermoelectric converters.

4.4 References:

1 Hofmann, A. I. *et al.* An Alternative Anionic Polyelectrolyte for Aqueous PEDOT Dispersions: Toward Printable Transparent Electrodes. *Angew Chem Int Ed Engl* **54**, 8506-8510, doi:10.1002/anie.201503024 (2015).

2 Sun, K. *et al.* Review on application of PEDOTs and PEDOT:PSS in energy conversion and storage devices. *Journal of Materials Science: Materials in Electronics* **26**, 4438-4462, doi:10.1007/s10854-015-2895-5 (2015).

3 Lindell, L. *et al.* Transparent, Plastic, Low-Work-Function Poly(3,4-ethylenedioxythiophene) Electrodes. *Chemistry of Materials* **18**, 4246-4252, doi:10.1021/cm061081m (2006).

4 Bubnova, O. & Crispin, X. Towards polymer-based organic thermoelectric generators. *Energy & Environmental Science* **5**, 9345, doi:10.1039/c2ee22777k (2012).

5 Chen, Y., Zhao, Y. & Liang, Z. Solution processed organic thermoelectrics: towards flexible thermoelectric modules. *Energy Environ. Sci.* **8**, 401-422, doi:10.1039/c4ee03297g (2015).

6 He, M., Qiu, F. & Lin, Z. Towards high-performance polymer-based thermoelectric materials. *Energy & Environmental Science* **6**, 1352, doi:10.1039/c3ee24193a (2013).

7 Kim, G. H., Shao, L., Zhang, K. & Pipe, K. P. Engineered doping of organic semiconductors for enhanced thermoelectric efficiency. *Nat Mater* **12**, 719-723, doi:10.1038/nmat3635 (2013).

8 Bubnova, O. *et al.* Semi-metallic polymers. *Nat Mater* **13**, 190-194, doi:10.1038/nmat3824 (2014).

9 Ashcroft, N. & Mermin, D. *Solid State Physics*. (Thomson Learning, 1976).

10 Geoghegan, M. & Hadziioannou, G. *Polymer Electronics*. (OUP Oxford, 2013).

11 Chen, G. *Nanoscale Energy Transport and Conversion: A Parallel Treatment of Electrons, Molecules, Phonons, and Photons*. (Oxford University Press, 2005).

12 Zhang, K. *et al.* Effect of host-mobility dependent carrier scattering on thermoelectric power factors of polymer composites. *Nano Energy* **19**, 128-137, doi:10.1016/j.nanoen.2015.11.005 (2016).

13 Coropceanu, V. *et al.* Charge Transport in Organic Semiconductors. *Chemical Reviews* **107**, 926-952, doi:10.1021/cr050140x (2007).

14 Mott, N. F. & Davis, E. A. *Electronic Processes in Non-Crystalline Materials*. (OUP Oxford, 2012).

15 Cutler, M. & Mott, N. F. Observation of Anderson Localization in an Electron Gas. *Physical Review* **181**, 1336-1340, doi:10.1103/PhysRev.181.1336 (1969).

16 Bubnova, O., Berggren, M. & Crispin, X. Tuning the thermoelectric properties of conducting polymers in an electrochemical transistor. *J Am Chem Soc* **134**, 16456-16459, doi:10.1021/ja305188r (2012).

17 Bubnova, O. *et al.* Optimization of the thermoelectric figure of merit in the conducting polymer poly(3,4-ethylenedioxythiophene). *Nat Mater* **10**, 429-433, doi:10.1038/nmat3012 (2011).

18 Khan, Z. U. *et al.* Acido-basic control of the thermoelectric properties of poly(3,4-ethylenedioxythiophene)tosylate (PEDOT-Tos) thin films. *J. Mater. Chem. C* **3**, 10616-10623, doi:10.1039/c5tc01952d (2015).

19 Petsagkourakis, I. *et al.* Structurally-driven Enhancement of Thermoelectric Properties within Poly(3,4-ethylenedioxythiophene) thin Films. *Scientific Reports* **6**, 30501, doi:10.1038/srep30501

20 Sun, P. *et al.* Large Seebeck effect by charge-mobility engineering. *Nat Commun* **6**, 7475, doi:10.1038/ncomms8475 (2015).

21 Ihnatsenka, S., Crispin, X. & Zozoulenko, I. V. Understanding hopping transport and thermoelectric properties of conducting polymers. *Physical Review B* **92**, doi:10.1103/PhysRevB.92.035201 (2015).

22 Kwok, H. L. Charge mobility and ZT in conducting organic thermoelectric. *Journal of Materials Science: Materials in Electronics* **23**, 2272-2275, doi:10.1007/s10854-012-0815-5 (2012).
23 Kwok, H. L. Thermoelectric Power and ZT in Conducting Organic Semiconductor. *Journal of Electronic Materials* **41**, 476-479, doi:10.1007/s11664-011-1863-y (2012).
24 Kim, G. & Pipe, K. P. Thermoelectric model to characterize carrier transport in organic semiconductors. *Physical Review B* **86**, 085208 (2012).
25 Shi, W., Zhao, T., Xi, J., Wang, D. & Shuai, Z. Unravelling Doping Effects on PEDOT at the Molecular Level: From Geometry to Thermoelectric Transport Properties. *Journal of the American Chemical Society* **137**, 12929-12938, doi:10.1021/jacs.5b06584 (2015).
26 Shi, W., Chen, J., Xi, J., Wang, D. & Shuai, Z. Search for Organic Thermoelectric Materials with High Mobility: The Case of 2,7-Dialkyl[1]benzothieno[3,2-b][1]benzothiophene Derivatives. *Chemistry of Materials* **26**, 2669-2677, doi:10.1021/cm500429w (2014).
27 K.Z. Xing , M. F., X.W. Chen , O. Inganas, W.R. Salaneck The electronic structure of poly(3,4-ethylene-dioxythiophene)": studied by XPS and UPS. *Synthetic metals* **89**, 161-165 (1997).
28 Sangeeth, C. S. S., Jaiswal, M. & Menon, R. Charge transport in transparent conductors: A comparison. *Journal of Applied Physics* **105**, 063713, doi:10.1063/1.3097759 (2009).
29 Kaiser, A. B. & Skakalova, V. Electronic conduction in polymers, carbon nanotubes and graphene. *Chem Soc Rev* **40**, 3786-3801, doi:10.1039/c0cs00103a (2011).
30 Sun, P. *et al.* Large Seebeck effect by charge-mobility engineering. *Nature Communications* **6**, 7475, doi:10.1038/ncomms8475
31 Koller, G. *et al.* Intra- and Intermolecular Band Dispersion in an Organic Crystal. *Science* **317**, 351-355, doi:10.1126/science.1143239 (2007).
32 Crispin, X. *et al.* Electronic Delocalization in Discotic Liquid Crystals: A Joint Experimental and Theoretical Study. *Journal of the American Chemical Society* **126**, 11889-11899, doi:10.1021/ja048669j (2004).
33 Massonnet, N., Carella, A., de Geyer, A., Faure-Vincent, J. & Simonato, J.-P. Metallic behaviour of acid doped highly conductive polymers. *Chem. Sci.* **6**, 412-417, doi:10.1039/c4sc02463j (2015).
34 Menon, R., Yoon, C. O., Moses, D., Heeger, A. J. & Cao, Y. Transport in polyaniline near the critical regime of the metal-insulator transition. *Physical Review B* **48**, 17685-17694, doi:10.1103/PhysRevB.48.17685 (1993).
35 Lee, K. *et al.* Metallic transport in polyaniline. *Nature* **441**, 65-68, doi:10.1038/nature04705 (2006).
36 Kaiser, A. B., Flanagan, G. U., Stewart, D. M. & Beaglehole, D. Heterogeneous model for conduction in conducting polymers and carbon nanotubes. *Synthetic Metals* **117**, 67-73, doi:http://dx.doi.org/10.1016/S0379-6779(00)00540-3 (2001).
37 Aleshin, A. N., Kiebooms, R. & Heeger, A. J. International Conference on Science and Technology of SyntheticMetallic conductivity of highly doped poly(3,4-ethylenedioxythiophene). *Synthetic Metals* **101**, 369-370, doi:http://dx.doi.org/10.1016/S0379-6779(98)00758-9 (1999).
38 Kronemeijer, A. J. *et al.* Universal scaling in highly doped conducting polymer films. *Phys Rev Lett* **105**, 156604, doi:10.1103/PhysRevLett.105.156604 (2010).
39 Aleshin, A. N. Charge carrier transport in conducting polymers on the metal side of the metal-insulator transition: A review. *Physics of the Solid State* **52**, 2307-2332, doi:10.1134/s106378341011017x (2010).
40 Kim, N. *et al.* Role of interchain coupling in the metallic state of conducting polymers. *Phys Rev Lett* **109**, 106405, doi:10.1103/PhysRevLett.109.106405 (2012).
41 Chen, T. *et al.* Metal-insulator transition in films of doped semiconductor nanocrystals. *Nat Mater* **15**, 299-303, doi:10.1038/nmat4486 (2016).

42 Ugur, A. *et al.* Low-Dimensional Conduction Mechanisms in Highly Conductive and Transparent Conjugated Polymers. *Adv Mater* **27**, 4604-4610, doi:10.1002/adma.201502340 (2015).
43 A.G. Zabrodskii, K. N. Z. e. Low-temperature conductivity and metal-insulator transition in compensate n-Ge *Journal of Experimental and Theoretical Physics* **59**, 425 (1983).
44 Veinger, A. I. *et al.* Low-temperature variation of magnetic order in a nonmagnetic n-Ge:As semiconductor in the vicinity of the metal-insulator phase transition. *Journal of Experimental and Theoretical Physics* **116**, 796-799, doi:10.1134/s1063776113050142 (2013).

Chapter 5: The anisotropic thermoelectric properties of Poly(3,4-ethylenedioxythiophene) thin films

Preface:

In the previous chapter a relationship between the Seebeck coefficient and the charge carrier mobility of the PEDOT:Tos material was established. However, to obtain a complete description of the thermoelectric efficiency, the accurate determination of the thermal conductivity is needed. This chapter acts as a final follow-up to the previous discussions with a strong emphasis on the relationships between the electronic and thermal conductivities. The electronic and thermal properties of PEDOT:Tos thin films were studied with respect to the structural anisotropy in the in-plane and out-of-plane directions. It was observed that the anisotropy between the charge carrier mobility and the thermal conductivity is amplified for higher degree of crystallinity. In parallel, these structural modification decrease the ratio between the electrical and thermal conductivities towards the value of a typical semimetal or a metal. This observed behavior is in agreement with the semimetallic behavior of the PEDOT:Tos at higher temperatures, presented in the previous chapters. Finally, a relationship is extracted between ZT and μ, allowing the estimation of the thermoelectric Figure of Merit from charge carrier mobility and charge carrier concentration measurements.

5.1 Introduction:

As the semi-crystalline PEDOT:Tos thin films are anisotropic, the measured electronic and thermal properties are dependent of the direction of the measurement.[1] For instance, the charge carrier mobility of the poly(3-hexylthiophene) (P3HT) thin films varies over few orders of magnitude between the directions along and perpendicular to the substrate.[1] This electronic anisotropy is related to the π-stacking chain conformation, which was normal to the substrate in this case. Indeed, when the chains are π-stacked, the interchain distance is reduced which benefits to the hopping transport of the charge carriers. When the direction of the π-stacking chains is along the thin film substrate, the chain conformation is called edge-on, while the opposite case is called face-on. This anisotropy was also reported for PEDOT:PSS thin films, for which the out-of-plane electrical conductivity was much lower than the in-plane electrical conductivity.[2,3]

As reported in the previous chapters, a high degree of crystallinity is beneficial to the thermoelectric efficiency of PEDOT:Tos thin films. As reported by Wei *et al*, the Seebeck coefficients of PEDOT derivatives measured along the in-plane and out-of-plane directions are of the same order of magnitude, implying that S is fairly independent of the structural anisotropy of such polymer thin film.[2] On the other hand, the thermal conductivity, κ, of conducting polymer thin films has been shown to follow an anisotropic behavior between the in-plane and out-plane directions.[2,4,5] The origin of this dissimilarity is not only the anisotropic structure of the polymer thin films but also the electronic contribution of the charge carriers to the thermal conductivity.[5,6]

In metals and heavily doped inorganic semiconductors, κ is separated into two contributions, the structural, κ_s, and the electronic contribution, κ_e, as the charge carriers of the material also contribute to the propagation of phonons in the material.[6,7] For metals the

electronic contribution is dominant in the thermal conductivity and the Lorenz number, L, is defined as the ratio between κ and σ :

$$\frac{\kappa}{\sigma T} = L \quad (1)$$

and is based on the fact that the charge carriers are involved in both the heat and charge transport in the material.[8] For metals the Lorenz number is equal to the Sommerfield value, $L_o = \frac{\pi^2}{3}\left(\frac{k_B}{e}\right)^2 \approx 2.45 \times 10^{-8}$ WΩ/K^2 and it is commonly used to calculate the thermal conductivity from the electrical conductivity in metals.[7] However, for inorganic semiconductors, the Lorenz number deviates from the Sommerfield value, due to the introduction of disorder into the system.[7] Weathers *et al*. reported in 2015 that the in-plane thermal conductivity of conducting PEDOT derivatives increases with the in-plane electrical conductivity, implying that this heavily doped semiconductor follows a behavior similar to that of the typical inorganic materials.[5] It was shown that the origin of this increase in the in-plane $\kappa_{//}$ was inherent not only to the anisotropic structure of the material, but also to the degree of crystallinity and the heavily doped nature of the material, as more crystalline and doped materials had also higher $\kappa_{//}$.[5,9] On the other hand, σ is also dependent on the doping and the structure of the material via the charge carrier concentration and the charge carrier mobility. Nevertheless, the electrical conductivity is more sensible than κ to any structural modifications of the polymer thin film, due to its linear dependence on μ. Thus, for a constant carrier concentration, the Lorenz number is expected to show a mild dependency to polymer structural modifications.

In the previous chapters, the electrical conductivity of PEDOT:Tos thin films were enhanced by various treatments. These treatments increased the thin film crystallinity without modifying the carrier concentration of the systems.[10] In this chapter, the thermal and

electronic properties of the PEDOT:Tos thin films are measured as a means to examine the dependence of the Lorenz number as regards to the thin film crystallinity.

5.2 Results and discussion: Anisotropic thermoelectric properties and their relationships to the structure in PEDOT:Tos thin films

Various PEDOT:Tos thin films were produced using the different synthetic strategies presented in the Chapters 2 and 3. The relative crystallinity was extracted from the GIWAXS patterns presented in the previous chapters. The in-plane charge carrier mobility, $\mu_{//}$, was extracted for these PEDOT:Tos systems from the transfer characteristic electrolyte-gated transistors (**Table 1** and Chapters 2-4).[11,12] As observed from **Figure 1**, the in-plane mobility of the PEDOT:Tos gradually increases with the relative crystallinity of the films, which is in agreement with other works on PEDOT:Tos systems.[10]

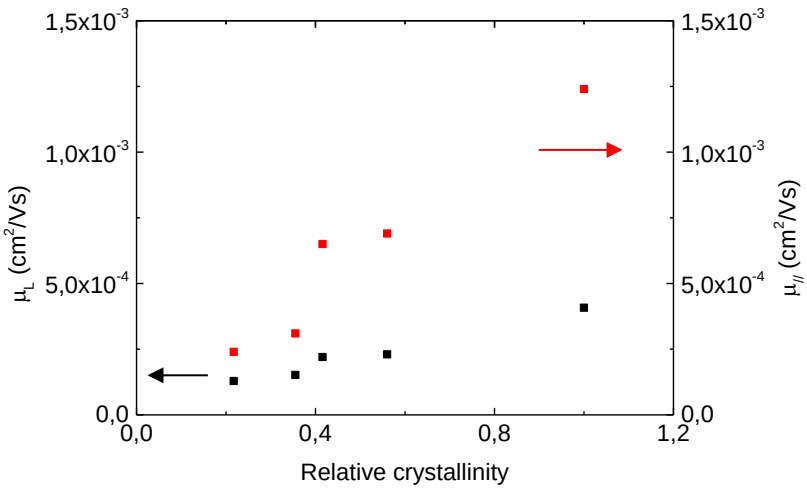

Figure 1: The out-of-plane (left, black) and in-plane (right,red) charge carrier mobilities for the PEDOT:Tos samples as a function of the relative thin film crystallinity.

A different approach was used for the extraction of the out-of-plane charge carrier mobility. Rutledge *et al*. calculated the out-of-plane mobility of PEDOT:PSS films from the

space-charge-limited-current (SCLC) region of the *J-V* curves for out-of-plane devices.[13] The authors had taken advantage of the relationship:

$$J = \frac{9}{8} \cdot \varepsilon_r \cdot \varepsilon_o \cdot \mu \cdot \frac{V^2}{d^3} \quad (2)$$

where, d is the polymer thickness, ε_r and ε_o the relative permittivity of the conducting polymer and of the free space respectively.[14]

The relative permittivity of the conducting polymers was taken as a constant and equal to 2.2.[13] At low voltages, below 1 V, the electrical behavior of the material follows an ohmic law, and thus **Equation (2)** is not valid. As opposed, in the higher voltage region (*i.e.* above 1 V), J follows a linear relationship wih V^2 in the space charge regime (as shown in **Figure 2b** for the most-conducting PEDOT:Tos thin film) and **Equation (2)** becomes valid, thus allowing the extraction of the out-of-plane charge carrier mobility.[13] Hence, this approach was used to extract the out-of-plane mobility of the PEDOT materials. Details on the device fabrication are presented in the **Appendix B**.

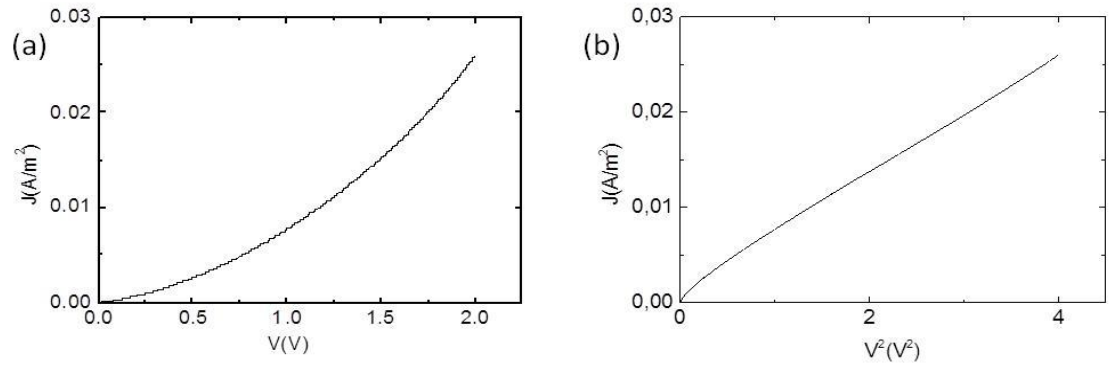

Figure 2: (a) The J-V curve for the most conducting PEDOT:Tos thin film (Pyr+DMSO). (b) The respective J-V^2 curve for the same material. In voltages above 1V the current follows a linear law with the V^2.

The resulted μ_L values are summarized in **Table 1** for the various PEDOT:Tos films. As observed in **Figure 1**, the out-of-plane mobility increases following a similar trend to that of the in-plane mobility as regards to the relative crystallinity of the thin films. Even if the out-of-plane mobility is lower than the in-plane mobility, the values are of the same order of magnitude. As observed from the GIWAXS patterns of the PEDOT:Tos materials presented in Chapters 2 and 3, face-on crystallites are also presented in the PEDOT:Tos films, and thus, contribute to the charge transport along the out-of-plane direction. Nevertheless, as the majority of the crystallites are oriented edge-on, a higher $\mu_{//}$ is retrieved. Consequently the ratio $\mu_{//}/\mu_L$ is indicative of the electronic anisotropy of the PEDOT:Tos films and is plotted in **Figure 3** with respect to the relative thin film crystallinity. It is observed that the anisotropy between the two parameters gradually increases with the degree of crystallinity. This has to be correlated with the increase of the amount of edge-on oriented crystallites with the thin film crystallinity (see Chapter 2 for details) which amplifies the structural and charge carrier mobility anisotropies.[10]

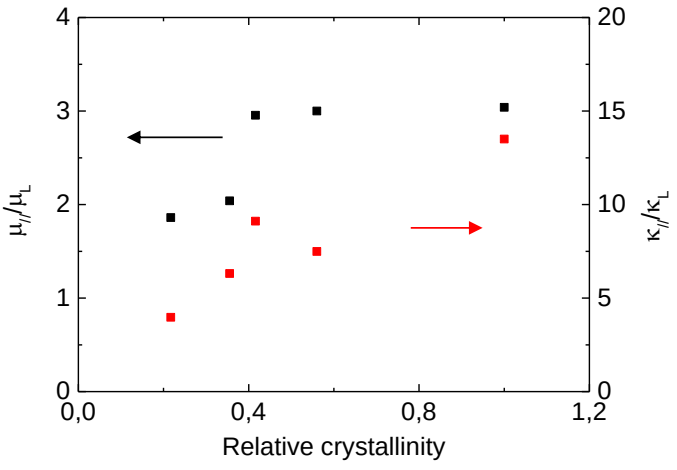

Figure 3: The ratio between the in-plane and out-of-plane charge carrier mobilities (black) and thermal conductivities (red) for the various PEDOT:Tos films.

Additionally, as shown by Wei *et al*., the thermal conductivity of PEDOT:PSS is also affected by the structural anisotropy of the material.[2] The electronic contribution to κ is affected by the direction of the bipolaronic conduction, along the π-π stacking.[5] The out-of-plane thermal conductivity, κ_L, was measured by heterodyne picosecond time-domain thermoreflectance,[15] and the results are summarized in **Table 1** and **Figure 4**. It appears that κ_L is not significantly affected (≈ 0.15-0.2 W/mK) by the thin film crystallinity as shown in **Figure 4**.

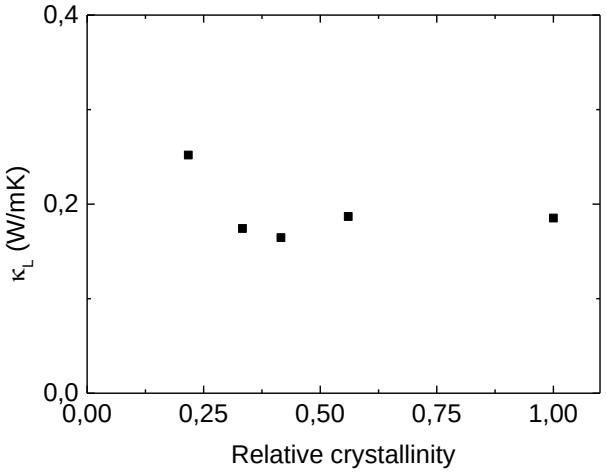

Figure 4: The out-of-plane thermal conductivity versus the relative crystallinity of the various PEDOT:Tos films.

However, the electronic contribution, κ_e, to the thermal conductivity is benefitted by the direction of the π stacking in the system, as this contribution is dependent to the charge transport mechanism of the material. Hence, an edge-on orientation of the chains is not expected to benefit the out-of-plane thermal conductivity.[5] This argument is further supported by the measured κ_L values, which are similar to those of typical slightly doped or undoped polymer semiconductors in which the electronic contribution is nonexistent or not significant.[9] Although measurements of out-of-plane thermal conductivity are quite common

in the literature,[9,16,17] there are only a few reports on the measurements of the in-plane thermal conductivity, $\kappa_{//}$. One accurate way to calculate $\kappa_{//}$ is by measuring the thermal diffusivity along the direction normal to the substrate.[2,18] Then the thermal conductivity is calculated as the product between the density, ρ, the heat capacity, c_p, and the thermal diffusivity, D. Alternatively, Weathers *et al*. used a 4-probe measurement technique[19] based on the 3ω method to measure the in-plane thermal conductivity of conducting PEDOT systems.[5] They demonstrated that $\kappa_{//}$ is linearly correlated with the in-plane electrical conductivity (similarly to the inorganic semiconductors) ($\kappa \approx 2.3 \cdot L_o \cdot T \cdot \sigma$). Consequently, we used this relationship in order to predict $\kappa_{//}$ from σ for the PEDOT:Tos thin film under study and the estimated $\kappa_{//}$ values are summarized in **Table 1**. The ratio between the in-plane and out-of-plane thermal conductivities was calculated and plotted versus the relative crystallinity (see **Figure 3**). It is noteworthy that the anisotropy in the thermal properties of the PEDOT:Tos materials follows a similar trend than the one observed for the electronic conductivity. A rationalization of this phenomenon can also be made by considering the increased amount of edge-on crystallites in the system for the most thermally anisotropic films since the heat transport is facilitated between the charge carriers in "metallic" domains.[5]

	Rel. cryst.	$\mu_{//}$ x10^{-4}(cm^2/Vs)	μ_L x10^{-4}(cm^2/Vs)	$\kappa_{//}$ (W/mK)	κ_L (W/mK)
Pristine	0.22	2.4±0.1	1.29±0.1	1	0.25±0.02
Toluene	0.36	3.2±0.3	1.52±0.1	1.1	0.17±0.02
DMSO	0.40	6.5±0.5	2.21±0.4	1.5	0.16±0.01
Pyridine	0.56	6.9±0.3	2.30±0.2	1.4	0.18±0.01
Pyridine+DMSO	1.00	12.4±1.0	4.08±0.6	2.5	0.18±0.01

Table 1: The relative crystallinity, in-plane and through plane charge carrier mobilities and thermal conductivities for the various PEDOT:Tos thin films.

The anisotropic thermal and electronic conductions in the PEDOT:Tos thin films is also expected to influence the Lorenz number. In fact two Lorenz numbers, the out-of-plane L_L and the in-plane $L_{//}$, can be derived. In order to calculate the Lorenz number, the determination of the electrical conductivity in the two directions is required. The in-plane electrical conductivity was measured with a 4-point probe setup.[10] From the values of $\sigma_{//}$ and $\mu_{//}$, the charge carrier concentration was calculated as 5.8×10^{24} carriers/cm^3. Consequently, by using the charge carrier concentration and the measured out-of-plane charge carrier mobility, the out-of-plane electrical conductivity was extracted and values are summarized in **Table 2**. The out-of-plane L_L and the in-plane $L_{//}$ were as well calculated and plotted against the relative degree of crystallinity (**Figure 5**). It is noteworthy that both values are in the same order of magnitude than the one obtained for metals and semimetals ($\approx 2.45 \times 10^{-8}$ WΩ/K^2),[7] which mirrors the semi-metallic behavior observed from the temperature dependent electrical conductivity measurements in the previous chapter.[20] However, as reported by Weathers *et al*, any deviations of the Lorenz number from the Sommerfield value for conducting polymers at high temperatures ($\approx$ 300 K) originates from the inelastic scattering of phonons in the material, which is inherent to a lower degree of crystallinity.[5,7] Consequently, the Lorenz number is expected to decrease towards the Sommerfield value with the increase of the degree of crystallinity, which is the tendency observed in **Figure 5**.

	$\sigma_{//}$(S/cm)	σ_L (S/cm)	$S_{//}$(μV/K)	L_L x10^{-8} (WΩ/K^2)	$L_{//}$x10^{-8} (WΩ/K^2)
Pristine	230±10	119±9	32±5	7.1±1.0	14.6±3.0
Toluene	310±10	141±9	32.1±5	4.1±0.7	11.9±2.0
DMSO	600±10	204±30	35±5	2.7±0.6	8.4±1.0
Pyridine	580±20	213±18	40±2	2.9±0.4	8.1±1.0
Pyridine+DMSO	1220±30	379±55	44±2	1.6±0.3	6.9±0.6

Table 2: The in-plane and out-of-plane electrical conductivities and Lorenz numbers for the various PEDOT:Tos films.

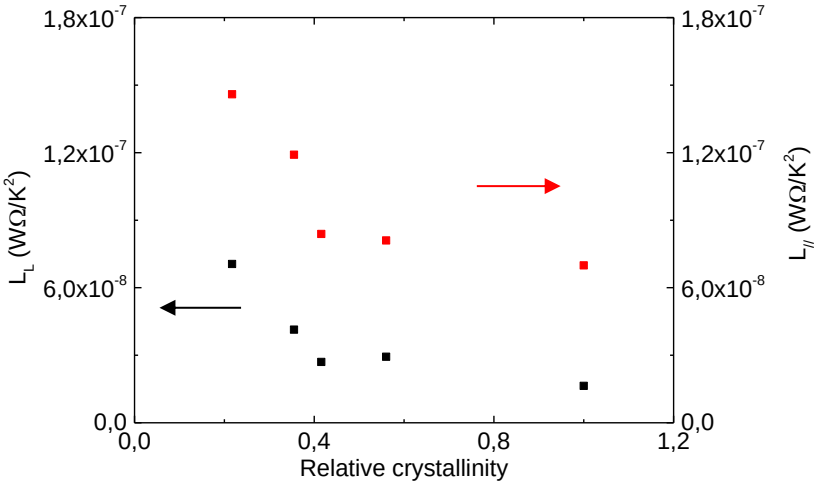

Figure 5: The out-of-plane and in-plane Lorenz numbers for the various PEDOT:Tos films.

However, in conventional inorganic thermoelectrics, a parallel increase of κ and σ usually originates from an increased charge carrier concentration, which is unfavorable for the Seebeck coefficient. As a result, such treatments are detrimental for the thermoelectric efficiency of the material, as the Figure of Merit, $ZT = S^2/L$, is eventually decreased.[6] On the other hand, when the charge carrier concentration is constant, the Lorenz number is indicative of the thermoelectric efficiency of the material, as a decreasing L is beneficial to the ZT. This is the case for the current study. As presented in **Figure 6,** the in-plane Figure of Merit is inversely proportionate to the in-plane Lorenz number, reaching a value of 0.03 for the lowest $L_{//}$. However, this behavior should originate from the increased degree of crystallinity of the systems, as the Lorenz number was shown to be decreasing with these structural modifications.

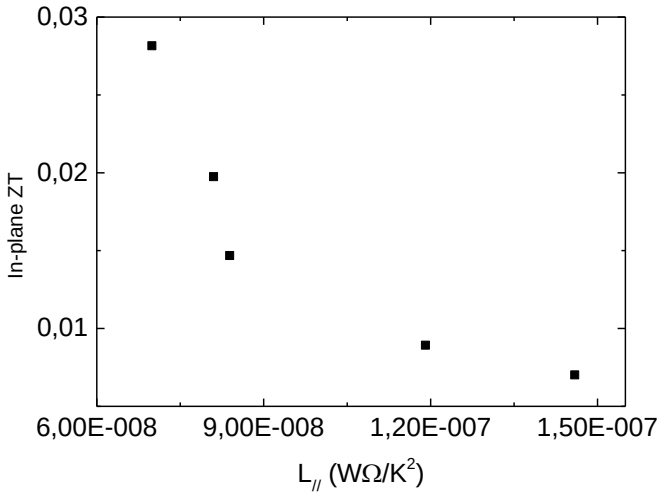

Figure 6: The in-plane ZT plotted against the in-plane Lorenz number for the various PEDOT systems.

In order to further elucidate this behavior, **Figure 7** presents the in-plane and out-of-plane Figure of Merit for the PEDOT:Tos systems plotted against the relative crystallinity. As shown by Wei *et al.*,[2] the out-of-plane Seebeck coefficient is close to the in-plane value, following a ratio of 0.9 for PEDOT derivatives. Based on this formalism, the out-of-plane Seebeck was calculated from the measured in-plane Seebeck using this particular ratio and the out-of-plane *ZT* was extracted. The increase of the thin film crystallinity appears to be beneficial to the *ZT*. This behavior originates not only from the decreasing Lorenz number, but also from an increased Seebeck coefficient with the degree of crystallinity (as shown in Chapter 4). As a result, for the most crystalline material, the Figure of Merit reached the values of 0.028 and 0.095 for the in-plane and out-of-plane directions, respectively. It should be noted though, that the lower out-of-plane thermal conductivity is the main factor resulting in the higher out-of-plane *ZT*.

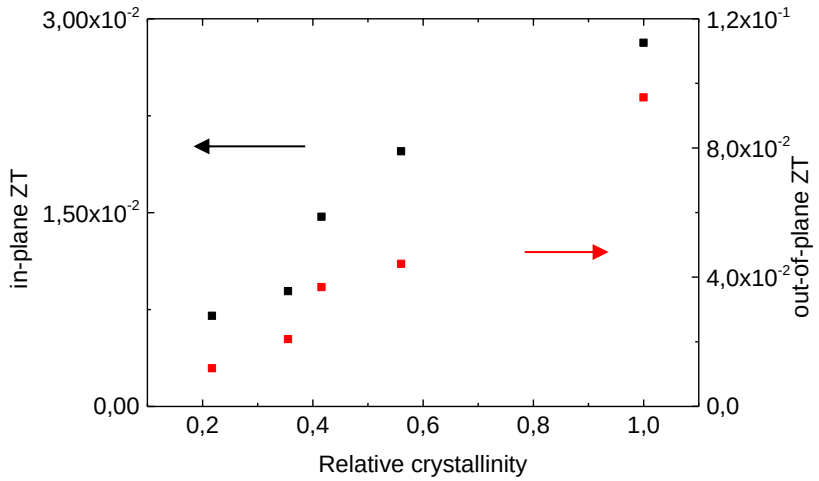

Figure 7: In-plane and out-of-plane ZT plotted against the relative crystallinity for the various PEDOT:Tos films

In the Chapter 4, it was shown that the in-plane Seebeck coefficient follows a power law with respect to the in-plane mobility ($S \approx \mu^{0.2}$). Considering that the electrical conductivity follows the law $\sigma = eN\mu$, and that the thermal conductivity is analogous to σ,[5] a relationship can be extracted between the in-plane Figure of Merit and the in-plane charge carrier mobility. Particularly, for constant charge carrier concentration, ZT can be derived as:

$$ZT \approx A \cdot \frac{\mu^{1.4}}{b \cdot \mu + c} \tag{3}$$

where A, b and c are fitting parameters (**Table 3**).

The parameter A is analogous to the N, T and the elemental charge q as:

$$A = \alpha \cdot q \cdot N \tag{4}$$

while the parameter b is analogous to the charge carrier concentration as:

$$b = w \cdot q \cdot N \tag{5}$$

Using these parameters and **Equation (3)**, a first estimation of the Figure of Merit for a material of given σ, N and μ could be extracted.

Parameters	Fitted values
A	671 $(Vs/cm^2)^{-1.4}$
α	$2.4x10^{-6}$ $((Vs/cm^2)^{-1.4}$ $cm^3/CK)$
b	1174 (Vs/cm^2)
w	$1.3x10^{-3}$ (Ωcm)
c	0.59

Table 3: The fitted parameters on equation (5) from the data plotted in Figure 5.

In **Figure 8** is plotted the in-plane *ZT* against the $\mu_{//}$ for the various PEDOT:Tos samples, while with a red line is presented the fit of the experimental data to **Equation (3)**. The *ZT* appears to be correctly described by **Equation (5)**, and the fitted parameters are presented in the **Table 3**. This finding not only highlights the importance of the electronic and structural properties to the thermoelectric efficiency of the material, but also provides a first estimation of the Figure of Merit for conducting polymers without the need of any thermal or thermoelectric measurements. Hence, the design of more thermoelectrically efficient polymer materials could be facilitated, as only the electrical and electronic measurements would be needed as a guiding rule for the development of new materials.

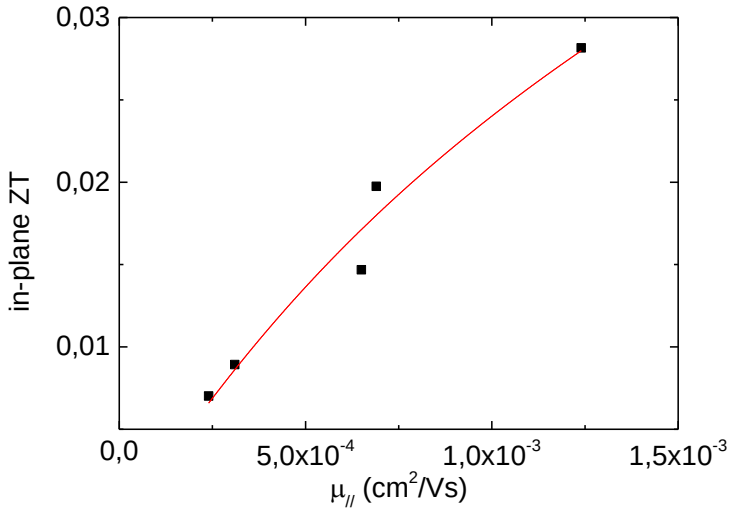

Figure 8: The in-plane ZT vs the in-plane charge carrier mobility. With red is the fitted line with respect to the model described by Equation (5).

5.3 Conclusions:

In this chapter we highlighted the anisotropy of the electronic and thermal properties of PEDOT:Tos materials. Due to its constant carrier concentration, the observed anisotropic properties were directly attributed to the polymer structural properties. The dependence of the charge carrier mobility of the conducting polymer to an preferential edge-on orientation of the crystallites is underlined as the in-plane charge carrier mobility is three orders of magnitude higher than out-of-plane one. The out-of-plane thermal conductivity was not significantly affected by the structural modifications. Afterwards, the Lorenz number was calculated in both directions and was found to decrease with the degree of crystallinity towards the typical values encountered for metals and semimetals. On the other hand, these structural modifications are beneficial for the Figure of Merit, which is increasing with the relative degree of crystallinity. Finally, a relationship was extracted between ZT and μ in the in-plane direction, which can be used to predict the thermoelectric efficiency of new polymer materials.

5.4 References:

1 Sirringhaus, H. *et al.* Two-dimensional charge transport in self-organized, high-mobility conjugated polymers. *Nature* **401**, 685-688 (1999).

2 Wei, Q., Mukaida, M., Kirihara, K. & Ishida, T. Experimental Studies on the Anisotropic Thermoelectric Properties of Conducting Polymer Films. *ACS Macro Letters* **3**, 948-952, doi:10.1021/mz500446z (2014).

3 Nardes, A. M. *et al.* Microscopic Understanding of the Anisotropic Conductivity of PEDOT:PSS Thin Films. *Advanced Materials* **19**, 1196-1200, doi:10.1002/adma.200602575 (2007).

4 Liu, J. *et al.* Thermal Conductivity and Elastic Constants of PEDOT:PSS with High Electrical Conductivity. *Macromolecules* **48**, 585-591, doi:10.1021/ma502099t (2015).

5 Weathers, A. *et al.* Significant electronic thermal transport in the conducting polymer poly(3,4-ethylenedioxythiophene). *Adv Mater* **27**, 2101-2106, doi:10.1002/adma.201404738 (2015).

6 Snyder, G. J. & Toberer, E. S. Complex thermoelectric materials. *Nat Mater* **7**, 105-114 (2008).

7 Chen, G. *Nanoscale Energy Transport and Conversion: A Parallel Treatment of Electrons, Molecules, Phonons, and Photons*. (Oxford University Press, 2005).

8 Charles, K. *Introduction to Solid State Physics*. 7 edn, (Wiley, 1995).

9 Maiz, J. *et al.* Enhancement of thermoelectric efficiency of doped PCDTBT polymer films. *RSC Adv.* **5**, 66687-66694, doi:10.1039/c5ra13452h (2015).

10 Petsagkourakis, I. *et al.* Structurally-driven Enhancement of Thermoelectric Properties within Poly(3,4-ethylenedioxythiophene) thin Films. *Scientific Reports* **6**, 30501, doi:10.1038/srep30501

11 Wei, Q., Mukaida, M., Naitoh, Y. & Ishida, T. Morphological change and mobility enhancement in PEDOT:PSS by adding co-solvents. *Adv Mater* **25**, 2831-2836, doi:10.1002/adma.201205158 (2013).

12 Herlogsson, L., Crispin, X., Tierney, S. & Berggren, M. Polyelectrolyte-Gated Organic Complementary Circuits Operating at Low Power and Voltage. *Advanced Materials* **23**, 4684-4689, doi:10.1002/adma.201101757 (2011).

13 Rutledge, S. A. & Helmy, A. S. Carrier mobility enhancement in poly(3,4-ethylenedioxythiophene)-poly(styrenesulfonate) having undergone rapid thermal annealing. *Journal of Applied Physics* **114**, 133708, doi:10.1063/1.4824104 (2013).

14 Campbell, A. J., Bradley, D. D. C. & Lidzey, D. G. Space-charge limited conduction with traps in poly(phenylene vinylene) light emitting diodes. *Journal of Applied Physics* **82**, 6326-6342, doi:doi:http://dx.doi.org/10.1063/1.366523 (1997).

15 Pernot, G. *et al.* Precise control of thermal conductivity at the nanoscale through individual phonon-scattering barriers. *Nat Mater* **9**, 491-495, doi:http://www.nature.com/nmat/journal/v9/n6/suppinfo/nmat2752_S1.html (2010).

16 Bubnova, O. *et al.* Optimization of the thermoelectric figure of merit in the conducting polymer poly(3,4-ethylenedioxythiophene). *Nat Mater* **10**, 429-433, doi:10.1038/nmat3012 (2011).

17 Kim, G. H., Shao, L., Zhang, K. & Pipe, K. P. Engineered doping of organic semiconductors for enhanced thermoelectric efficiency. *Nat Mater* **12**, 719-723, doi:10.1038/nmat3635 (2013).

18 Wei, Q., Uehara, C., Mukaida, M., Kirihara, K. & Ishida, T. Measurement of in-plane thermal conductivity in polymer films. *AIP Advances* **6**, 045315, doi:doi:http://dx.doi.org/10.1063/1.4948447 (2016).

19 Mavrokefalos, A., Pettes, M. T., Zhou, F. & Shi, L. Four-probe measurements of the in-plane thermoelectric properties of nanofilms. *Review of Scientific Instruments* **78**, 034901, doi:doi:http://dx.doi.org/10.1063/1.2712894 (2007).
20 Bubnova, O. *et al.* Semi-metallic polymers. *Nat Mater* **13**, 190-194, doi:10.1038/nmat3824 (2014).

Chapter 6: Silicon / PEDOT:Tos hybrid thermoelectric generators.

Preface:

The previous chapters aimed at the enhancement of the thermoelectric properties of a p-type polymer thermoelectric material. Nevertheless, a n-type component is also needed for the fabrication of a thermoelectric generator. The PEDOT:Tos thin films synthesized in the previous chapters were thus combined with inorganic n-type materials towards the fabrication of hybrid thermoelectric generators. PEDOT:Tos thin films were deposited on silicon substrates of various doping and electrical conductivities. It was observed that the measured Seebeck coefficient of the junction was dependent of the thickness of the PEDOT:Tos layer. A model of two voltage sources connected in parallel is proposed in order to describe the PEDOT:Tos-Si junction. Additionally, charge exchanges between the two materials were observed by the Capacitance vs Voltage graphs (Mott-Schotky plots) and UPS measurements. The thermoelectric converters that were fabricated with this procedure were exceeding the correspondent inorganic converters. Consequently, a power output of 671 nW was measured for a 5-legs generator.

6.1 Introduction:

Harvesting waste heat by thermoelectric generators (TEG) acts as a potential alternative to conventional petroleum based fuels. Currently, TEGs fabricated from inorganic thermoelectric materials are dominant in the market due to their higher efficiencies, $ZT = \frac{\sigma S^2 T}{\kappa}$.[1,2] State-of-the-art thermoelectric inorganic materials can reach *ZT* as high as 1 close to room temperature.[1] An less conventional approach for the fabrication of TEGs is to use conducting polymer materials.[3-5] As opposed to their inorganic equivalents, conducting polymers are characterized by an intrinsic low thermal conductivity (≈ 0.6W/mK), whereas high values of σ (≈ 1200 S/cm) can be achieved by a proper tuning of the polymer structure.[3,5] Considering their lower cost and higher processability, TEGs based on conducting polymers show great promises even if *ZT* values comparable to the ones of inorganic materials need yet to be achieved.

The main detrimental feature of organic materials for thermoelectricity is related to the intrinsically low Seebeck coefficient.[1,3,5-8] Furthermore, a strong bottleneck for the development of organic TEGs is the n-type thermoelectric polymers which are usually unstable and less efficient than their p-type compartments. Consequently most published reports on polymer thermoelectrics involved either strategies to enhance the Seebeck coefficient of the organic materials[3-5,9-12] or novel synthetic routes towards efficient and stable n-type polymers.[13] Common approaches for the engineering of new n-type materials involved macromolecular engineering,[13-16] structural tuning,[5,11,17,18] charge carrier optimization[4,9,10] and polymer/inorganic nanocomposites,[19-23] with the later showing encouraging results in producing an n-type leg. Indeed, by controlling the interface between the organic matrix and the inorganic charge, the electronic structure of the polymer can be modified leading to a tuning of its electrical and thermoelectric properties.[19,24] Another remarkable approach was

recently presented by Ireland *et al*. where $SnCl_2$ was introduced into n-type polymer semiconductors leading to Power Factor as high as 100 μW/mK^2.[22] Alternatively, p- or n-doped carbon nanotubes blended into a semiconducting polymer matrix were used to fabricate a printed TEG, in which the n-type leg was formed from the bend of n-type carbon nanotube with a p-type semi-conducting polymer.[21] Following those reports, an alternative approach is presented herein, in which PEDOT:Tos thin films are deposited on p- and n-type Si substrates leading to a controlled modulation of the Seebeck coefficient of the junction.

6.2 Results and discussion: Si/PEDOT hybrid materials

Silicon was chosen as the inorganic substrates due to its high industrial importance and its fair thermoelectric (S ≈ 700-1000 μV/K) and thermal (κ ≈ 100 W/mK) properties at room temperature. Although the thermal conductivity of the silicon can be decreased by introducing holes and defects in the structure,[25] the main drawback of silicon is its inherent low electrical conductivity (1-20 S/cm), in comparison to the conventional bismuth telluride (> 2000S/cm).[2,25-27] On the other hand, conducting polymers, like poly(3,4-ethylenedioxythiophene) doped with toluenesulfonate counter ions (PEDOT:Tos), have a relatively high electrical conductivity (500-1200 S/cm) but exhibit a small Seebeck coefficient (≈ 30 μV/K).[5,18] A combination of silicon substrates and PEDOT:Tos thin films could potentially result in a hybrid material that benefits from the advantages of the two components, hindering their corresponding drawbacks.

PEDOT:Tos thin films were deposited on top of silicon wafers, by in-situ polymerization of the polymer on the wafer. The synthesis procedure is described in **Appendix B**. The neat polymer thin film displays on glass substrate an electrical conductivity of 1200 S/cm and a Seebeck coefficient of 44 μV/K (See Chapters 2 and 3). The silicon substrates chosen for this study were of p- and n-type with various electrical conductivities (**Table 1**). The Seebeck coefficients of the p- and n-type silicon substrates were measured as 1000 μV/K and -1100 μV/K, comparable to the reported values.[26,28] Details on the Seebeck measurements are provided in the **Appendix B**. Upon deposition of the PEDOT:Tos films, the electrical conductivity of the system measured with a 4-probe set-up remained unchanged, equal to the value of the PEDOT:Tos thin film on glass, while a remarkable increase of the measured Seebeck coefficient was observed as presented in **Figure 1**.

Substrates	σ_{Si} (S/cm)
n-Si	0.05 , 0.2 , 0.7 , 2.0, 20.0
p-Si	0.7, 20.0

Table 1: The electrical conductivities of the various Silicon substrates used.

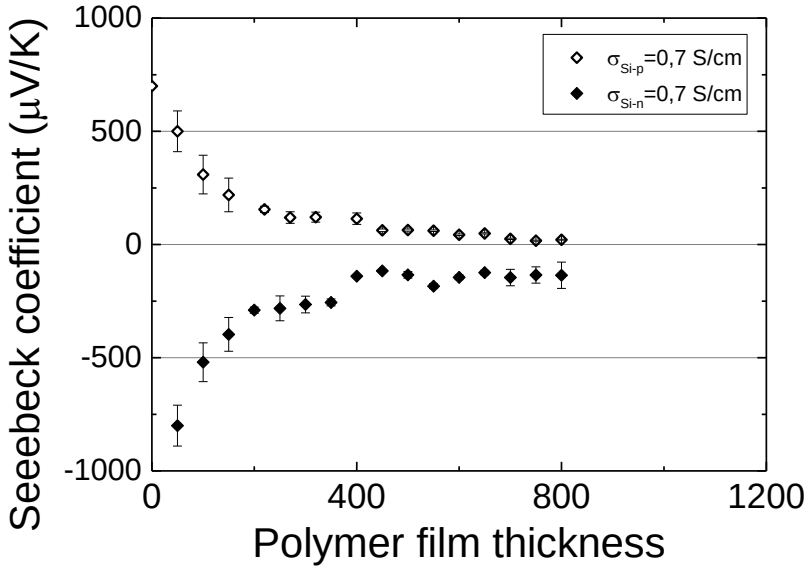

Figure 1: Seebeck coefficient of the hybrid systems against the thickness of the deposited PEDOT:Tos films. With filled points are the values corresponding to n-doped wafers, while the blank points represent p-doped wafers.

A first striking feature apparent in **Figure 1** is that the absolute value of the Seebeck coefficient increases with reduction of the polymer thickness towards the values measured for the Si substrates. For high PEDOT:Tos film thicknesses, the Seebeck coefficient reaches a plateau value dependent of the Si substrate doping type. For the case of a p-type silicon subsatrte, the measured Seebeck coefficient of the thicker PEDOT:Tos samples (800nm) is of the same order of magnitude as the one of the PEDOT:Tos on glass. On the other hand, a

negative value is retrieved for PEDOT:Tos films on n-type Si substrate showing the strong influence of the substrate doping on the thermopower. Consequently this approach allows the tuning of the Seebeck coefficient sign depending of the doping of the substrate.

This behavior was investigated for Si substrates of various doping and conductivities as shown in **Figure 2** and the measured Seebeck coefficient was accordingly tailored by both the PEDOT:Tos film thickness and the doping level of the substrates. Interestingly the plateau value obtained for thick PEDOT:Tos film shows a strong dependence to the intrinsic conductivity of the Si substrates.

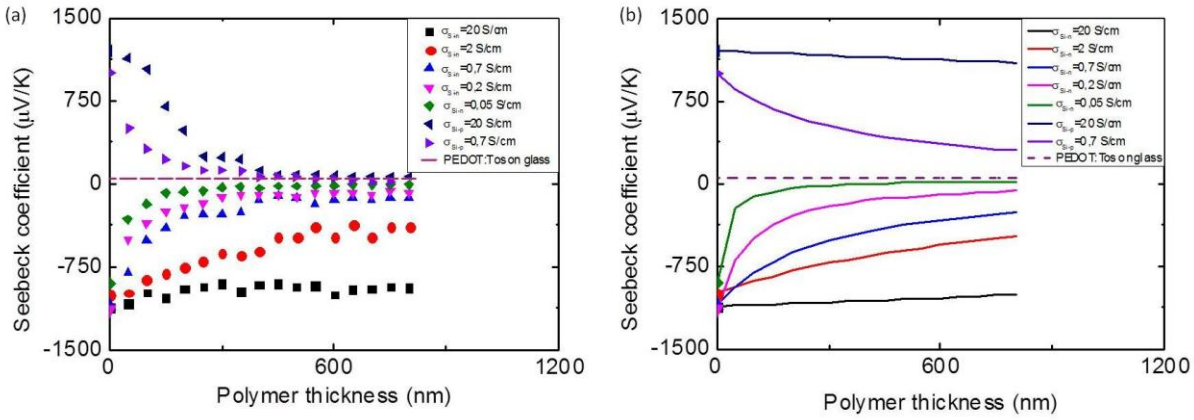

Figure 2: (a) The Seebeck coefficient plotted against the thickness of the polymer layer for the various doping Silicon wafers. (b) With lines are depicted the results of the model (See Equation 1). The thickness of all Silicon wafers used in this study is 500 µm.

In order to gain some insights into the origin of these measured thermoelectric effects, a model considering the PEDOT:Tos-Silicon system as two sources with resistances in parallel was applied to the experimental data (see **Figure 3**). Hence, the calculated total Seebeck coefficient for the junction is described as:

$$S_{measured} = S_{Si} \cdot \frac{1+\frac{S_{pol} \cdot \sigma_{pol} \cdot t_{pol}}{S_{Si} \cdot \sigma_{Si} \cdot t_{Si}}}{1+\sigma_{pol} \cdot \frac{t_{pol}}{\sigma_{Si} \cdot t_{Si}}} \quad (1)$$

where S_{Si}, S_{pol}, σ_{Si}, σ_{pol}, t_{Si} , t_{pol} are the Seebeck coefficient, the electrical conductivity and the thicknesses of the Si substrate and PEDOT:Tos film, respectively.

This resulting Seebeck coefficient data are plotted along the experimental Seebeck coefficient for the various devices on **Figure 2**.

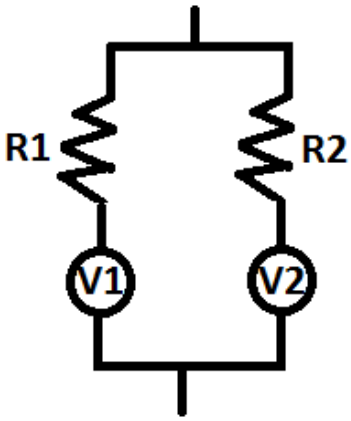

Figure 3: The model system of the two voltage sources and resistances connected in parallel, which was used to describe the thermoelectric properties of the hybrid materials.

This model allows to satisfactorily fit the experimental data for the n-Si/PEDOT:Tos junction but fails to accurately predict the observed behavior of the p-Si/PEDOT:Tos junction. One possible explanation for these discrepancies is related to the role of the interface between the two components which has been shown to play an important role for thermoelectric "nanocomposite" systems.[19,24] As reported by Kislyuk *et al.* and Jackle *et al.*, Schottky junctions are formed between PEDOT:Tos thin films and p-type inorganic semiconductors,[29] while a p/n junction is retrieved for n-type inorganic substrates.[30] This asymmetry is a possible explanation to the different thermoelectric behaviors observed for p- and n-type

substrates. To investigate the role of the interface in these Si/PEDOT:Tos junctions, the interface between the Si substrate and the PEDOT:Tos thin film was severed with a passivation layer following a methodology described by Chua *et al*.[31,32] The passivation layer is a benzocyclobutene derivative which is crosslinkable upon thermal annealing, resulting in films (≈ 50nm) that severe the junction between the inorganic material and the polymer.[31,32] For the passivated junction, the measured Seebeck coefficient was comparable to bulk PEDOT:Tos samples ($S \approx 20$ μV/K) for both p- and n-type substrates which supports the role of the interface in the observed modifications of the Seebeck coefficient. We further exanimated the role of the interface by using Si substrates with a fresh native oxide layer (obtained after a plasma treatment of the wafers). As summarized in **Table 2**, the measured thermoelectric properties of the resulting junctions were similar to the ones measured for the junctions fabricated from as-received Si wafers. However, for silicon wafers of thicker SiO_x layer, the phenomenon is again diminishing, as the measured Seebeck values are comparable to the ones of the polymer on glass (**Table 2**). This behavior can be supported by a tunneling effect in the SiO_x thin layer, which is severed when the oxide layer becomes too thick or when a passivation layer is applied on top of the wafer.[33,34]

Substrates	Seebeck coefficient (μV/K)
Plasma treated n-Si (σ=2S/cm)	-900 ± 50
n-Si with 100nm SiOx	+11± 3
n-Si (σ=2S/cm)	-983 ± 30
Plasma treated p-Si (σ=0.7S/cm)	452 ± 32
p-Si (σ=0.7S/cm)	499 ± 65

Table 2: The Seebeck coefficient of devices fabricated with etched and un-etched Silicon wafers.

However, this tunneling effect does not provide an explanation of the measured high Seebeck coefficient. The Seebeck coefficient of the polymer material is dependent to its Density of States. Thus, any changes in the shape of the DoS, the filling of the DoS, or the Fermi position have to affect the material thermoelectric behavior.[4,5] As shown in Chapters 3 and 4, PEDOT:Tos with higher charge carrier mobility and higher Seebeck coefficient had also a steeper Density of States at the Fermi Level. Ireland *et al*. had reported that the shape of DoS of a polymer/nanocomposite material is affected by both the DoS of the polymer and the DoS of the inorganic compartment.[22] So, PEDOT:Tos of different DoS shapes (and different charge carrier mobilities) should result in hybrid materials of different Seebeck coefficients. Subsequently, PEDOT:Tos of two different DoS shapes (presented in Chapters 3-4) were deposited on the various Si substrates. As presented in **Figure 4**, for polymer films of higher carrier mobility, the absolute Seebeck values were lower for n-doped wafers and higher for p-doped wafers, than that of the lower mobility PEDOT films. Consequently, the hybrid material obtained from the polymer with a steeper DoS at the Fermi Level had also a Seebeck coefficient closer to the bulk values of PEDOT:Tos.

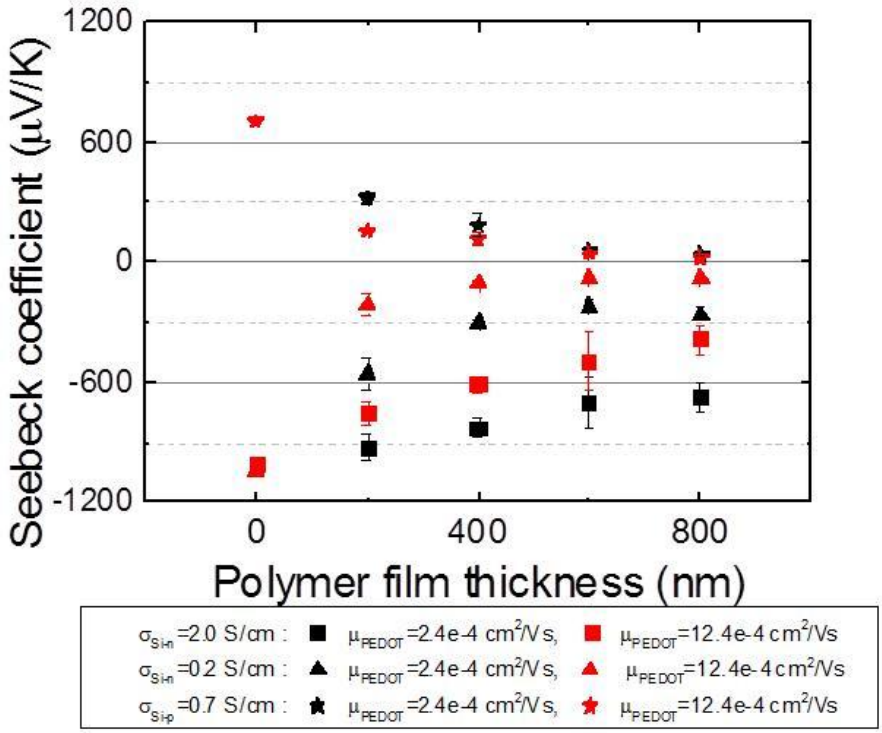

Figure 4: The measured Seebeck coefficient versus the thickness of the deposited PEDOT layer of varying carrier mobility and for p and n-doped wafers of varying electrical conductivity.

In order to correlate these findings to the Density of States of the systems, Ultraviolet Photoelectron Spectroscopy (UPS) was conducted on the PEDOT films with different mobilities on the various Si substrates (details on the UPS measurement are provided in the **Appendix B**). The UPS spectra are presented in **Figure 5** and clear signatures of the inelastic scattering of electrons in the surface at high binding energies and of the PEDOT:Tos HOMO bands at lower binding energies are retrieved. The work functions of the various materials can be extracted from the UPS data and are presented in **Table 3**. Band alignment is evident for n-Si/PEDOT:Tos junctions for the n-Si substrate of higher conductivity as shown in the **Figure 5b**, where the work function of the n-Si/PEDOT:Tos and the bare n-Si overlapped, as opposed to the one of glass/PEDOT:Tos. Additionally, in the lower binding energy area, the band edge of the n-Si/PEDOT:Tos and Glass/PEDOT:Tos overlapped. Consequently, the different

Seebeck coefficients measured on n-Si/PEDOT:Tos and Glass/PEDOT:Tos do not originate from modifications of the band edge structure. Thus, the different Seebeck coefficients were attributed to probable charge exchange at the interface. On the other hand, for n-Si/PEDOT:Tos of lower charge carrier mobility, the work function of the material differs from the one of n-Si substrate, which is indicative of dipoles at the interface of the two materials (**Figure 5a and 5d)**. Additionally, for the p-Si/PEDOT:Tos junctions (**Figure 5c),** the work function is also different to that of the p-Si substrate, regardless of the PEDOT:Tos mobility, implying again the formation of dipoles between the two materials. This finding also highlights the difference between the junctions of the p-Si/PEDOT and n-Si/PEDOT, for the highly conducting PEDOT:Tos films.

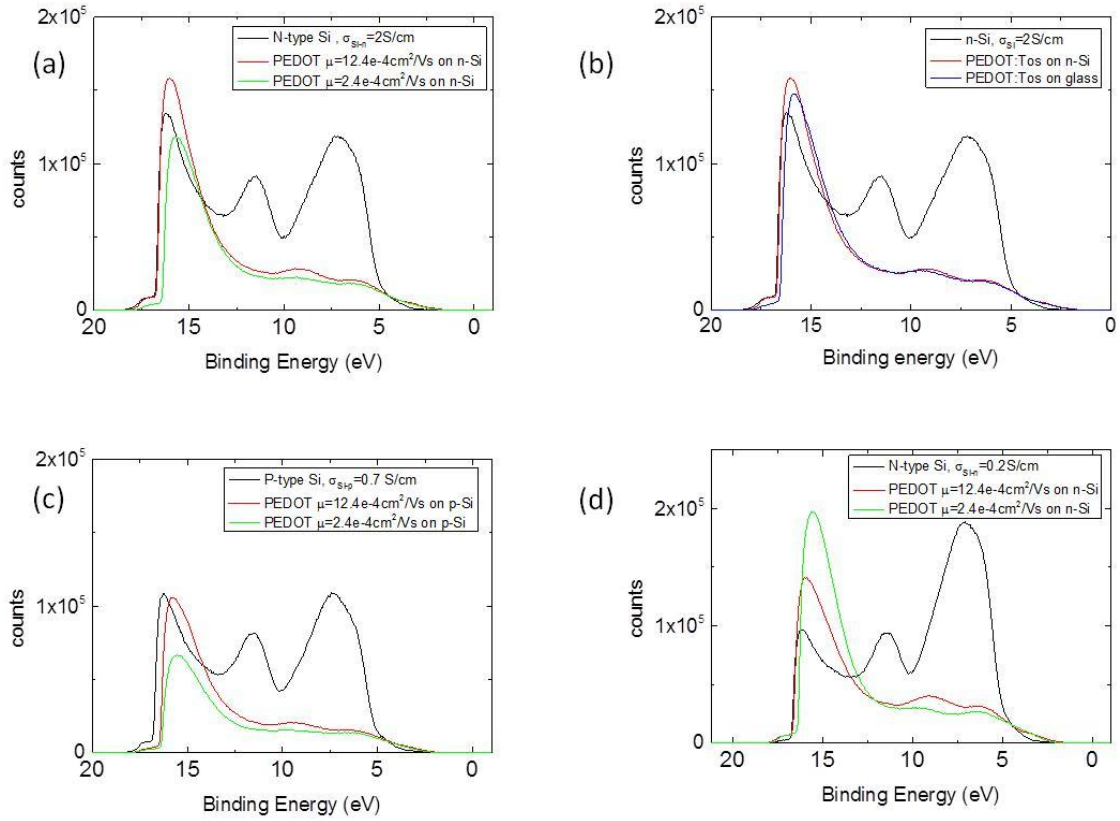

Figure 5: The UPS spectra of the PEDOT:Tos samples on the Silicon substrates with n-doping and σ_{Si}=2S/cm (a) and comparatevely for PEDOT:Tos (μ=12.4x10^{-4} cm^2/Vs) on glass (b) , p-doping and σ_{Si}=0.7S/cm (c) and n-doping and σ_{Si}=0.2S/cm (d)

Substrates	Bare wafer Work function (eV)	PEDOT:Tos (μ=12.4x10^{-4}cm^2/Vs) Work function (eV)	PEDOT:Tos (μ=2.4x10^{-4}cm^2/Vs) Work function (eV)
n-Si (σ=2S/cm)	4.4	4.4	4.8
n-Si (σ=0.2S/cm)	4.4	4.5	4.8
p-Si (σ=0.7S/cm)	4.4	4.8	4.7
glass	--	4.7	--

Table 3: The work function of the PEDOT:Tos films on the various Silicon wafers.

A strong tool to further study the interfacial effects between the Si substrate and the PEDOT:Tos film is the measurement of the capacitance of the system versus the applied voltage. Details on the device fabrication are provided in **Appendix B**. Through the Mott-Schotky plots ($1/C^2$ *versus* V), valuable information on interfacial effects can be obtained such as the presence of depletion/inversion layers,[30,35-38] the Density of States at the interface,[37,39,40] and injection phenomenon of majority or minority charge carriers along the interface.[41] In **Figure 6** the Mott-Schotky plots for devices with a 200 nm PEDOT:Tos film are presented for different doping of the Si substrates. A distinct peak at reverse bias is observed for all the samples on n-doped Si. This peak is due to inductive effects which originate from the injection of minority carriers (*i.e.* electrons) from the Si substrate to the PEDOT:Tos film through the interface. This result is in accordance with the work on Stallinga *et al*. on the interfacial behavior of Si and semiconducting polymer junctions.[41] This feature becomes more distinct with the increase of the silicon electrical conductivity (doping) leading to an increased injection of electrons in the PEDOT:Tos film for higher doping. On the other hand, for the p-

Si/PEDOT:Tos junction, the injection signature appears at forward bias. Consequently, holes are injected from the p-doped Si substrate into the PEDOT:Tos film. In both cases, charge exchange phenomena are observed in the Mott-Schottky graphs.

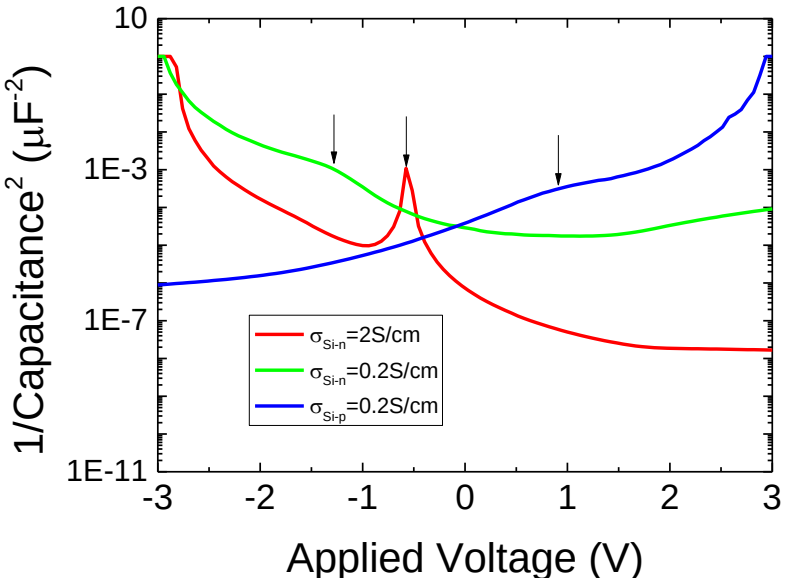

Figure 6: The Mott-Schotky plots for the various Si/PEDOT:Tos junctions. For clarity, the inverse of the square capacitance of the samples on n-doped silicon were normalized to their corresponding value at 3V, while for the p-doped sample it was normalized with respect to the value at -3V.

The Voc/Isc measurements (Fig. 7) for the individual hybrid materials also confirm macroscopically the observed charge transfer effects discussed here above. The V_{oc}/I_{sc} response of the n-Si/PEDOT and the bare Silicon are overlapping (**Figure 7a**). This observation is in agreement with the HOMO alignment and the strong charge exchange as were verified in **Figures 5a** and **6** for the n-Si/PEDOT:Tos (for σ_{Si}=2S/cm). Additionally, the V_{oc}/I_{sc} responce of the less conducting n-Si/PEDOT (**Figure 7b**) and p-Si/PEDOT systems (**Figure 7c**) are also coherent with the observations in **Figures 5** and **6**.

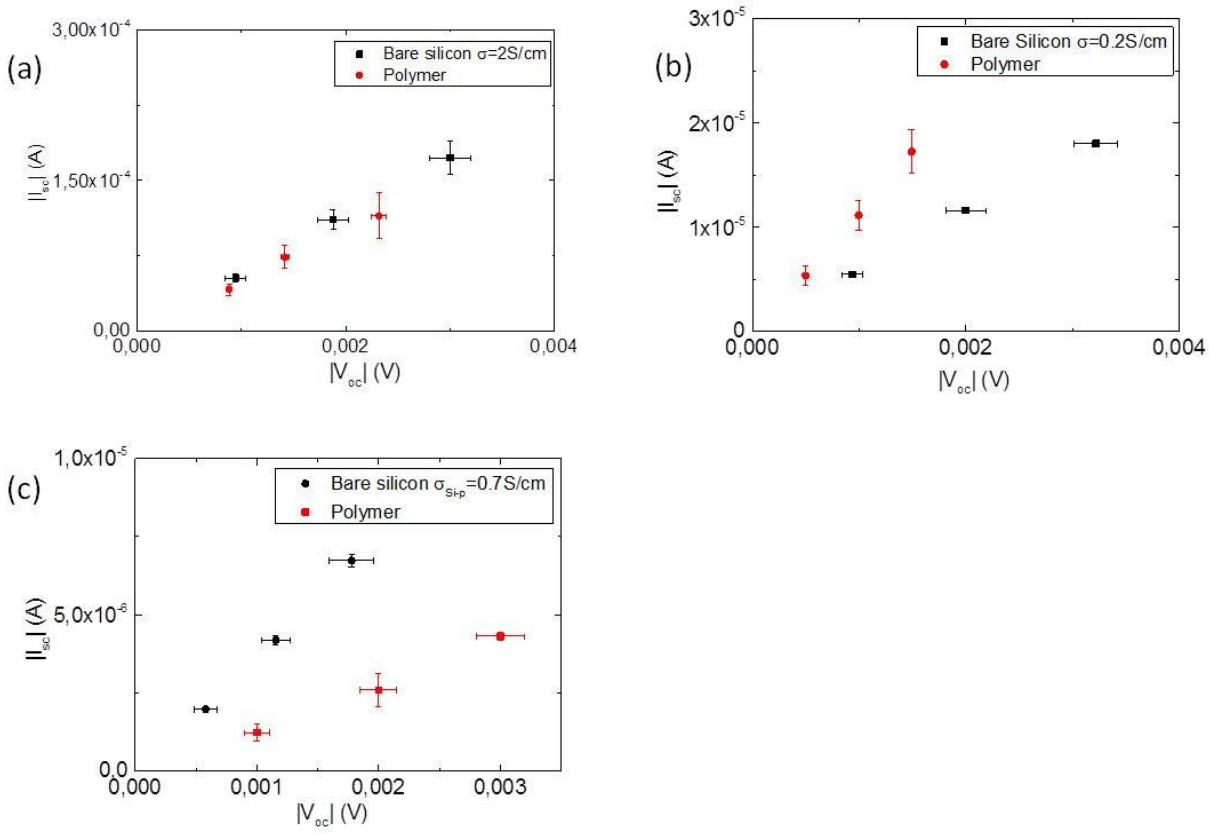

Figure 7: The I_{sc} vs V_{oc} of the separated legs for n-silicon of (a) 2S/cm and (b) 0.2S/cm and for p-silicon of 0.7S/cm

The observed charge carrier exchanges between the PEDOT:Tos film are strictly related to a filling/unfilling of the Density of States of the two materials (i.e the PEDOT DoS is filled and the Si DoS is unfilled). Considering the sensibility of the Seebeck coefficient to the filling of the DoS, these findings indirectly provide an explanation to the increased Seebeck values of the hybrid materials. Additionally, Kislyuk *et al* demonstrated that the Density of States of a CdS/PEDOT system is modified with the thickness of the polymer films.[29] They reported that the UPS spectra of thinner PEDOT films on CdS are comparable to the bare CdS spectra, while the HOMO of the PEDOT would be only measured for thicker films. These findings are coherent with the differences in Seebeck coefficient values observed

for the PEDOT:Tos films under study, as the value of the Seebeck coefficient is modified with the polymer thickness (**Figure 1**).

To strengthen our experimental observations on the Seebeck measurements of Si/PEDOT:Tos junctions, thermoelectric converters were fabricated using this hybrid configurations. More details on the device fabrication are presented in the **Appendix B**. Measurements in short circuit conditions were conducted inside a Faraday cage using the same Seebeck measurement setup. For these TEGs, n-doped Si (2 S/cm) and p-doped Si (0.7 S/cm) substrates were used and 50 nm PEDOT:Tos films were deposited on top of the substrates. The resulted thermovoltages were 1.4, 1.55 and 1.7 mV for a temperature difference of 1 K at room temperature, and increased to 7.8, 8.8 and 11 mV for a 5 K gradient for devices with 3, 4 and 5 legs, respectively. In order to compare the hybrid devices with the respective inorganics, TEGs with only Silicon were also fabricated. As presented in **Figure 8**, the devices with only Silicon provide a higher thermovoltage but lower short circuit current comparatively to the hybrid devices, which is translated in lower generator internal resistance for the hybrids.

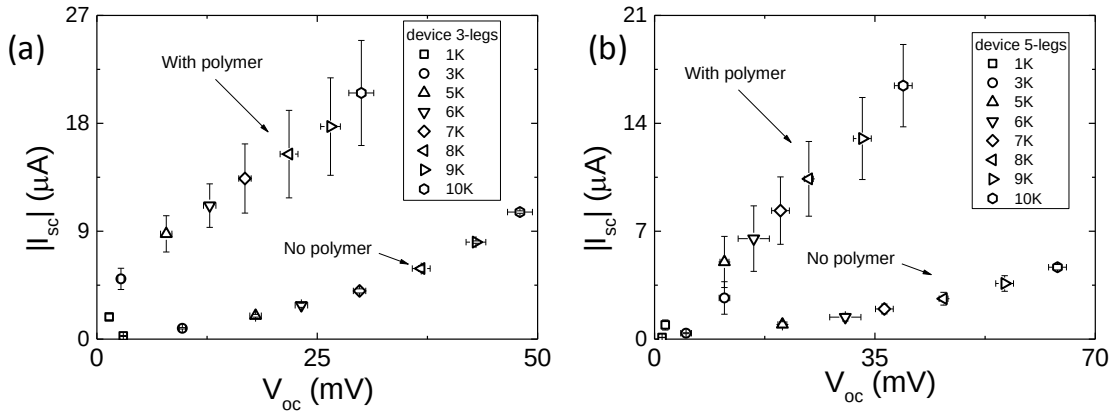

Figure 8: The short circuit current plotted against the thermovoltage for devices with 3(a), and 5(b) legs, for temperature differences form 1 to 10K.

The Power Output was subsequently calculated as the product between the short circuit current and the thermovoltage.[3,42] **Figure 9** presented the output power as function of the temperature gradient for the TEGs examined in this study.

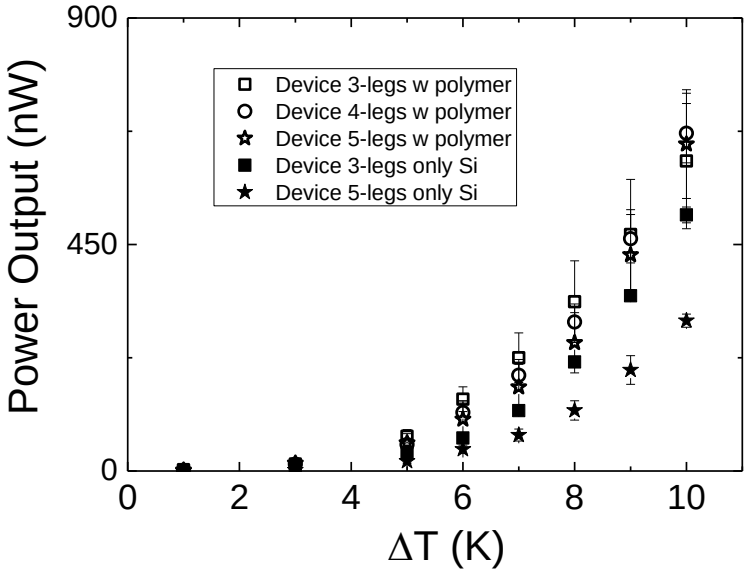

Figure 7: Power Output for the various TEGs, plotted against the applied temperature difference, at room temperature.

It is observed that the power output increased with the temperature difference in a similar manner to the one reported in the literature for organic thermoelectric generators.[3,4,8] The highest output power, 671nW, was obtained for the device with 5 legs at T_{diff} = 10K. It is noteworthy the power output of the Si/PEDOT:Tos junctions exceeded that of the Si devices. The origin of this feature is attributed to the higher I_{sc} current measured for the Si/polymer devices (**Figure 8**). Nevertheless, to our best knowledge this is a record high Power Output for a thermoelectric generator with only 5 legs, utilizing a conducting polymer. By increasing

the legs connected in-series the power output shall also increase, thus higher efficiencies are expected for devices of i.e. 100 legs.

6.3 Conclusion:

In the present study, the influence of various doping Si-substrates on the Seebeck coefficient of a Si/PEDOT:Tos junction was examined. It was shown that the Seebeck coefficient of such junctions can be tuned in magnitude and sign depending of the Si doping type and electrical conductivity. These findings were explained from modifications on the Density of States of the hybrid material, which was supported by measuring devices fabricated with different PEDOT materials and further elucidated by UPS measurements, where charge exchange phenomena were observed. These phenomena were translated as the migration of minority charge carriers at the interface between the Silicon and polymer. That was justified by Capacitance - Voltage characteristics of the systems. Thermoelectric Generators were also fabricated, utilizing these hybrid materials by putting to our advantage the observed Seebeck modifications. The Power Output per area was increasing with the number of legs per generator and with the applied temperature difference, thus resulting to a record high power of 671 nW, for a 5-legs generator at $\Delta T = 10K$ near room temperature.

6.4 References:

1 Zhao, L. D. Ultrahigh power factor and thermoelectric performance in hole-doped single-crystal SnSe. *Science* **351**, 141-144 (2016).

2 Snyder, G. J. & Toberer, E. S. Complex thermoelectric materials. *Nat Mater* **7**, 105-114 (2008).

3 Bubnova, O. & Crispin, X. Towards polymer-based organic thermoelectric generators. *Energy & Environmental Science* **5**, 9345, doi:10.1039/c2ee22777k (2012).

4 Bubnova, O. *et al.* Optimization of the thermoelectric figure of merit in the conducting polymer poly(3,4-ethylenedioxythiophene). *Nat Mater* **10**, 429-433, doi:10.1038/nmat3012 (2011).

5 Bubnova, O. *et al.* Semi-metallic polymers. *Nat Mater* **13**, 190-194, doi:10.1038/nmat3824 (2014).

6 Chen, Y., Zhao, Y. & Liang, Z. Solution processed organic thermoelectrics: towards flexible thermoelectric modules. *Energy Environ. Sci.* **8**, 401-422, doi:10.1039/c4ee03297g (2015).

7 Ghosh, S., Maiyalagan, T. & Basu, R. N. Nanostructured conducting polymers for energy applications: towards a sustainable platform. *Nanoscale* **8**, 6921-6947, doi:10.1039/c5nr08803h (2016).

8 He, M., Qiu, F. & Lin, Z. Towards high-performance polymer-based thermoelectric materials. *Energy & Environmental Science* **6**, 1352, doi:10.1039/c3ee24193a (2013).

9 Bubnova, O., Berggren, M. & Crispin, X. Tuning the thermoelectric properties of conducting polymers in an electrochemical transistor. *J Am Chem Soc* **134**, 16456-16459, doi:10.1021/ja305188r (2012).

10 Khan, Z. U. *et al.* Acido-basic control of the thermoelectric properties of poly(3,4-ethylenedioxythiophene)tosylate (PEDOT-Tos) thin films. *J. Mater. Chem. C* **3**, 10616-10623, doi:10.1039/c5tc01952d (2015).

11 Kim, G. H., Shao, L., Zhang, K. & Pipe, K. P. Engineered doping of organic semiconductors for enhanced thermoelectric efficiency. *Nat Mater* **12**, 719-723, doi:10.1038/nmat3635 (2013).

12 Kim, G.-H., Kim, J. & Pipe, K. P. Humidity-dependent thermoelectric properties of poly(3,4-ethylenedioxythiophene):poly(styrene sulfonate). *Applied Physics Letters* **108**, 093301, doi:10.1063/1.4942598 (2016).

13 Russ, B. *et al.* Power factor enhancement in solution-processed organic n-type thermoelectrics through molecular design. *Adv Mater* **26**, 3473-3477, doi:10.1002/adma.201306116 (2014).

14 Oshima, K., Shiraishi, Y. & Toshima, N. Novel Nanodispersed Polymer Complex, Poly(nickel 1,1,2,2-ethenetetrathiolate): Preparation and Hybridization for n-Type of Organic Thermoelectric Materials. *Chemistry Letters* **44**, 1185-1187, doi:10.1246/cl.150328 (2015).

15 Shi, K. *et al.* Toward High Performance n-Type Thermoelectric Materials by Rational Modification of BDPPV Backbones. *J Am Chem Soc* **137**, 6979-6982, doi:10.1021/jacs.5b00945 (2015).

16 Sun, Y. *et al.* Organic thermoelectric materials and devices based on p- and n-type poly(metal 1,1,2,2-ethenetetrathiolate)s. *Adv Mater* **24**, 932-937, doi:10.1002/adma.201104305 (2012).

17 Petsagkourakis. Synergetic optimization of the thermoelectric properties of conducting polymers. (to be submitted).

18 Petsagkourakis, I. *et al.* Structurally-driven Enhancement of Thermoelectric Properties within Poly(3,4-ethylenedioxythiophene) thin Films. *Scientific Reports* **6**, 30501, doi:10.1038/srep30501

19 Coates, N. E. *et al.* Effect of interfacial properties on polymer-nanocrystal thermoelectric transport. *Adv Mater* **25**, 1629-1633, doi:10.1002/adma.201203915 (2013).

20 Yee, S. K., Coates, N. E., Majumdar, A., Urban, J. J. & Segalman, R. A. Thermoelectric power factor optimization in PEDOT:PSS tellurium nanowire hybrid composites. *Phys Chem Chem Phys* **15**, 4024-4032, doi:10.1039/c3cp44558e (2013).
21 Dorling, B. *et al.* Photoinduced p- to n-type Switching in Thermoelectric Polymer-Carbon Nanotube Composites. *Adv Mater* **28**, 2782-2789, doi:10.1002/adma.201505521 (2016).
22 Ireland, R. M. *et al.* ZT > 0.1 Electron-Carrying Polymer Thermoelectric Composites with In Situ SnCl2Microstructure Growth. *Advanced Science* **2**, n/a-n/a, doi:10.1002/advs.201500015 (2015).
23 Wang, H. *et al.* Thermally Driven Large N-Type Voltage Responses from Hybrids of Carbon Nanotubes and Poly(3,4-ethylenedioxythiophene) with Tetrakis(dimethylamino)ethylene. *Adv Mater* **27**, 6855-6861, doi:10.1002/adma.201502950 (2015).
24 Malen, J. A., Yee, S. K., Majumdar, A. & Segalman, R. A. Fundamentals of energy transport, energy conversion, and thermal properties in organic–inorganic heterojunctions. *Chemical Physics Letters* **491**, 109-122, doi:10.1016/j.cplett.2010.03.028 (2010).
25 Tang, J. *et al.* Holey silicon as an efficient thermoelectric material. *Nano Lett* **10**, 4279-4283, doi:10.1021/nl102931z (2010).
26 Boukai, A. I. *et al.* Silicon nanowires as efficient thermoelectric materials. *Nature* **451**, 168-171, doi:10.1038/nature06458 (2008).
27 Yamamoto, A., Ogawa, K. & Takeuchi, T. Effect of Chemical Potential on Thermoelectric Power of Bi2Te3 and Bi2Se3. *Materials Transactions* **52**, 1539-1545, doi:10.2320/matertrans.E-M2011809 (2011).
28 Geballe, T. H. & Hull, G. W. Seebeck Effect in Silicon. *Physical Review* **98**, 940-947, doi:10.1103/PhysRev.98.940 (1955).
29 Kislyuk, V. V., Fedorchenko, M. I., Smertenko, P. S., Dimitriev, O. P. & Pud, A. A. Interfacial properties and formation of a Schottky barrier at the CdS/PEDOT : PSS hybrid junction. *Journal of Physics D: Applied Physics* **43**, 185301, doi:10.1088/0022-3727/43/18/185301 (2010).
30 Jackle, S. *et al.* Junction formation and current transport mechanisms in hybrid n-Si/PEDOT:PSS solar cells. *Sci Rep* **5**, 13008, doi:10.1038/srep13008 (2015).
31 Chua, L.-L., Ho, P. K. H., Sirringhaus, H. & Friend, R. H. High-stability ultrathin spin-on benzocyclobutene gate dielectric for polymer field-effect transistors. *Applied Physics Letters* **84**, 3400, doi:10.1063/1.1710716 (2004).
32 Chua, L.-L. *et al.* General observation of n-type field-effect behaviour in organic semiconductors. *Nature* **434**, 194-199, doi:http://www.nature.com/nature/journal/v434/n7030/suppinfo/nature03376_S1.html (2005).
33 Waxman, A., Shewchun, J. & Warfield, G. Tunneling in MIS structures—II. *Solid-State Electronics* **10**, 1187-1198, doi:http://dx.doi.org/10.1016/0038-1101(67)90060-3 (1967).
34 Terman, L. M. An investigation of surface states at a silicon/silicon oxide interface employing metal-oxide-silicon diodes. *Solid-State Electronics* **5**, 285-299, doi:http://dx.doi.org/10.1016/0038-1101(62)90111-9 (1962).
35 Aydoğan, Ş., Sağlam, M. & Türüt, A. Reverse bias capacitance–voltage characteristics of Al/polyaniline/p-Si/Al structure as a function of temperature. *Journal of Non-Crystalline Solids* **354**, 4991-4995, doi:10.1016/j.jnoncrysol.2008.07.015 (2008).
36 Lin, Y.-J. *et al.* Capacitance–voltage and current–voltage characteristics of Au Schottky contact on n-type Si with a conducting polymer. *Journal of Physics D: Applied Physics* **42**, 165104, doi:10.1088/0022-3727/42/16/165104 (2009).
37 Shrotriya, V. & Yang, Y. Capacitance–voltage characterization of polymer light-emitting diodes. *Journal of Applied Physics* **97**, 054504, doi:10.1063/1.1857053 (2005).
38 Yu, X. *et al.* High Efficiency Organic/Silicon-Nanowire Hybrid Solar Cells: Significance of Strong Inversion Layer. *Sci Rep* **5**, 17371, doi:10.1038/srep17371 (2015).

39 Kuik, M. *et al.* 25th anniversary article: charge transport and recombination in polymer light-emitting diodes. *Adv Mater* **26**, 512-531, doi:10.1002/adma.201303393 (2014).
40 Kavak, P., Deneb Menda, U., Alturk Parlak, E., Özdemir, O. & Kutlu, K. Excess current/capacitance observation on polymer–fullerene bulk heterojunction, studied through I–V and C/G–V measurements. *Solar Energy Materials and Solar Cells* **103**, 199-204, doi:10.1016/j.solmat.2012.03.026 (2012).
41 Stallinga, P. *et al.* Minority-carrier effects in poly-phenylenevinylene as studied by electrical characterization. *Journal of Applied Physics* **89**, 1713, doi:10.1063/1.1334634 (2001).
42 Goupil, C., Seifert, W., Zabrocki, K., Müller, E. & Snyder, G. J. Thermodynamics of Thermoelectric Phenomena and Applications. *Entropy* **13**, 1481 (2011).

Thesis Conclusions

The main objective of this Ph.D. thesis, the fabrication of an efficient polymer thermoelectric material was successfully tackled. The basic philosophy of the work was to elucidate the relationship between structure and thermoelectric/electronic properties of the material, towards efficient thermoelectric design. Alternatively, the interfacial effects between the polymer material and an inorganic wafer were utilized in order to fabricate a novel hybrid thermoelectric generator.

The structure of the PEDOT:Tos systems was tuned via various different methods, all of which had left unaffected the carrier concentration of the material. In Chapter 2, high boiling point solvents like DMSO were added to the oxidant solution and acted as plasticizers during the annealing step of the PEDOT deposition. As a result, the electronic and electrical properties of the material were enhanced by a factor of 3, resulting to a Power Factor of 75 $\mu W/mK^2$.

Afterwards, in Chapter 3, the Power Factor was further increased via the simultaneous addition of pyridine and DMSO to the synthesis. An organic base like pyridine acts as an inhibitor to the polymerization process, slowering down the reaction process. As a result, the crystallinity of the PEDOT:Tos material was highly increased. This lead to a simultaneous increase of the electrical conductivity, the Seebeck coefficient and the charge carrier mobility of the material. Hence, the Power Factor was enhanced up to 236 $\mu W/mK^2$, which is up to 10 times more than the value of the pristine material, without any additives.

The observed enhancements in the Power Factor of the material presented in the Chapters 2 and 3 were structurally and mobility driven. Thus, it rose the question if there is a correlation between Seebeck coefficient and the charge carrier mobility. This question was

answered in Chapter 4, where the Seebeck coefficient was shown to follow a mild dependence on the charge carrier mobility. This correlation was also supported by UPS measurements were a broadened band edge was observed for the material with the higher Seebeck coefficient and higher degree of crystallinity. Insights on the charge transport mechanism were also extracted from low temperature electrical conductivity measurements. All systems were found to follow the VRH transport model, while a transition was observed at low temperatures.

The Figure of Merit of those PEDOT:Tos materials was calculated and presented in Chapter 5. Particularly, the structural anisotropy that was found in Chapters 2 and 3 were resulting in an anisotropy in both the electronic and the thermal properties of the material. It was found that the lorenz number of the PEDOT material was decreasing towards the Sommerfield value with increasing degree of crystallinity, which agreed to the findings on the conduction mechanism of Chapter 4. Finally, a relationship between the Figure of Merit and the charge carrier mobility, in the in-plane direction was extracted, as a means to predict the thermoelectric efficiency of future materials.

In the final chapter of this thesis, the PEDOT:Tos material was combined with p and n type Silicon wafers. It was observed that the measured Seebeck value of the hybrid material could be tuned via increasing the thickness of the polymer layer. Although the origin of this behavior is not completely clarified, it could be appointed to interfacial charge transfer phenomena. That hypothesis was solidified by UPS and capacitance measurements were charge transfer in the interface of the two materials was observed. Thermoelectric generators were fabricated by using these hybrid systems and their behavior was recorded with respect to the temperature difference. A high power output of 671 nW was recorded for a TEG of 5 legs and a temperature difference 10K. Comparatevely to the literature, this is the highest output

reported for a hybrid TEG, opening the road for an alternative fabrication of novel thermoelectric devices.

Direct perspectives of this thesis are not only to thoroughly elucidate the underlying phenomena after the observation on the polymer/inorganic systems. A different inorganic material could be used instead of Silicon, while doped inorganic charges could be introduced in the conducting polymer in order to tune the properties of the hybrid material. Additionally, further studies should be done with respect the optimized design of the hybrid thermoelectric generator, as its dimensions are playing important role in the device efficiency.

Appendix A: Theoritical background

A.1 Classical thermodynamic approach of thermoelectric phenomena:

Thermoelectric phenomena are characterized by a coupling between the heat flux and the electric current in a material. Thermoelectric devices can either harvest waste heat into useful energy or act as heat sinks upon an applied voltage. In the first case, a temperature gradient results in the production of a voltage, the so-called Seebeck effect. As opposed, the Peltier effect describes the presence of heating or cooling at an electrified junction of two different conductors. Although, thermoelectric effects were discovered in the 19th century by Johann Seebeck (1821) and Jean Peltier (1834), actual applications only appears in the 1950's, due to the complexity to engineer thermoelectric devices[1-3]. Thermoelectric effects are thus a unique category of thermodynamic phenomena, where fluxes between the charge carriers, $\overrightarrow{J_N}$, and heat carriers $\overrightarrow{J_Q}$, are intervened, resulting in coupling between the electrochemical potential μ_{ec} and the temperature T.[2-4] Without any temperature gradient, the system is at equilibrium without any concerted charge carriers diffusion. Whereas, when a temperature gradient is being applied, the "hot" carriers diffuse from the hot side to the cold side leading to the establishment of a particle flux. For this system, the conservation of energy ($\overrightarrow{J_E}$ being the energy flux) is described as:

$$\overrightarrow{J_E} = \overrightarrow{J_Q} + \mu_{ec} \cdot \overrightarrow{J_N} \qquad (1)$$

Given that the heat and entropy flows are related as:

$$\overrightarrow{J_Q} = T \cdot \overrightarrow{J_S} \qquad (2)$$

The equation (1) can be transformed as:

$$\overrightarrow{J_E} = T \cdot \overrightarrow{J_S} + \mu_{ec} \cdot \overrightarrow{J_N} \quad (3)$$

Following the description of Onsager and Callen,[1-3,5-8] linear relationships can be established between the fluxes and the potentials, since μ_{ec} and T are the driving potentials for the phenomena described by equation (3):

$$\begin{bmatrix} \overrightarrow{J_N} \\ \overrightarrow{J_S} \end{bmatrix} = -\begin{bmatrix} L_{11} & L_{12} \\ L_{21} & L_{22} \end{bmatrix} \cdot \begin{bmatrix} \vec{\nabla}\mu_{ec} \\ \vec{\nabla}T \end{bmatrix} \quad (4)$$

The equation (4) can be transformed considering an electrical field $\vec{E} = -q\vec{\nabla}\mu_e$:

$$\begin{bmatrix} \overrightarrow{J_e} \\ \overrightarrow{J_Q} \end{bmatrix} = \begin{bmatrix} q^2L_{11} & qL_{12} \\ TqL_{21} & TL_{22} \end{bmatrix} \cdot \begin{bmatrix} \vec{\mathrm{E}} \\ -\vec{\nabla}T \end{bmatrix} \quad (5)$$

where $\overrightarrow{J_e}$ is the flux of electricity and $\underline{\sigma} = \begin{bmatrix} q^2L_{11} & qL_{12} \\ TqL_{21} & TL_{22} \end{bmatrix}$ is the conductivity matrix (L_{12} and L_{21} obey Onsager's symmetry leading to $L_{12} = L_{21}$).

If the system is not under a temperature gradient, then the equation (5) is reduced to the Ohm's law:

$$\overrightarrow{J_e} = q^2L_{11} \cdot \vec{E} \quad (6)$$

Consequently the electrical conductivity is given by:

$$\sigma = q^2 L_{11} \tag{7}$$

On the other hand, if a temperature gradient is applied to the system (**Figure 1b**), a coupling takes place between the heat and particle fluxes. This temperature gradient generates an electric current which is directly related to the measured thermovoltage. Thus, by applying a field equal to the produced thermovoltage in order to counter the particle flux (therefore $\overrightarrow{J_N}$ = 0), the equation (5) can be rewritten as:

$$q^2 L_{11} \cdot \vec{\mathrm{E}} - \ qL_{12} \cdot \vec{\nabla} T = 0$$

Hence the Seebeck coefficient is defined as:

$$S \equiv \frac{E}{\nabla T_{|\overrightarrow{J_N}=0}} = \frac{L_{12}}{qL_{11}} \tag{8}$$

Furthermore, given the same conditions, the heat flux can be rewritten as the Fourier law:

$$\overrightarrow{J_Q} = \left(-\frac{L_{12}}{qL_{11}} TqL_{21} \ + \ TL_{22}\right) \cdot \left(-\vec{\nabla} T\right) \tag{9}$$

in which the thermal conductivity, κ, is defined as $\kappa = -\frac{L_{12}}{qL_{11}} TqL_{21} \ + \ TL_{22}$

For the case of the Peltier effect, an external applied field results in a heat flux, without the application of an external applied temperature difference. Thus, the equation (5) can be rewritten as:

$$\begin{bmatrix} \overrightarrow{J_e} \\ \overrightarrow{J_Q} \end{bmatrix} = \begin{bmatrix} q^2 L_{11} \\ TqL_{21} \end{bmatrix} \cdot \begin{bmatrix} \vec{\mathrm{E}} \end{bmatrix}$$

Consequently, the Peltier coefficient is defined as:

$$\Pi \equiv \frac{\overrightarrow{J_Q}}{\overrightarrow{J_e}_{|\nabla T=0}} = \frac{TL_{21}}{qL_{11}} \qquad (10)$$

Due to Onsager's symmetry, $L_{12} = L_{21}$ and taking into account the definition of the Seebeck coefficient, $S \equiv \frac{E}{\nabla T_{|\overrightarrow{J_N}=0}} = \frac{L_{12}}{qL_{11}}$, one can write:

$$\Pi = S \cdot T \qquad (11)$$

Equation (13) implies the reversibility between the two sister thermoelectric phenomena, the Seebeck and the Peltier effect.[1-4,8]

Using the relationships (8) and (10), the conductivity matrix can be re-written as:

$$\underline{\sigma} = \begin{bmatrix} \sigma & S\sigma \\ TS\sigma & \kappa(1+ZT) \end{bmatrix}$$

In which the dimensionless figure of merit ZT is defined as:

$$ZT = \frac{S^2\sigma}{\kappa} T \qquad (12)$$

As implied by equations (4), (5) and (11), the observed thermoelectric effects are heavily dependent of the intrinsic material properties[2]. Consequently an adequate tailoring of the material properties is essential for an efficient thermoelectric converter.

A thermoelectric module is comprised of two compartments – the so-called "legs" - where the one is conducting holes (p-type) and the other is conducting electrons (n-type) (**Figure 1**). With this configuration of dissimilar materials, the current can flow in the circuit under a temperature gradient, and hence produce power.

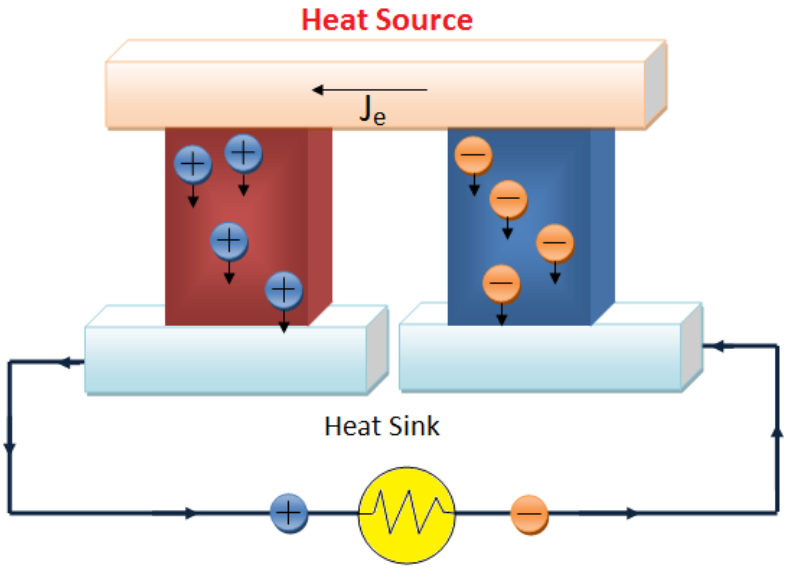

Figure 1: A schematic representation of a thermoelectric generator. The hole conducting (p-type) and electron conducting (n-type) thermoelectric legs are represented in red and blue, respectively.

For such thermoelectric generator, the efficiency of a thermodynamic cycle is defined as:

$$\eta = \left(1 - \frac{T_C}{T_H}\right) \cdot \frac{W}{Q_H} \qquad (13)$$

where W is the produced work and Q_H is the provided heat, while $\left(1 - \frac{T_C}{T_H}\right)$ is the efficiency of an ideal Carnot engine.

For a thermoelectric cycle, the efficiency can be expressed as a function of *ZT:*[1,3,4,8,9]

$$\eta_{Max} = \left(1 - \frac{T_C}{T_H}\right) \cdot \left(\frac{\sqrt{1+ZT}-1}{\sqrt{1+ZT}+1}\right) \quad (14)$$

As a result, in order to maximize the efficiency of a thermoelectric device, the figure of merit, *ZT*, must be also maximized. From a thermodynamic point of view, an efficient thermoelectric material must have low thermal conductivity and high electrical conductivity and Seebeck coefficient, at a given temperature. The pursuit of this "balance" between the three aforementioned properties is the very heart of the thermoelectric materials research society. In the following paragraph, a solid state description of the parameters influencing these properties will be presented.

A.2 Thermoelectric properties - a general solid state physics approach:

By using the notion of the Density of States, the electrical conductivity and the Seebeck coefficient can be derived for thermoelectric systems. The Density of available states or Density of States, *D(E)*, is defined as the number of possible states that an electron can occupy per unit volume and per energy interval. [10-12] **Figure 2** presents a typical Density of States diagram for a bulk crystal.[10,11] Although the notion of the Density of States is a mathematical concept, its shape and filling can be used to apprehend the electrical, electronic and thermoelectric properties of a material.

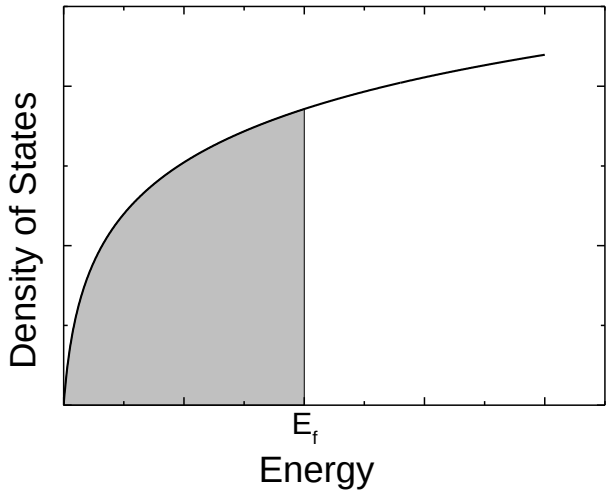

Figure 2: Density of States of electrons in a bulk crystal at 0 K. The occupied states are depicted with the gray area, while the highest filled level is the Fermi Level.

In electron rich systems, quasi-continuous bands (energy levels) are formed, separated by continuous forbidden regions called band gaps. At 0 K, the charge carriers always fill the lowest energy level first, inside the valence band, while the highest filled energy state is called

the Fermi Level, E_f. The electronic band above the Fermi Level is called the conduction band and the forbidden region between them is the Band Gap, E_g , as shown in **Figure 3** .[10-13] The possibility of an electron to occupy a certain available state/level of these bands at an absolute temperature T is described by the Fermi-Dirac distribution $f_0(E)$:[12]

$$f_0(E) = \frac{1}{1+\exp\left(\frac{E-\mu}{k_B T}\right)} \qquad (15)$$

where μ is the chemical potential and k_B the Boltzmann constant.

At temperatures close to 0 K, the aforementioned chemical potential equals the Fermi level, E_f [11].

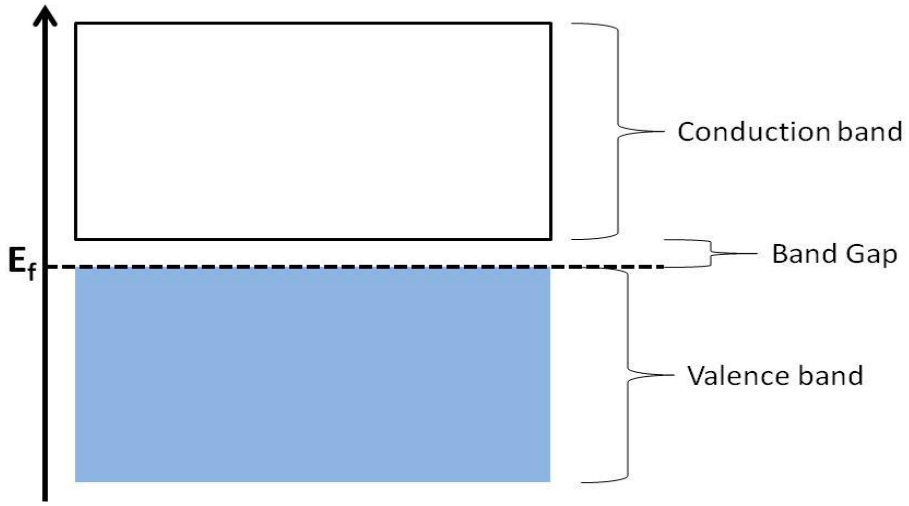

Figure 3: Band structure of a material (at T = 0 K) with filled valence band (blue), and unfilled conduction band with the Band Gap separating them. This band structure is representative of a typical semiconductor or insulator.

Considering that $D(E)$ is the number of available states that the carriers can occupy, and that $f_0(E)$ is the probability of an electron to occupy a state, the integral of their product on

all possible energy levels represents the actual number of charge carriers per volume in the system, *N*. Hence, for *T*>0 and with energy *E* in the system:[10-12]

$$N = \int_o^\infty f_0(E) \cdot D(E) dE \qquad (16)$$

N is also called the carrier concentration or the charge carrier density, and is one of the key parameter in order to tune the properties of semiconducting materials.

A material can be classified as insulator, semiconductor and metal depending on its band gap and the filling of its Density of States.[11,14] In **Figure 4** the various cases of band structures for insulator, semimetal, metal and semiconductor are presented.

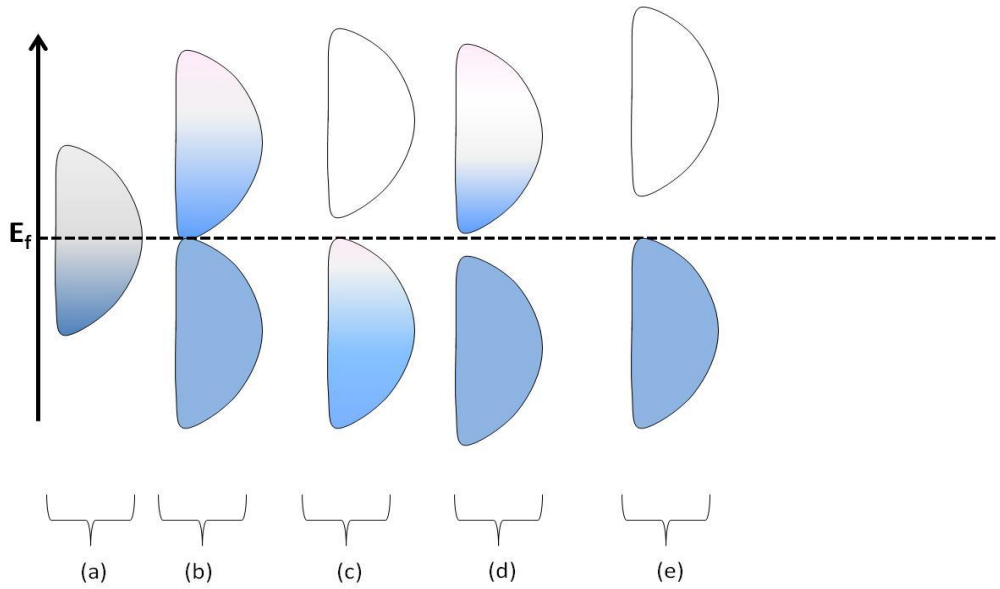

Figure 4: Band structure for a metal, (a), a semimetal, (b), a p-type semiconductor, (c), a n-type semiconductor, (d), and an insulator, (e). With white and blue colour are the unfilled and filled states respectively. With light-blue appear, the partially filled bands.

In metals there is a full overlap between the valence and the conduction bands (**Figure 4a**), while for semimetals only the bottom of the conduction band overlaps with the top of the

valence band (**Figure 4b**). In both cases the band gap is inexistent and the Fermi Level exists inside one of these two bands. On the other hand, insulators (**Figure 4e**) usually have a filled valence band and a band gap above 2 eV. The fourth case, the semiconductor, is an intermediate case between a metal and an insulator. A semiconductor has a band gap E_g < 2 eV, while differences between the filling of the two bands can result in a p- or n-type semiconductor. When the conduction band is unfilled and the valence band is semi-filled, the material is a p-type semiconductor (**Figure 4c**), and holes (the absence of an electron) are the major charge carriers. On the opposite, a semiconductor that conducts electrons is denominated as n-type (**Figure 4d**). Its valence band is fully filled and there are also filled states in the conduction band. This partial filling of bands in semiconductors allows to finely tune the band structure. This tuning can occur either by filling/emptying the states or by modifying the shape of the Density of States.[10-14]

The effect of those modifications in *D(E)* become apparent to the macroscopic properties of the materials, when they are expressed as a function of the Density of States. The electric current, J_e (A/m^2), can be re-expressed as:[12]

$$J_e = \frac{q}{3} \cdot \int v^2 \cdot \tau \cdot \left(q\epsilon \frac{\partial f_0}{\partial E}\right) D(E)dE + \frac{q}{3} \cdot \int v^2 \cdot \tau \cdot \left(\frac{\partial f_0}{\partial x}\right) D(E)dE \qquad (17)$$

where ϵ is the one-dimensional field $\vec{E}$, τ is the relaxation time and v the drift velocity of the charge carriers in the system.

Equation (17) can also be reformulated as:

$$J_e = q \cdot N \cdot \mu_e \cdot \epsilon + q \cdot a \cdot \frac{\partial N}{\partial x} \qquad (18)$$

where, *N*, is the carrier concentration as defined in equation (16), μ_e is the charge carrier mobility (m^2/Vs) and *a* is the carrier diffusivity (m^2/s).

Equation (18) is also called the drift-diffusion equation[12]. In the first part of this relationship, the electrical conductivity can be identified as

$$\sigma = q \cdot N \cdot \mu_e \tag{19}$$

where:

$$\mu_e = \frac{\frac{q}{3}\int_o^\infty v^2 \cdot \tau \cdot \left(\frac{\partial f_0}{\partial E}\right) \cdot D(E)dE}{\int_o^\infty f_0(E) \cdot D(E)dE} \tag{20}$$

Consequently the electrical conductivity can be defined as:

$$\sigma = \frac{q}{3} \cdot \int_o^\infty v^2 \cdot \tau \cdot \left(\frac{\partial f_0}{\partial E}\right) \cdot D(E)dE \tag{21}$$

The importance of the shape and the filling of the Density of States to material properties is highlighted in the extracted relationships for electrical conductivity and charge carrier mobility. Practically speaking, the electrical conductivity of a semiconducting material can be increased either by increasing the carrier concentration (i.e. the filling the states) or by increasing the carrier mobility. Considering that the carrier mobility is the measure of the mobile properties of individual electrons in the system, tuning of μ_e can be achieved by modifications of the material structure. For example, the mobility of an amorphous semiconductor is lower than the mobility of a semi-crystalline or crystalline one as the amorphous material exhibits more structural defects inhibiting the transport of electrons.

Furthermore, following equation (18), the diffusivity of the charge carriers can be written as:

$$a = \frac{\frac{1}{3}\int_o^\infty v^2 \cdot \tau \cdot f_0 \cdot D(E)dE}{\int_o^\infty f_0(E) \cdot D(E)dE} \approx \frac{k_B T}{q} \cdot \mu_e \tag{22}$$

Equation (22) is called the Einstein relationship and correlates the mobility with the diffusivity. This equation is only valid when the distribution function follows a Boltzmann distribution law.[12,15,16]

Additionally, the Seebeck coefficient can be derived from the Onsager relationships that connect *S* with σ, so *S* is written as:

$$S = \frac{\frac{1}{qT}\cdot\int_o^\infty v^2\cdot\tau\cdot(E-\mu)\cdot\left(\frac{\partial f_0}{\partial E}\right)\cdot D(E)dE}{\int_o^\infty v^2\cdot\tau\cdot\left(\frac{\partial f_0}{\partial E}\right)\cdot D(E)dE} \quad (23)$$

The influence of the Density of States on the Seebeck coefficient is also evident in the relation (23). But, in contrast to the electrical conductivity, the Seebeck coefficient appears to have a strong dependence to the position of the chemical potential with respect to the Density of States, as implied by the (E-μ) term inside the integral. Effectively, equation (23) shows that the Seebeck coefficient is a measure of the average energy of a carrier above the chemical potential under open circuit conditions, weighted against the differential electrical conductivity at each energy level.[12]

At low temperature close to 0 K, the value of the chemical potential is close to the Fermi Level. Thus the charge carrier density $N(E)$ is equal to the Density of States, $D(E)$. Additionally to these assumptions, if metallic conduction is also assumed, equation (21) can be re-written as:[14,17,18]

$$\sigma = \sigma(E,T) = \frac{q}{3}\cdot\frac{v^2\cdot\tau}{k_B\cdot T}\cdot D(E) \quad (24)$$

where $\sigma(E,T)$ it the Mott's energy dependent electrical conductivity.

With the same assumptions of low temperature and metallic conduction, the mobility can be re-written as energy dependent:

$$\mu_e(E,T) = \frac{q}{3}\cdot\frac{v^2\cdot\tau}{k_B\cdot T} \quad (25)$$

and the diffusion coefficient:

$$a(E,T) = \frac{1}{3} \cdot v^2 \cdot \tau \tag{26}$$

Subsequently, the Seebeck coefficient is derived as:

$$S(E,T) = \frac{\pi^2}{3} \cdot \frac{{k_B}^2 T}{q} \cdot \left(\frac{\partial ln(\sigma(E))}{\partial E}\right)_{E=E_f} \tag{27}$$

which can be re-written as:[14,17,18]

$$S(E,T) = \frac{\pi^2}{3} \cdot \frac{{k_B}^2 T}{q} \cdot \left(\left(\frac{1}{\mu_e(E,T)} \cdot \frac{\partial(\mu_e(E,T))}{\partial E}\right)_{E=E_f} + \left(\frac{1}{D(E,T)} \cdot \frac{\partial(D(E,T))}{\partial E}\right)_{E=E_f}\right) \tag{28}$$

Consequently the Seebeck coefficient is analogous to:

- the slope of the Density of States at Fermi Level
- the slope of the energy dependent "metallic" mobility at Fermi Level

Following these arguments, the DoS slope for a metal is close to zero, resulting in low Seebeck coefficient, as shown in **Figure 5a**. For a semimetal and a semiconductor, both the value and the sign of the Seebeck coefficient is adjusted by tuning the position of the Fermi Level with respect to the Density of States, as shown in **Figures 5b-5d.** If the slope is negative at the Fermi level, like for the n-type semiconductor (**Figure 5d**), the Seebeck coefficient is negative. On the other hand, a p-type semiconductor has a positive slope and thus a positive Seebeck coefficient.[11,14,19]

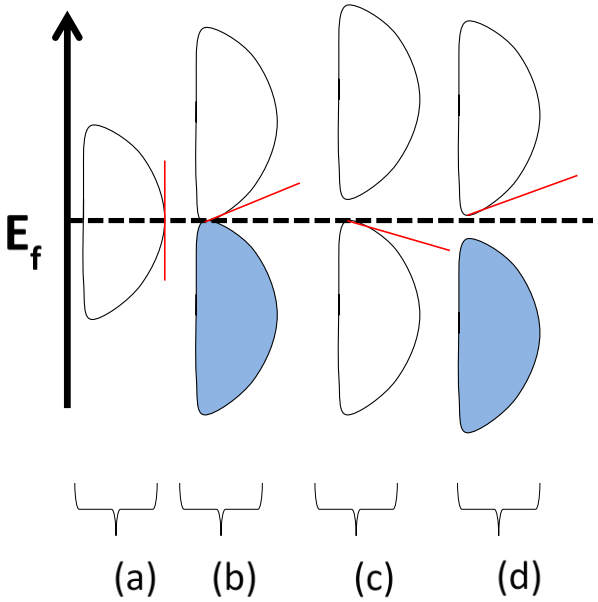

Figure 5: The band structure at T close to 0 K for a metal (a), a semimetal (b), a p-type semiconductor (c), and a n-type semiconductor (d). The red line is representative of the slope of the Density of States at the Fermi Level. The figure is adapted from Kittel *et al*. [20]

Nevertheless these relationships are only effective at T close to 0 K. When the temperature starts to increase, the chemical potential is shifting away from the Fermi Level due to the presence of defects in the material (e.g. structural defects). These defects modify the distribution of carriers in the different states (i.e. the Fermi-Dirac distribution).[11,12] As a result, the equations (24)-(28) are strictly valid at low temperatures close to 0 K and energies near the Fermi position.

A.3 Charge transport in π-conjugated systems:

The field of polymer electronics was given birth by the discovery of Shirakawa, Mac Diarmid and Heeger in 1977, that oxidized conjugated polymers could behave electrically as a metal. Upon exposure to iodine vapors, the doped polyacetylene (**Figure 6a**) become as electrically conductive as typical metals, like copper. [10,21,22]

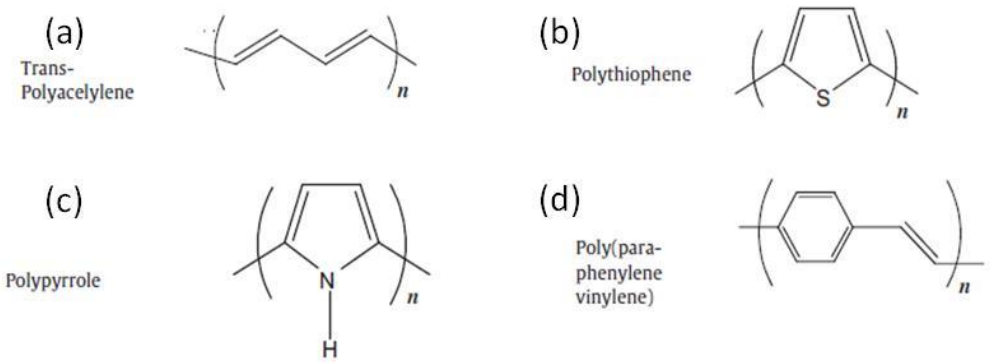

Figure 7: Typical semiconducting polymers[22]

Since then, many other polymer architecture have been synthesized, bearing similar electrical properties to that of polyacetylene, like polythiophene, polypyrrole and poly (paraphenylvinylidene) (**Figure 6b-6d**). All these polymers have a common structural characteristic; they are all π-conjugated systems.

In a π-conjugated system, the electrons of the carbon molecules of the units are delocalized in an extended π-system due to the double bonds (like in Polyacetylene) or benzyl groups (like in PPV). [10,23] This electron delocalization is prerequisite for the expression of the electronic properties of the polymer, as systems with electron delocalization exhibit a (semi)conducting behavior. In fact, these π-bonds where the electrons are delocalized are the HOMO of the material and the π*-anti-bonds are the respective LUMO. If the band gap of the organic substance is too large, like for ethylene or a simple benzene molecule (bang gap >

4eV), the material is insulating. For a conjugated chain, the extension of each π-π* bond in the system results in the recombination of the unit π-orbitals, which is electronically translated to the addition of states to the HOMO and the LUMO. Consequently, the band gap is being reduced and the material acts a semiconductor.[10,23-25]

Hence, Polyacetylene, due to its structure of alternated π-bonds, is intrinsically semiconducting. Upon oxidation with iodine vapors, radical ions are formed on the polyacetylene chain, which are called solitons (**Figure 7**). The solitons add extra states to the HOMO-LUMO levels, lowering even more the band gap of the polymer. Hence the polymer shows increased electrical conductivity associated with a metallic behavior.[22,26-29]

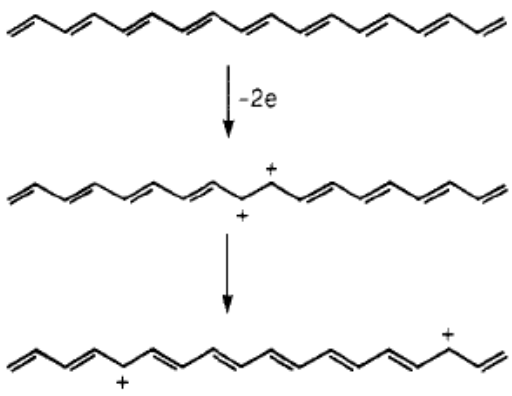

Figure 7: Polyacetylene (upper) and the formed solitons on the chain upon oxidation (middle and down) [25]

On the other hand, materials like undoped polythiophenes are not intrinsically semiconducting and they have to be doped in order to achieve a semiconducting (or conducting) behavior. In such un-doped polymers, the electrons are only localized in the π-orbitals of their unit. When the chain is oxidized (for a π-doped polymer) or reduced (for a n-doped polymer), an electron is taken (for p) or given (for n) to the polymer units. Consequently, the thiophene rings configuration is changed to the quinoid form (**Figure 8**), so the newly formed double bonds enable the recombination of the π-orbitals, extending the π-

system along the chain. As a result, the charge carriers (holes in p-type and electrons in n-type) are being delocalized in the doped polymer chain, which reduces the band gap and grants to the material a semiconduncting behavior.[10,23,25,30]

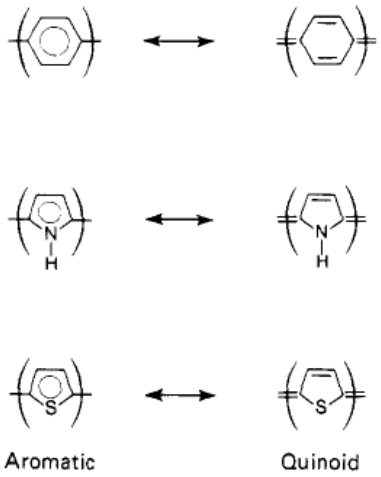

Figure 8: Aromatic to quinoid form for various semiconducting polymers.[25]

The charge carriers that are formed in these extrinsically semiconducting polymers are called polarons or bipolarons. Upon the redox doping, the chain conformation changes from an aromatic to a quinoid form, leading to a chain lattice relaxation; a polaron. In π-conjugated systems, a polaron extends over three monomer units (**Figure 9**) and assists in the extension of the π-system. As a result, electronic states are added in the HOMO and the LUMO levels (**Figure 10**), and are referred to polaron bands.[24,25,30,31]

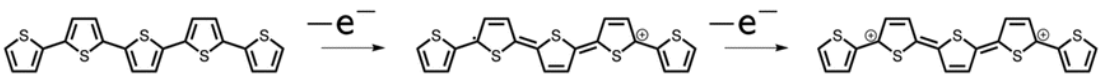

Figure 9: Formation of a polaron (center) and a bipolaron (left) for an oligothiophene [32].

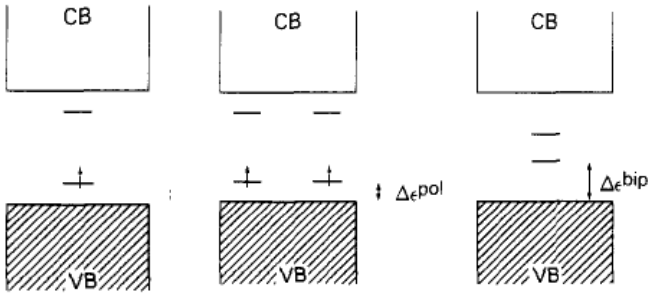

Figure 10: Band structure of 1 polaron (left), 2 polarons (center) and one bipolaron (right) [25]

Additional doping of the system results in formation of bipolarons instead of multiple polarons. When a second polaron is being formed in a chain, a bipolaron is spontaneously created (**Figure 10**). A bipolaron is an extended lattice relaxation that gives an energy ΔE_K to the system, which is larger than the repulsion between the two ions. Hence, it is thermodynamically more favorable to form a new polaron besides the already existing polaron of the chain, than to anywhere else in the chain. Therefore, a bipolaron band of higher energy is formed (**Figure 10**). At even higher dopant concentration, the number of bipolarons is further increased, resulting in the formation of widened bipolaron bands in the material (**Figure 11**). [24,25,31]

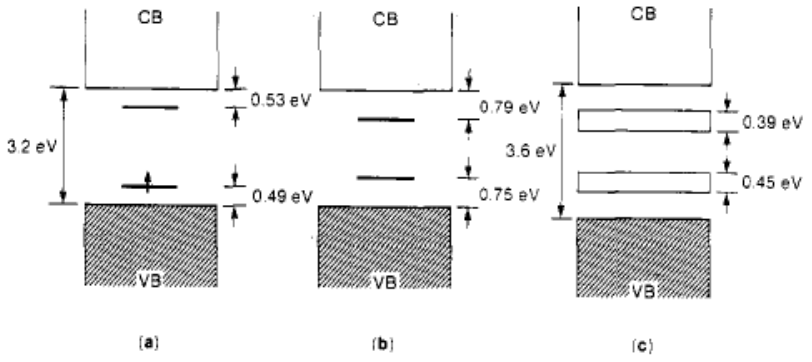

Figure 11: Evolution of the polypyrrole band structure upon doping: (a) low doping level, polaron formation; (b) moderate doping level, bipolaron formation; (c) high (33%) doping level, formation of bipolaron bands [25]

All these electronic states (solitons, polarons or bipolarons) formed in the system, constitute the Density of States of the polymer, which is filled with the redox processes. At low dopant concentration, the DoS of the polymer resembles that of a conventional inorganic semiconductor. On the other hand, when the doping is increased (and the band gap is decreased), the polymer DoS resembles that of a metal or a semimetal. In these synthetic metals, the HOMO of the highly doped polymer is the work function of the material.[24,25,30]

The formation of those energy bands, should result in *band transport* mechanism of the charge carriers between the different energy bands in the polymer material. But band transport prerequisites to have a perfect crystal in the material, which is not the case for polymers. In reality, the main charge transport mechanism is the thermally activated hopping transport in which the charge carriers 'hop' between the different units in an interchain and intrachain level (**Figure 12**).[10,21,23,33]

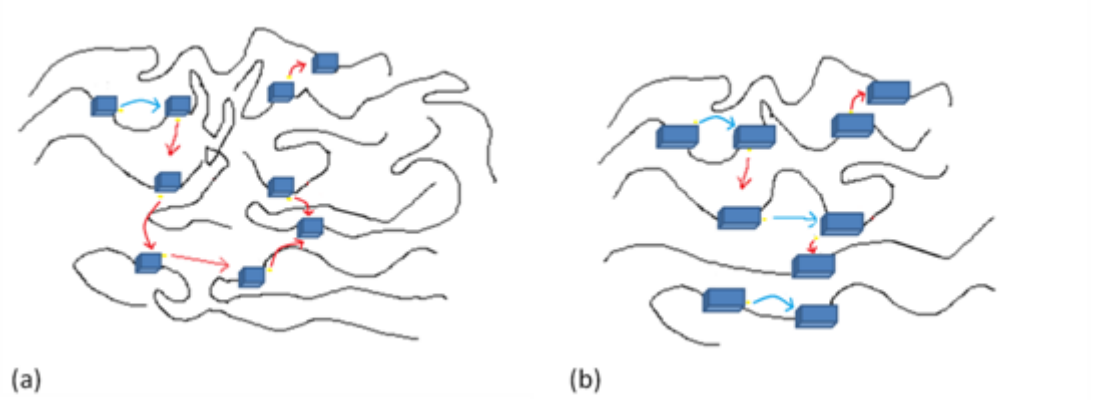

Figure 12: (a) Hopping transport in a conducting polymer of low degree of crystallinity, where the hopping transport occurs mainly in one direction. The red and the blue arrows show the hopping of the charge carriers between the metallic islands at the interchain level and at a intrachain level, respectively. (b) Hopping transport in a higher crystallinity system where a 2-D hopping behavior becomes more dominant.

These hopping sites are the extended π-systems formed between the chain units, which are inherently conducting. In highly doped conducting polymers, these conducting formations are called "metallic" islands and are dispersed inside the amorphous polymer matrix.[33] Concerning the DoS of the polymer, the distribution of these metallic islands in the amorphous matrix heavily affects the shape of the Density of States. Consequently, the electronic structure and electronic properties of doped polymer materials are highly dependent on the structural properties such as the degree of crystallinity and the chain orientation.

In a material with a high degree of crystallinity, π-orbitals are able to be recombined, resulting in a much extended π-system. Hence, larger "metallic islands" are formed in the amorphous insulating matrix and charge carriers are more mobile in the material. Also, the chains with a higher conjugation length benefit from the intrachain hopping transport resulting in an enhanced charge carrier mobility. On an interchain level, the hopping transport occurs either normal to level of the chain backbone or out-of-normal to the polymer backbones. The latter configuration is more beneficial to charge transport since the π-orbitals are at a closer distance leading to an increased hopping between the sites. Hence, the charge carriers are more mobile along the π-stacking distance, which is usually equal to 3.4 Å.[34] In a conducting polymer material where all three aforementioned structural parameters are being satisfied at the intrachain and interchain levels, the π-orbitals recombine into a much extended π-system (**Figure 13**), called a "bipolaron network".[35]

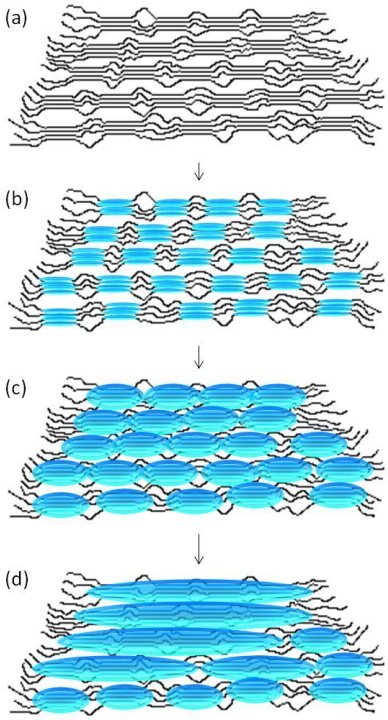

Figure 13: A “bipolaron network”. (a) A semicrystalline doped polymer, where bipolarons are the charge carriers. (b) The same polymer depicted with the π-orbitals of the individual doped conjugated chains (in blue). The π-orbitals of the various chains recombine (c), extending the π-system. Finally, due to the high crystallinity of the doped chains, the various π-orbitals overlap, resulting in a much wider π-system (d), a bipolaron network.[21,35]

From a thermoelectric point of view, that ideal conformation of the "bipolaron network" benefits the Seebeck coefficient of the material. The Mott's equation on thermoelectricity (equation 27) dictates that the Seebeck coefficient of a material is analogous to the slope of the DoS at the Fermi Level. In a doped conducting polymer with a “bipolaron network”, the band edge is broader due to the extended π-system. Hence, the slope of the DoS at E_F is steeper and the Seebeck coefficient of the material is higher.

Of course, for thermoelectric optimization, doping levels of the material must be also considered. Increasing the carrier concentration will add more states to the HOMO, narrowing

the band gap. Thus, the slope of the DoS will be decreased, resulting to a lower Seebeck coefficient of the material. Consequently, proper and detailed material design is needed in order to achieve high performance thermoelectric materials.[21]

In most highly conducting systems, like poly(3,4-ethylenedioxythiophene), the electrical conductivity of the material follows the thermally activated variable range hopping (VRH) model, proposed by Mott (equation 29).[14,33]

$$\sigma = \sigma_o \cdot e^{-(\frac{T_o}{T})^p} \quad (29)$$

In this equation, the prefactor σ_o has a negligible temperature dependence, while the parameter T_o is related to the Fermi position of the polymer and the localization length of the polymer charge carriers on the chains. The parameter p is connected to the dimensionality, d, of the hopping transport ($p = \frac{1}{1+d}$) and can take a value between 0.5, 0.33 and 0.25 which correspond to 1-D, 2-D and 3-D hopping transport. This dimensionality is an indication of the preferential hopping direction of the charge carriers.[33,36,37] Due to their semicrystalline nature, conducting polymers are effectively 3-D systems. Nevertheless, in highly crystalline materials, the hopping transport occurs either mainly along the π-stacking (thus resembling a 1-D behavior) or both along the π-stack and along the chain backbone (resembling a 2-D system).[38,39]

In the case of p=0.5, the model is called Efros-Shklovski and the parameter T_0 of equation 29 is written as:

$$T_{ES} = \frac{Cq^2}{\varepsilon_r k_B \xi} \quad (30)$$

where ε_r is the dielectric constant, $C \approx 9.6$, a numerical constant and ξ is the charge carrier localization length.[36,40,41]

The charge transport behavior of most reported amorphous conducting polymers like poly(3,4-ethylenedioxythiophene):poly(styrene sulfonate) (PEDOT:PSS) was successfully described by this model.[33,37,42-45] Of course, there are case studies of deviations to the general VRH model[33]. For example, at low temperatures (<50K), systems of low doping, like PCDTBT, the coulomb interactions between the electrons become significant and the *J-V* curves that are used to calculate the electrical conductivity do not follow the typical linear Ohm's law. Instead, the polymers behaves as a one dimensional Luttinger liquid at these low temperatures. Thus, the electric current density is accordingly modified:

$$J = J_0 T^{1+\alpha} \sinh\left(\gamma \frac{qV}{k_B T}\right) \left|\Gamma\left(1 + \frac{\alpha}{2} + i\gamma \frac{qV}{\pi k_B T}\right)\right| \qquad (31)$$

where α is an experimentally derived parameter, J_0 and γ are fitting parameters, while q and k_B are the electric charge and the Boltzmann constant respectively, and Γ is the gamma function[38].On the other hand, systems of higher degree of crystallinity and doping may follow a $(1/T)^b$ law, instead of an exponential behavior. Hence, the material shows a linear or constant trend in the σ over T graphs.[33]

Besides the charge transport mechanism, information on the behavior of the conduction of the system is also obtained from those plots. Particularly, a doped semiconductor can belong in three distinct conduction behavior regimes, depending on its σ over T law; the metallic regime, the critical regime and the insulating regime of Mott's Metal-Insulator Transition (MIT).[14] In order to distinguish the material behavior, the reduced activation energy W, $\left(W = \frac{\partial ln\sigma}{\partial lnT}\right)$ must be plotted against the temperature. The slope of the plot defines in which regime of MIT belongs the material. The material belongs to the

metallic regime, the critical and the insulating regime of MIT when the slope is positive, constant and negative, respectively. Most semiconducting materials, and thus most semiconducting and conducting polymers, fall into the insulating regime of the MIT. In specific case studies of heavily doped or high crystallinity systems, the material falls in the metallic regime or the critical regime, hence resembling the electrical behavior of a metal or a semimetal respectively.[14,40,44]

A.4 References:

1 Domenicali, C. A. Irreversible Thermodynamics of Thermoelectricity. *Reviews of Modern Physics* **26**, 237-275 (1954).

2 Goupil, C., Seifert, W., Zabrocki, K., Müller, E. & Snyder, G. J. Thermodynamics of Thermoelectric Phenomena and Applications. *Entropy* **13**, 1481 (2011).

3 Goupil, C. *et al.* in *Continuum Theory andModeling of Thermoelectric Elements* 1-74 (Wiley-VCH Verlag GmbH & Co. KGaA, 2016).

4 Goddard, J. D. On the Thermoelectricity of W. Thomson: Towards a Theory of Thermoelastic Conductors. *Journal of Elasticity* **104**, 267-280, doi:10.1007/s10659-011-9309-6 (2011).

5 Onsager, L. Reciprocal Relations in Irreversible Processes. I. *Physical Review* **37**, 405-426 (1931).

6 Onsager, L. Reciprocal Relations in Irreversible Processes. II. *Physical Review* **38**, 2265-2279 (1931).

7 Callen, H. B. The Application of Onsager's Reciprocal Relations to Thermoelectric, Thermomagnetic, and Galvanomagnetic Effects. *Physical Review* **73**, 1349-1358 (1948).

8 Manzanares José, A., Jokinen, M. & Cervera, J. in *Journal of Non-Equilibrium Thermodynamics* Vol. 40 211 (2015).

9 Goupil, C. Thermodynamics of the thermoelectric potential. *Journal of Applied Physics* **106**, 104907, doi:doi:http://dx.doi.org/10.1063/1.3257250 (2009).

10 Geoghegan, M. & Hadziioannou, G. *Polymer Electronics*. (OUP Oxford, 2013).

11 Ashcroft, N. & Mermin, D. *Solid State Physics*. (Thomson Learning, 1976).

12 Chen, G. *Nanoscale Energy Transport and Conversion: A Parallel Treatment of Electrons, Molecules, Phonons, and Photons*. (Oxford University Press, 2005).

13 Singleton, J. *Band Theory and Electronic Properties of Solids*. (OUP Oxford, 2001).

14 Mott, N. F. & Davis, E. A. *Electronic Processes in Non-Crystalline Materials*. (OUP Oxford, 2012).

15 Wetzelaer, G. A., Koster, L. J. & Blom, P. W. Validity of the Einstein relation in disordered organic semiconductors. *Phys Rev Lett* **107**, 066605, doi:10.1103/PhysRevLett.107.066605 (2011).

16 Xiao-Hong, S., Jiu-Xun, S. & Chun-Hua, X. Dependence of general Einstein relation on density of state for organic semiconductors. *Organic Electronics* **35**, 65-73, doi:http://dx.doi.org/10.1016/j.orgel.2016.04.042 (2016).

17 Cutler, M. & Mott, N. F. Observation of Anderson Localization in an Electron Gas. *Physical Review* **181**, 1336-1340, doi:10.1103/PhysRev.181.1336 (1969).

18 Jonson, M. & Mahan, G. D. Mott's formula for the thermopower and the Wiedemann-Franz law. *Physical Review B* **21**, 4223-4229 (1980).

19 Ihnatsenka, S., Crispin, X. & Zozoulenko, I. V. Understanding hopping transport and thermoelectric properties of conducting polymers. *Physical Review B* **92**, doi:10.1103/PhysRevB.92.035201 (2015).

20 Charles, K. *Introduction to Solid State Physics*. 7 edn, (Wiley, 1995).

21 Bubnova, O. & Crispin, X. Towards polymer-based organic thermoelectric generators. *Energy & Environmental Science* **5**, 9345, doi:10.1039/c2ee22777k (2012).

22 Heeger, A. J. Nobel Lecture: Semiconducting and metallic polymers: The fourth generation of polymeric materials. *Reviews of Modern Physics* **73**, 681-700 (2001).

23 Coropceanu, V. *et al.* Charge Transport in Organic Semiconductors. *Chemical Reviews* **107**, 926-952, doi:10.1021/cr050140x (2007).

24 Brédas, J. L., Wudl, F. & Heeger, A. J. Polarons and bipolarons in doped polythiophene: A theoretical investigation. *Solid State Communications* **63**, 577-580, doi:http://dx.doi.org/10.1016/0038-1098(87)90856-8 (1987).

25 Bredas, J. L. & Street, G. B. Polarons, bipolarons, and solitons in conducting polymers. *Accounts of Chemical Research* **18**, 309-315, doi:10.1021/ar00118a005 (1985).
26 Park, Y. W., Heeger, A. J., Druy, M. A. & MacDiarmid, A. G. Electrical transport in doped polyacetylene. *The Journal of Chemical Physics* **73**, 946, doi:10.1063/1.440214 (1980).
27 Moses, D. *et al.* Inter-soliton electron hopping transport in trans-(CH)x. *Solid State Communications* **40**, 1007-1010, doi:http://dx.doi.org/10.1016/0038-1098(81)90055-7 (1981).
28 Park, J. G. *et al.* Tunneling conduction in polyacetylene nanofiber. *Synthetic Metals* **135-136**, 299-300, doi:10.1016/s0379-6779(02)00547-7 (2003).
29 Park, Y. W. *et al.* Proceedings of the International Conference on Science and Technology of Synthetic Metals Conductivity and thermoelectric power of the newly processed polyacetylene. *Synthetic Metals* **28**, D27-D34, doi:http://dx.doi.org/10.1016/0379-6779(89)90670-X (1989).
30 Brédas, J. L., Thémans, B., Fripiat, J. G., André, J. M. & Chance, R. R. Highly conducting polyparaphenylene, polypyrrole, and polythiophene chains: An \textit{ab initio} study of the geometry and electronic-structure modifications upon doping. *Physical Review B* **29**, 6761-6773 (1984).
31 Chance, R. R., Brédas, J. L. & Silbey, R. Bipolaron transport in doped conjugated polymers. *Physical Review B* **29**, 4491-4495 (1984).
32 Beverina, L., Pagani, G. A. & Sassi, M. Multichromophoric electrochromic polymers: colour tuning of conjugated polymers through the side chain functionalization approach. *Chem Commun (Camb)* **50**, 5413-5430, doi:10.1039/c4cc00163j (2014).
33 Kaiser, A. B. & Skakalova, V. Electronic conduction in polymers, carbon nanotubes and graphene. *Chem Soc Rev* **40**, 3786-3801, doi:10.1039/c0cs00103a (2011).
34 Sirringhaus, H. *et al.* Two-dimensional charge transport in self-organized, high-mobility conjugated polymers. *Nature* **401**, 685-688 (1999).
35 Bubnova, O. *et al.* Semi-metallic polymers. *Nat Mater* **13**, 190-194, doi:10.1038/nmat3824 (2014).
36 Skinner, B., Chen, T. & Shklovskii, B. I. Theory of hopping conduction in arrays of doped semiconductor nanocrystals. *Physical Review B* **85**, doi:10.1103/PhysRevB.85.205316 (2012).
37 Aleshin, A. N., Kiebooms, R. & Heeger, A. J. International Conference on Science and Technology of SyntheticMetallic conductivity of highly doped poly(3,4-ethylenedioxythiophene). *Synthetic Metals* **101**, 369-370, doi:http://dx.doi.org/10.1016/S0379-6779(98)00758-9 (1999).
38 Kronemeijer, A. J. *et al.* Universal scaling in highly doped conducting polymer films. *Phys Rev Lett* **105**, 156604, doi:10.1103/PhysRevLett.105.156604 (2010).
39 Brondijk, J. J. *et al.* Two-dimensional charge transport in disordered organic semiconductors. *Phys Rev Lett* **109**, 056601, doi:10.1103/PhysRevLett.109.056601 (2012).
40 Chen, T. *et al.* Metal-insulator transition in films of doped semiconductor nanocrystals. *Nat Mater* **15**, 299-303, doi:10.1038/nmat4486 (2016).
41 Efros, A. L. & Shklovskii, B. I. Coulomb gap and low temperature conductivity of disordered systems. *Journal of Physics C: Solid State Physics* **8**, L49 (1975).
42 Menon, R., Yoon, C. O., Moses, D., Heeger, A. J. & Cao, Y. Transport in polyaniline near the critical regime of the metal-insulator transition. *Physical Review B* **48**, 17685-17694, doi:10.1103/PhysRevB.48.17685 (1993).
43 Lee, K. *et al.* Metallic transport in polyaniline. *Nature* **441**, 65-68, doi:10.1038/nature04705 (2006).
44 Sangeeth, C. S. S., Jaiswal, M. & Menon, R. Charge transport in transparent conductors: A comparison. *Journal of Applied Physics* **105**, 063713, doi:10.1063/1.3097759 (2009).
45 Aleshin, A. N. Charge carrier transport in conducting polymers on the metal side of the metal-insulator transition: A review. *Physics of the Solid State* **52**, 2307-2332, doi:10.1134/s106378341011017x (2010).

Appendix B: Experimental Section

B.1 Materials and Processing:

- ***PEDOT:Tos formulations:***

The oxidant solution (40% in 1-butanol) was purchased from Heraus (Clevios B40), while EDOT, its derivative, 2-methanol-3,4-ethylenedioxythiophene (HOM-EDOT) and all other additives and solvents were purchased from Sigma-Aldrich and used without further purification. In case of high boiling point solvent-containing films, the various solvent additives were introduced in the oxidant solutions before EDOT addition, at a constant volume fraction of 5% v/v with respect to the solution volume. When pyridine is incorporated in the formulation, pyridine was added in the $Fe(Tos)_3$ oxidant solution in a ratio of 0.5 mol of pyridine to 1 mol of oxidant. For the samples including both pyridine and solvent additives, the solvent additives were added in a volume fraction of 3% with respect to the oxidant solution volume.

All oxidant/additives solutions were stirred for 12 hours in ambient conditions and stored at 4°C for subsequent use. The EDOT monomers were added to the $Fe(Tos)_3$ oxidant solution with an oxidant-to-monomer ratio equal to 2.3:1 based on the fact that 2 moles of oxidant are needed to polymerize the monomer, plus 0.3 moles to dope the system. The oxidant/EDOT dispersion was spin-coated on 15×15 mm glass substrates at 1.5 krpm for 30s to form 180 nm thick films. Films were thermally annealed at 100°C for 15 min to initiate the polymerization reaction. Afterwards the films were sequentially washed with 1-butanol and ethanol, to remove the remaining oxidant, and dried under nitrogen flow. Films were further dried under vacuum overnight.

- ***Materials for device fabrication:***

Poly(vinylidenefluoride-co-hexafluoropropylene) (P(VDF-HFP)) and 1-ethyl-3-methylimidazolium bis(trifluoromethylsulfonyl)amide ([EMI][TFSA]) used for the fabrication of the electrolyte gated transistors were purchased from Sigma-Aldrich. $LiClO_4$ and Propylene Carbonate used in chronocoulometry experiments were purchased as well from Sigma-Aldrich.

Before the polymer deposition, the silicon or glass substrates were washed in baths of acetone, isopropanol and ethanol for 15 min per washing step.

B.2 Methods and Characterizations:

- ***Electrical conductivity measurement***

Sheet resistance, $R_{\square}$, was measured directly on the film surface *via* a 4-point probe set-up utilizing a Lucas Lab S-302-4 station having R recorded with a Keithley 2450. The film thickness, t, measured with a Dektak XT stylus profilometer allowed calculation of the electrical conductivity *via* $\sigma = 1/(R_{\square}.t)$.

- ***Seebeck coefficient measurement***

The Seebeck coefficient was measured in a thin film geometry with a homemade setup[1] utilizing two tungsten-pins to measure the voltage, V, (Keithley 2450), whilst the temperature, T, was recorded with 2 T-type thermocouples (Omega T-08). Substrates were coated with four 100 nm Au electrodes to ensure proper electrical contact. Temperature gradients were directly controlled through Peltier plates below the samples fixed using

thermal pastes. Applied gradients were between 0-5°C at room temperature and the resulting *V/T* slope was calculated as the Seebeck coefficient.

To minimize the potential errors on the Seebeck coefficient determination, the measurement configuration was optimized following a methodology described by van Reenen *et al*.[2] Consequently the geometry of the Au electrodes and the channel length (gap between the Au electrodes) were chosen such as the channel and electrode aspect ratios (defined as the ratio of the electrode width to the channel and electrode length, respectively) are lower than 1. This geometrical configuration allow to minimize errors on the Seebeck coefficient determination.[2] The device configuration and dimensions are presented in **Figure 1** and **Table 1**.

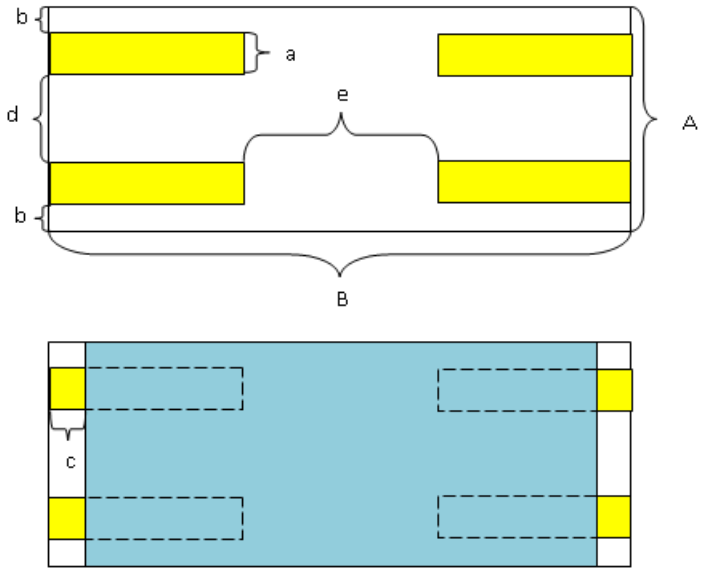

Figure 1: (top panel) The geometry of the used device for the thermoelectric measurement (with yellow the gold electrodes), (bottom panel) with the polymer on top (blue). The depicted dimensions are presented in **Table 1**.

Letter	Dimension (mm)
A	12
B	25
a	2
b	1
c	2
d	5
e	8

Table 1: Configuration used for the thermoelectric measurements of the PEDOT:Tos thin films.

To further asset the validity of the Seebeck coefficient determination, Ni foil was used for calibration of the Seebeck measurement set-up. In **Figure 2** the thermovoltage *vs.* temperature gradient for Ni foil calibrant is displayed. Value of the Seebeck coefficient obtained for this material was 19.5 ± 0.2 μV/K which is in accordance with reported values in the literature.[3] Also, in order to reassure that there is not any errors to the measurement of the Silicon and hybrid materials due to dissipated heat, the high Seebeck coefficient of those systems was also measured under vacuum and no discrepancies were found with the results obtained in ambient conditions (**Figure 3**).

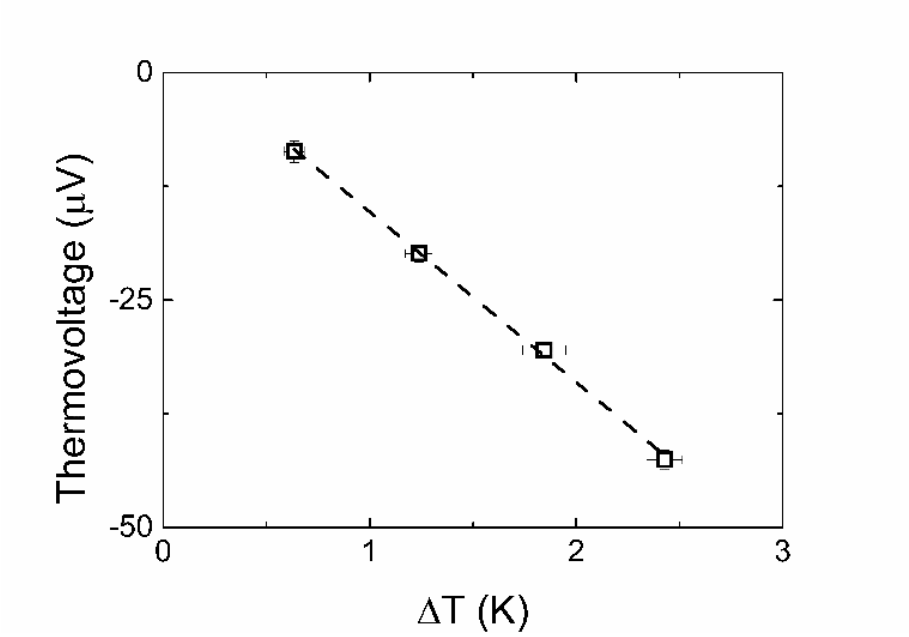

Figure 2. Thermovoltage versus temperature gradient for Ni foil calibrant. The dashed line is the linear fit, whose slope is used for the Seebeck coefficient calculation.

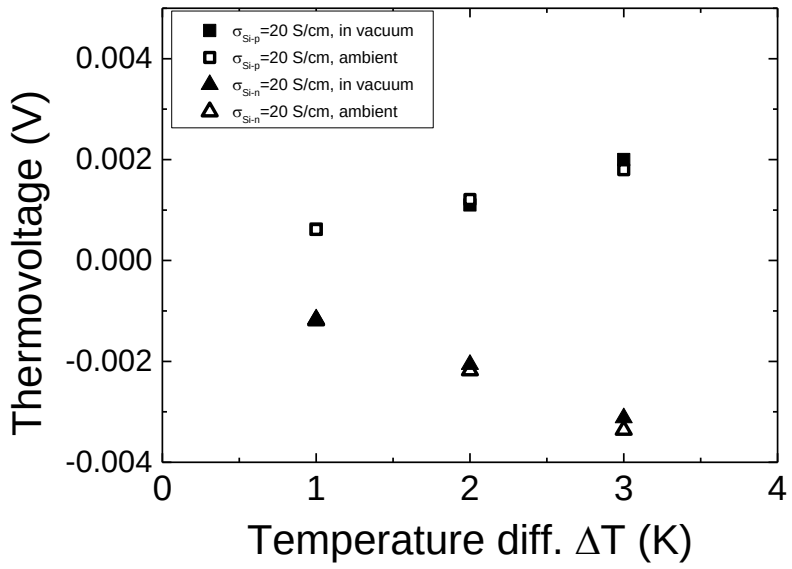

Figure 3: Thermovoltage vs the temperature difference for PEDOT:Tos on Silicon measured under vacuum and ambient conditions. The thickness of the PEDOT:Tos sample was 200 nm and its electrical conductivity, 1222 S/cm.

- ***In-plane charge carrier mobility measurement***

Electrolyte-gated transistors were fabricated and used for the calculation of the in-plane mobility of the PEDOT:Tos thin films.[4] On top of the PEDOT:Tos thin films deposited on glass substrates, gold electrodes of 100 nm were evaporated via thermal evaporation for the transistor source-drain and the gate electrodes. The device capacitative effect of the gate electrode was taken into consideration in device fabrication.[5,6] Afterwards, an ion gel solution in acetone comprised of P(VDF-HFP) and [EMI][TFSA] was drop-casted and then annealed for 1 hr at 50°C to remove the excess solvent. The ion gel film had a 6 μm thickness. If the transistor device was considered as an OFET, then mobility would be calculated following the relationship:

$$\mu = \frac{dg_d}{dV_G} \cdot \frac{L}{W \cdot C} \quad (1)$$

using the slope of the linear region. However, the dedoping procedure that is observed in conventional devices does not happen in a monolayer of PEDOT:Tos, (as in the case of top gated OFET), but it occurs in the bulk of the transistor device. Hence, the transistor should be considered as an Organic Electrochemical Transistor (OECT). This might result in an overestimation of the value of the charge carrier mobility. Consequently, the equation for the calculation of mobility should be re-visited. If Q_{ch} is the charge in the OECT channel:

$$I_D = -Q_{ch}/t_{tr} \quad (2)$$

where I_D the drain source and t_{tr} the transit time in the channel ($t_{tr} = \frac{L^2}{\mu \cdot V_D}$ with L = 50μm the channel length, V_D the drain voltage and μ the charge carrier mobility).

Consequently, the charge passing from the channel is equal to

$$Q_{ch} = -C \cdot (V_G - V_T) \quad (3)$$

where C is the capacitance, V_T and V_G the threshold and gate voltages.

Hence, the charge carrier mobility can be extracted as:

$$I_D = \mu \cdot \frac{C}{L^2} \cdot (V_G - V_T) \cdot V_D \quad (4)$$

A Princeton Potensiostat was used for the calculation of the polymer capacitance.

To further elaborate the differences between the two methods (OFET and OECT), the charge carrier mobility of the commercial PEDOT:PSS was calculated from electrolyte-gated transistors. Due to the difference in capacitance between gold and gold/PEDOT, the device would be able to turn off for lower gate voltages, allowing the correct estimation of the charge carrier mobility of PEDOT:PSS. These features become clear in the **Figure 4**. In **Figure 4a,4c** and **4b,4d** are presented the output curves and transfer curves of the devices fabricated with PEDOT:PSS treated with DMSO. The curves of **Figure 4a** and **4b** represent devices fabricated only with gold as the gate electrode and the **Figure 4c** and **4d** are extracted for devices where PEDOT is added to the gate electrode. As observed in **Figures 4a** and **4c**, the latter devices are able to turn off in lower gate voltages, allowing a correct estimation of the charge carrier mobility.

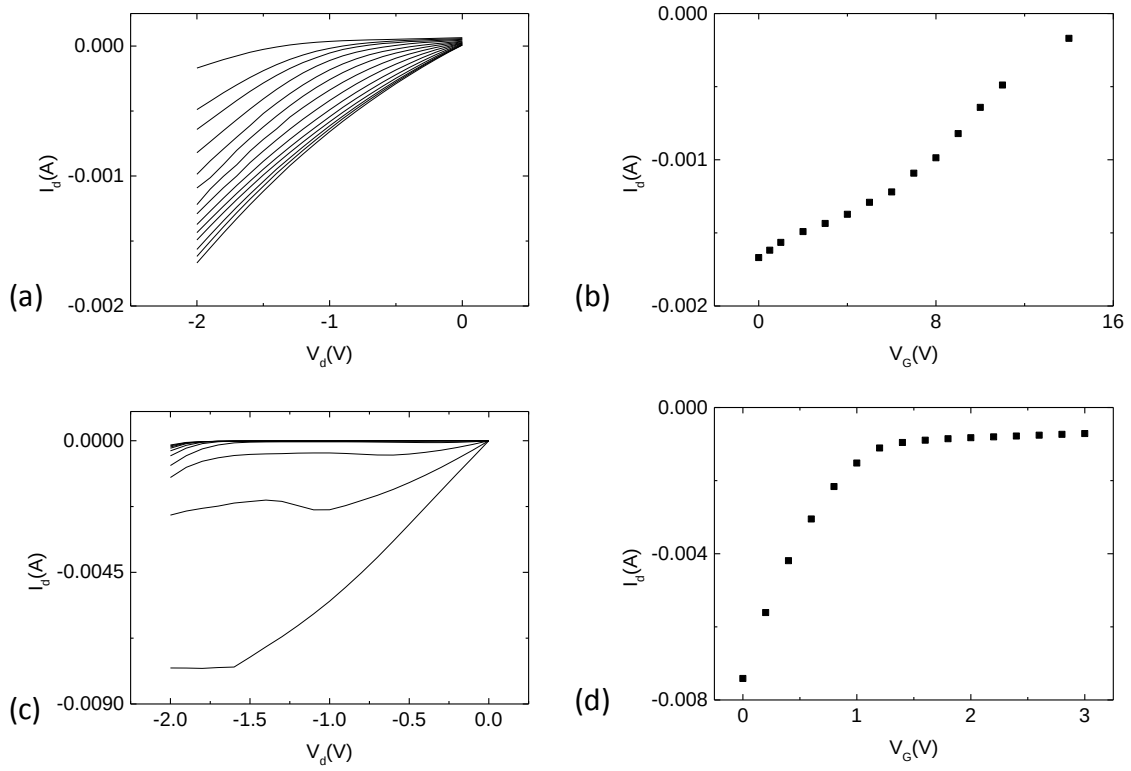

Figure 4: The output curves of transistor devices of PEDOT:PSS where the gate electrode was gold (a) and where PEDOT was also included in the gate electrode (c). The respective transfer curves (b) and (d) are also presented.

Using equation for a ion-gel capacitance of 10 μF/cm^2, a channel length of 50μm and a channel width of 1.5mm, the mobility is calculated as μ = 0.6 cm^2/Vs. This value is in the same order of magnitude to the one reported from Wei *et al* [4]. However, when equation (4) is used for the new devices, the calculated μ would be quite different. For a PEDOT layer capacitance of around 7.5 μF (as in Chapter 2) the new charge carrier mobility is 3.3x10^{-4} cm^2/Vs, which is three orders of magnitude lower. Additionally, when devices of PEDOT:PSS without DMSO are fabricated, the calculated mobility is equal to 7.8x10^{-6} cm^2/Vs, which is also three orders of magnitude lower than the value (0.045 cm^2/Vs) reported by Wei *et al* [4]. These new values on the charge carrier mobilities of PEDOT:PSS allow the

calculation of the charge carrier concentration of the material, N, as 1.15×10^{25} carriers/cm^3, which is also three orders of magnitude higher. This overestimated values of μ for PEDOT:PSS might lead in misinterpreted correlations between charge carrier mobility and other material properties , i.e. the Seebeck coefficient .

- ***Out-of-plane charge carrier mobility measurements***

Sandwich-like devices were fabricated for the calculation of the out-of-plane charge carrier mobility of the PEDOT:Tos thin films, following the report of Rutledge *et al.*[7] The PEDOT:Tos films were deposited on top of ITO and consequently Al electrodes (100nm) were evaporated on top of the polymer films.

- ***Chronocoulometry***

For the chronocoulometric analysis, a Princeton Versastat 3 setup was used. An Ag electrode was used as a counter electrode. The same device geometry as the Seebeck measurement was used to connect the sample to the voltage source. The PEDOT film and the counter electrode were bathed in a 0.1M $LiClO_4$ solution in Propylene Carbonate.

- ***Out-of-plane thermal conductivity***

The calculation of the out-of-plane thermal conductivity was made through heterodyne picosecond thermoreflectance in the Laboratoire Ondes Matiere d'Aquitaine (LOMA). A metal layer of silver with diameter 2mm is deposited on the PEDOT:Tos films. Two femtosecond oscillators were used as pump and probe beams. Their repetition periods are

slightly different and the two beams are focused on the sample with a microscope objective; their wavelengths can be adjusted independently. The probe beam is detected with a photodiode and the signal is recorded by a digital oscilloscope. A beam splitter deviates a part of the two reflected beam to a photodiode to obtain a synchronization signal. Subsequently, the thermal conductivity was extracted through optimization of the fitting of the experimental signal with a theoritical thermal model on the thermal conductivities of the active layer and the metal film.[8]

- ***Grazing Incidence Wide Angle X-ray Scattering GIWAXS***

The internal structure of the PEDOT:Tos thin films was probed using Grazing Incidence Wide Angle X-ray Scattering (GIWAXS). GIWAXS measurements were performed on the Dutch-Belgian Beamline (DUBBLE CRG), station BM26B, at the European Synchrotron Radiation Facility (ESRF), Grenoble, France.[9] The energy of the X-rays was 12 keV, the sample-to-detector distance and the angle of incidence, α_i, were set at 11 cm and 0.16°, respectively. The diffracted intensity was recorded by a Frelon CCD camera and was normalized by the incident photon flux and the acquisition time (30 s). Flat field, polarization, solid angle and efficiency corrections were subsequently applied to the 2D GIWAXS images.[10] The scattering vector q was defined with respect to the center of the incident beam and has a magnitude of $q = (4\pi/\lambda)\sin(\theta)$, where 2θ is the scattering angle and λ is the wavelength of the X-ray beam. Herein we opted to present the wedge-shaped corrected images where q_r and q_z are the in-plane and near out-of-plane scattering vectors, respectively. The scattering vectors are defined as follows: $q_x = (2\pi/\lambda)(\cos(2\theta_f)\cos(\alpha_f)-\cos(\alpha_i))$, $q_y = (2\pi/\lambda)(\sin(2\theta_f)\cos(\alpha_f))$, $q_z = (2\pi/\lambda)(\sin(\alpha_f)+\sin(\alpha_i))$, $q_r^2 = q_x^2 + q_y^2$, where α_f is the exit angle in the vertical direction and $2\theta_f$ is the in-plane scattering angle, in agreement with standard GIWAXS notation.[11]

- ***Ultraviolet photoelectron spectroscopy UPS***

UPS measurements were carried out in a UHV surface analysis system equipped with a Scienta-200 hemispherical analyzer. The base pressure of a sample analysis chamber is 2×10^{-8} mbar. UPS was performed using a standard He-discharge lamp with HeI 21.22 eV as excitation source and an energy resolution of 50 meV.

- ***Device fabrication for capacitance measurements of PEDOT/Silicon systems***

Upon deposition of the PEDOT:Tos films on top of 15x15mm silicon substrates, Gold (100nm) electrodes were evaporated on both sides (top and bottom) of the film.[12] The bottom electrode fully covered the silicon in contact, while on the top of the PEDOT films four electrodes were evaporated with dimensions depicted in **Figure 5.** The capacitance was measured with a SI 1260 Impedance/Gain-Phase Analyser.

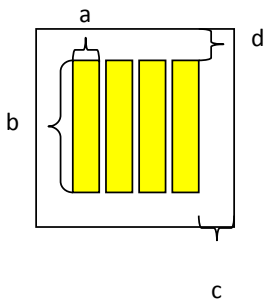

Figure 5: The device configuration for the capacitance measurements. a=0.2cm, b=1cm, c=0.275cm , d=0.25cm. With yellow are depicted the gold electrodes.

- ***Thermoelectric generators***

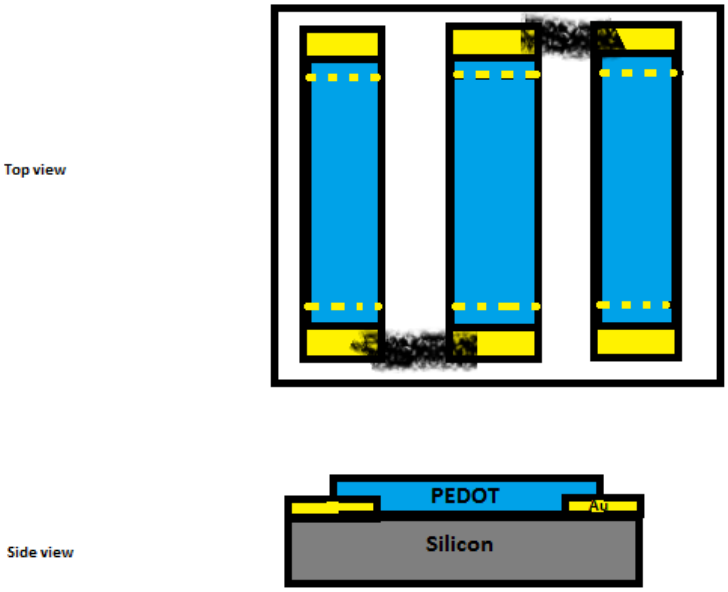

Figure 6: Schematic representation of the prototype thermoelectric generator.

Thermoelectric converters were fabricated for demostration of the phenomena reported in this study. PEDOT:Tos was deposited on top of the n and p doped silicon wafers. The PEDOT+Si wafers were then cut with diamond cutter in dimensions 25x3mm. The legs were stuck with glue on top of a glass substrate and the connection between the legs was being made by carbon paste. To further asset the device functionality, the short circuit current was measured for each device configuration. The measurement took place in the same setup used for the Seebeck measurement inside the closed Faraday cage.

B.3 References:

1 Wüsten, J. & Potje-Kamloth, K. Organic thermogenerators for energy autarkic systems on flexible substrates. *Journal of Physics D: Applied Physics* **41**, 135113, doi:10.1088/0022-3727/41/13/135113 (2008).

2 Reenen, S. v. & Kemerink, M. Correcting for contact geometry in Seebeck coefficient measurements of thin film devices. *Organic Electronics* **15**, 2250-2255, doi:http://dx.doi.org/10.1016/j.orgel.2014.06.018 (2014).

3 Zhao, L. D. Ultrahigh power factor and thermoelectric performance in hole-doped single-crystal SnSe. *Science* **351**, 141-144 (2016).

4 Wei, Q., Mukaida, M., Naitoh, Y. & Ishida, T. Morphological change and mobility enhancement in PEDOT:PSS by adding co-solvents. *Adv Mater* **25**, 2831-2836, doi:10.1002/adma.201205158 (2013).

5 Andersson, P., Forchheimer, R., Tehrani, P. & Berggren, M. Printable All-Organic Electrochromic Active-Matrix Displays. *Advanced Functional Materials* **17**, 3074-3082, doi:10.1002/adfm.200601241 (2007).

6 Herlogsson, L., Crispin, X., Tierney, S. & Berggren, M. Polyelectrolyte-Gated Organic Complementary Circuits Operating at Low Power and Voltage. *Advanced Materials* **23**, 4684-4689, doi:10.1002/adma.201101757 (2011).

7 Rutledge, S. A. & Helmy, A. S. Carrier mobility enhancement in poly(3,4-ethylenedioxythiophene)-poly(styrenesulfonate) having undergone rapid thermal annealing. *Journal of Applied Physics* **114**, 133708, doi:10.1063/1.4824104 (2013).

8 Pernot, G. *et al.* Precise control of thermal conductivity at the nanoscale through individual phonon-scattering barriers. *Nat Mater* **9**, 491-495, doi:http://www.nature.com/nmat/journal/v9/n6/suppinfo/nmat2752_S1.html (2010).

9 Bras, W. *et al.* Recent experiments on a small-angle/wide-angle X-ray scattering beam line at the ESRF. *Journal of Applied Crystallography* **36**, 791-794, doi:10.1107/s002188980300400x (2003).

10 Müller-Buschbaum, P. The Active Layer Morphology of Organic Solar Cells Probed with Grazing Incidence Scattering Techniques. *Advanced Materials* **26**, 7692-7709, doi:10.1002/adma.201304187 (2014).

11 Renaud, G., Lazzari, R. & Leroy, F. Probing surface and interface morphology with Grazing Incidence Small Angle X-Ray Scattering. *Surface Science Reports* **64**, 255-380, doi:http://dx.doi.org/10.1016/j.surfrep.2009.07.002 (2009).

12 Jackle, S. *et al.* Junction formation and current transport mechanisms in hybrid n-Si/PEDOT:PSS solar cells. *Sci Rep* **5**, 13008, doi:10.1038/srep13008 (2015).

Appendix C:

C.1 Optimization of the PEDOT:Tos synthesis.

C.1.1 Introduction:

In-situ polymerized Poly(3,4-ethylenedioxthiophene) was first reported by Jonas *et al*, who were working for Bayer in 1991,[1] as an antistatic coating. Its synthesis was presented in details the later years, highlighting the importance of a rigorous and detailed synthetic route for an electrically efficient material.[2-7] PEDOT can be obtained either by in-situ oxidative polymerization, or electrochemical polymerization or by oxidative dispersion polymerization.[8] In the present Ph.D., the PEDOT was synthesized with oxidative in-situ chemical polymerization using iron p-toluenesulfonate as oxidant, resulting to the PEDOT:Tos derivatives exhibiting high electrical and thermoelectric performance.[9-11]

C.1.2 Results and discussion:

The in-situ oxidative chemical polymerization of EDOT is a rather simple but rigorous synthetic procedure, as a deviation from the experimental protocol leads to low performance PEDOT films. Upon adding the EDOT monomer to the FeTos solution (40% in n-butanol, purchased as Clevios B40 from Heraus), the dispersion is spin coated at 1500 rpm for 30s at a 800 rpm/s^2 acceleration rate. The resulted thin films were annealed on a hot plate (100°C) in ambient conditions for 15 min. Afterwards the films were bathed subsequently in n-butanol baths (twice) and in an ethanol bath for 5 min each. The role of the bathing steps is to remove the unreacted and insulating oxidant that remained after the end of the polymerization.

Considering that the FeTos used in the synthesis was dissolved in n-butanol, this solvent is chosen as a first bathing step. The second and third bathing steps are added to further remove any remaining oxidant. After the bathing steps, the films are dried with Nitrogen gas.

The most important step of the synthetic route for the production of PEDOT:Tos films is the stoichiometric addition of EDOT to the oxidant solution.[5-8] The oxidation procedure under the presence of Iron p-toluenesulfonate (FeTos) oxidant is presented in **Figure 1**. Upon oxidation, a free radical is formed on the EDOT monomer, which further reacted to form EDOT dimers leading susbsequently to PEDOT chains. The ratio between the EDOT monomer and the oxidant should follow a stoichiometric ratio of oxidant/EDOT = 2.3.

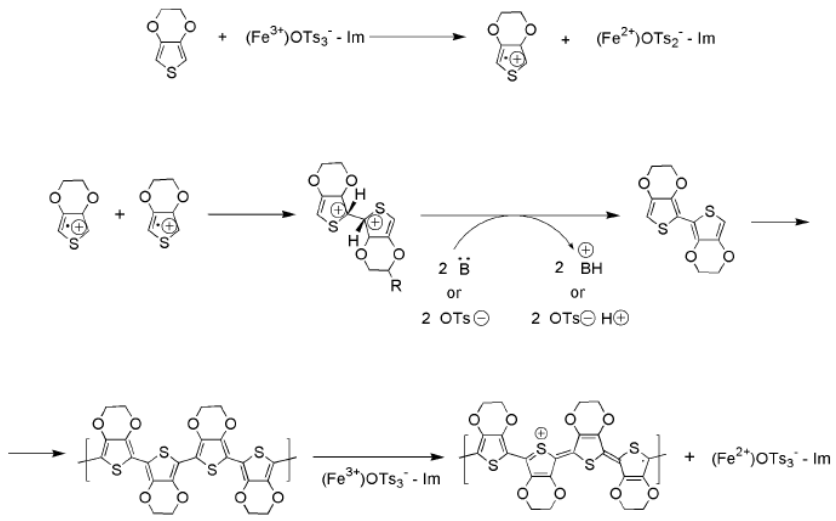

Figure 1: The oxidative polymerization of EDOT to PEDOT using Iron Toluenesulfonate oxidant. The effect of a base like Imidazole is highlighted.[5]

This stoichiometry originates from the fact that two equivalent moles of oxidant are needed to open the aromatic ring of the EDOT monomer, forming the radical ions, and the 0.3 equivalent moles are used to dope the material. Any declination from this ratio would result in either underdoped or overdoped PEDOT material which would not have the optimum

electrical properties.[5-7] This is clearly observed in **Figure 2**, where the electrical conductivity of the in-situ polymerized PEDOT:Tos films is plotted against the Oxidant/EDOT ratio. The Electrical conductivity of the in-stu synthesized PEDOT:Tos films appears to reach an optimum peak around the 2.3 ratio, which is in agreement with the theoretical stoichiometry. However, the Seebeck coefficient of the polymer films seems to not be significantly affected by this ratio.

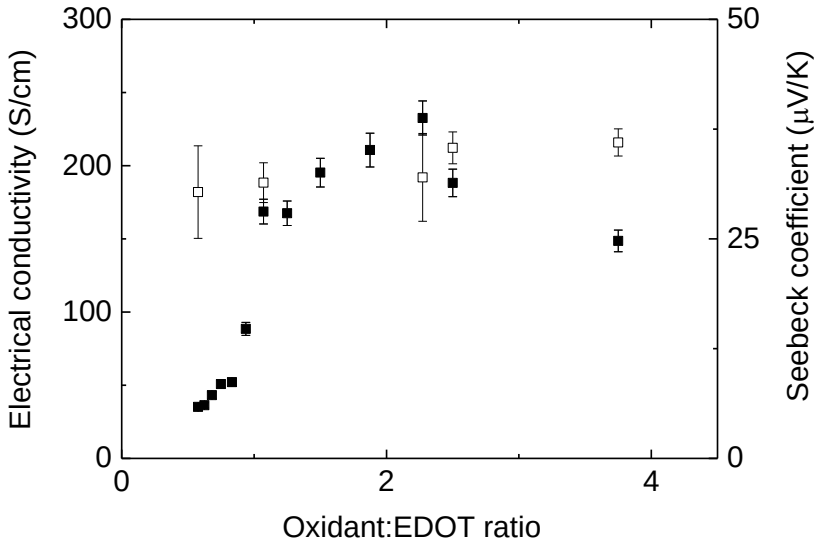

Figure 2: Electrical conductivity and Seebeck coefficient vs Oxidant:EDOT ratio.

As highlighted by Ha *et al*.[5]and Winther-Jensen *et al*.[12], an organic base like imidazole or pyridine can inhibit the oxidative polymerization of PEDOT. During the oxidative polymerization, free protons are released in the media and accelerate the polymerization procedure. Hence, organic bases act as proton scavengers and inhibit the polymerization kinetics, allowing the synthesis of longer PEDOT chains and films with more efficient electrical properties.[5,13] However, an excess addition of the organic base to the oxidant solution might be detrimental for the PEDOT:Tos electrical performance. As the mole ratio

between the base and the oxidant increases, the polymerization is hindered and eventually stopped (see **Figure 3**).

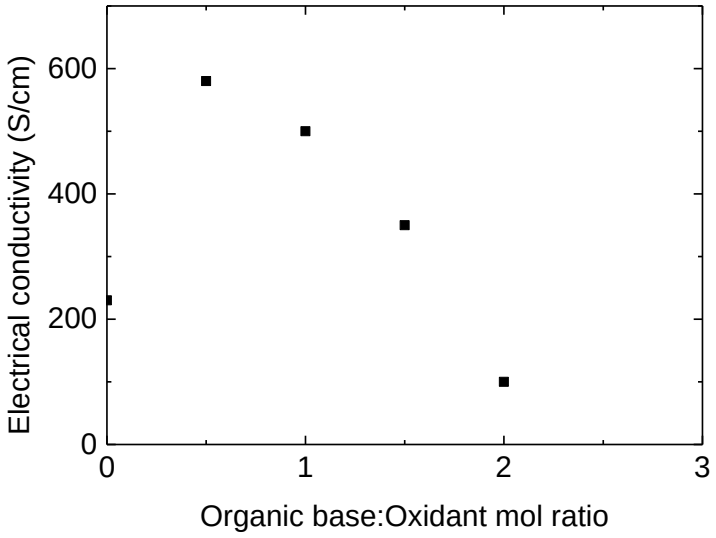

Figure 3: The electrical conductivity of PEDOT:Tos thin films versus the mole ratio between the organic base and the oxidant.

The pKa of an organic base can act as a means to compare the ability of an organic base to capture a free proton. Hence, various organic bases (**Table 1**) were added to the iron toluenesulfonate solution, in order to study the proton scavenging effect on the electrical properties of PEDOT:Tos. All bases were added in a ratio of 0.5 mol of base to 1 mol of oxidant. As observed in **Figure 4**, an increase of the pKa of the organic base has a beneficial effect on the electrical conductivity.

Organic base	pKa	T_b (°C)	σ (S/cm)	S (μV/K)	μx10^{-4} (cm^2/Vs)	σ (with addition of DMSO) (S/cm)
2,6 di-tert-butyl-pyridine	3.58	100	450±20	n.d.	n.d.	890±10
Pyridine	5.25	115	551±10	40±5	6.9±0.3	1220±32
2-ethylpyridine	5.89	149	683±30	43±4	7.4±0.4	1000±12
4-ethylpyridine	6.08	168	770±40	n.d.	n.d.	950±22
2,6 lutidine	6.60	144	800±50	44±3	8.9±0.5	1400±150
Collidine	7.40	170	855±40	45±5	9.0±0.3	1100±50

Table 1: The various organic bases used for the synthesis of PEDOT:Tos thin films and their respective pKa and boiling points. Thermoelectric properties are reported as well. (n.d. non determined)

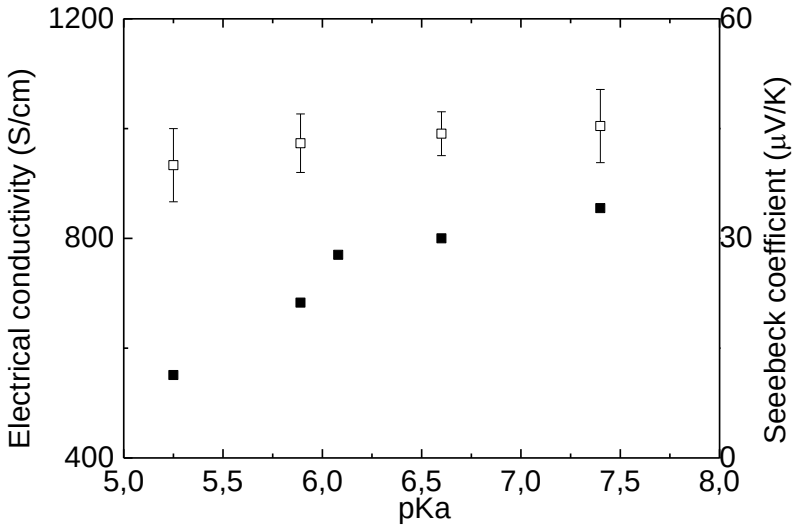

Figure 4: Electrical conductivity and Seebeck coefficient versus pKa for the various PEDOT:Tos thin films synthesized by the addition of the different organic bases.

Additionally, the Seebeck coefficient seems to be slightly improved by the addition of the various bases. However, from **Table 1** it appears that organic bases with high pKa also have a high boiling point. The main solvent being n-butanol (T_b = 117°C), the bases with a

boiling point above this value also act as a plasticizer.[14,15] As a result, for organic bases with pKa higher than that of , it is not clear whether the observed enhancement of σ is due to the proton scavenging effect of the base or to a plasticizing effect. Nevertheless, this information can used in order to synthesize a highly conducting PEDOT:Tos material.

The increased conductivity of pyridine formulated samples has been shown to be inherent to a higher charge carrier mobility. Consequently, electrolyte gated transistors were fabricated in order to evaluate the charge carrier mobility as a function of the base used in the formulation. The calculated mobilities are summarized in **Table 1** and it appears that the addition of the organic bases is beneficial for the charge carrier mobility, in agreement with the observations reported in the Chapter 3.

C.1.3 Conclusions:

The in-situ synthesis of PEDOT:Tos thin films was studied in order to produce films of high thermoelectric performance. The importance of the stoichiometry between the oxidant and the EDOT monomers is underlined in order to retrieve a highly conducting PEDOT:Tos film. Besides it was shown that organic bases can act as proton scavengers during the PEDOT polymerization, which appears beneficial to the film properties. Finally, the organic bases can be combined with a high boiling point solvent additive, like DMSO, in order to lead to highly conducting and thermoelectrically efficient films. Hence, films treated with 2,6 lutidine and DMSO exhibited a σ=1400±150S/cm, S=48±6μV/K, and a Power Factor of 322±75 μW/mK^2.

C.1.4 References:

1 Jonas, F., Heywang, G., Schmidtberg, W., Heinze, J. & Dietrich, M. (Google Patents, 1991).

2 Jonas, F. & Morrison, J. T. 3,4-polyethylenedioxythiophene (PEDT): Conductive coatings technical applications and properties. *Synthetic Metals* **85**, 1397-1398, doi:http://dx.doi.org/10.1016/S0379-6779(97)80290-1 (1997).

3 Jonas, F. & Schrader, L. Conductive modifications of polymers with polypyrroles and polythiophenes. *Synthetic Metals* **41**, 831-836, doi:http://dx.doi.org/10.1016/0379-6779(91)91506-6 (1991).

4 de Leeuw, D. M., Kraakman, P. A., Bongaerts, P. F. G., Mutsaers, C. M. J. & Klaassen, D. B. M. Electroplating of conductive polymers for the metallization of insulators. *Synthetic Metals* **66**, 263-273, doi:http://dx.doi.org/10.1016/0379-6779(94)90076-0 (1994).

5 Ha, Y. H. *et al.* Towards a Transparent, Highly Conductive Poly(3,4-ethylenedioxythiophene). *Advanced Functional Materials* **14**, 615-622, doi:10.1002/adfm.200305059 (2004).

6 Elschner, A., Kirchmeyer, S., Lovenich, W., Merker, U. & Reuter, K. *PEDOT: Principles and Applications of an Intrinsically Conductive Polymer*. (CRC Press, 2010).

7 Lövenich, W. PEDOT-properties and applications. *Polymer Science Series C* **56**, 135-143, doi:10.1134/s1811238214010068 (2014).

8 Groenendaal, L. B. e. a. Poly(3,4-ethylenedioxythiophene) and its derivatives: Past, Present and Future. *Advanced Materials* **12**, 481 (2000).

9 Bubnova, O. *et al.* Optimization of the thermoelectric figure of merit in the conducting polymer poly(3,4-ethylenedioxythiophene). *Nat Mater* **10**, 429-433, doi:10.1038/nmat3012 (2011).

10 Bubnova, O. *et al.* Semi-metallic polymers. *Nat Mater* **13**, 190-194, doi:10.1038/nmat3824 (2014).

11 Bubnova, O. & Crispin, X. Towards polymer-based organic thermoelectric generators. *Energy & Environmental Science* **5**, 9345, doi:10.1039/c2ee22777k (2012).

12 Winther-Jensen, B., Breiby, D. W. & West, K. Base inhibited oxidative polymerization of 3,4-ethylenedioxythiophene with iron(III)tosylate. *Synthetic Metals* **152**, 1-4, doi:http://dx.doi.org/10.1016/j.synthmet.2005.07.085 (2005).

13 Huang, J.-H. & Chu, C.-W. Achieving efficient poly(3,4-ethylenedioxythiophene)-based supercapacitors by controlling the polymerization kinetics. *Electrochimica Acta* **56**, 7228-7234, doi:10.1016/j.electacta.2011.03.044 (2011).

14 Palumbiny, C. M. *et al.* The Crystallization of PEDOT:PSS Polymeric Electrodes Probed In Situ during Printing. *Adv Mater* **27**, 3391-3397, doi:10.1002/adma.201500315 (2015).

15 Rogers, J. T., Schmidt, K., Toney, M. F., Bazan, G. C. & Kramer, E. J. Time-resolved structural evolution of additive-processed bulk heterojunction solar cells. *J Am Chem Soc* **134**, 2884-2887, doi:10.1021/ja2104747 (2012).

16 Koller, G. *et al.* Intra- and Intermolecular Band Dispersion in an Organic Crystal. *Science* **317**, 351-355, doi:10.1126/science.1143239 (2007).

17 Crispin, X. *et al.* Electronic Delocalization in Discotic Liquid Crystals: A Joint Experimental and Theoretical Study. *Journal of the American Chemical Society* **126**, 11889-11899, doi:10.1021/ja048669j (2004).

C.2 Hydroxymethylated PEDOT derivatives as thermoelectric material.

Preface:

In this chapter the structural and electrical properties of a Hydroxymethylated PEDOT derivative are investigated. The presence of the hydroxymethyl group attached to the PEDOT unit is expected to modify the crystallization behavior of the polymer, and thus a tailoring of the electrical properties of the material in the thin film configuration. The synthesized P(HOM-EDOT):Tos films had an electrical conductivity of 150 S/cm, lower than the 230 S/cm obtained for PEDOT:Tos films. The decrease in the electrical conductivity is related to an increase in the π-π distance due to the hydroxylmethyl moities. Additionally, a shift in the S(2p) position of the Tos XPS spectra indicated the existence of weak hydrogen bonds between the polymer chain and the Tos counter-ions. In order to further improve the electrical conductivity of the PEDOT derivative, DMF was added in the formulation resulting in films of higher crystallinity, higher charge carrier mobility and eventually increased electrical conductivity (450 S/cm). This procedure did not significantly affected the Seebeck coefficient of the material. Finally, the Power Factor of the formulated P(HOM-EDOT):Tos material was estimated to 64 $\mu W/mK^2$, a value lower than the one obtained for PEDOT:Tos thin films.

C.2.1 Introduction

Conducting polymers have gained the attention of the scientific community during the recent years due to unique properties inherent to their π-conjugated structure. Upon proper design, these materials were integrated in various organic devices such as sensors[1], OPVs,[2] and thermoelectric devices.[3] The electrical behavior of these π-conjugated systems origins from the hopping transport of the charge carriers between the conducting sites in the amorphous polymer matrix.[4] Hence the structural features of the polymers are highly influential to its electrical properties. As shown in Chapters 2-4, a higher degree of crystallinity of PEDOT:Tos thin films benefits its electrical conductivity and its thermoelectric performance.

Another important structural parameter is the orientation of the polymer chains. Specifically it was shown by Sirringhaus *et al*. that the direction of the π-stacking chain conformation is important for the electronic properties of the polymer thin film.[5] In the π-stacked conformation, the chains are packed at a distance of 3.4 Å, which assists to the overlapping of the π-orbitals of the chain units. This extended π-system is beneficial to the intermolecular hopping transport of the charge carriers, resulting in materials of higher charge carrier mobility.[5,6] The importance of the chain orientation for conducting polymers like Poly(3,4-ethylenedioxythiophene) (PEDOT) was recently highlighted by Palumbiny *et al.*[7,8] Specifically, these authors investigated the structural origin of the enhancement of the electrical properties of PEDOT:PSS thin films after treatments with high boiling point solvents (DMSO). They reported that such treatment would recrystallize the PEDOT chains and shift the chain orientation from face-on to edge-on, highlighting the importance of the π-stacking for the electrical conductivity of these systems.[7] In Chapter 2 and 3, we have demonstrated that the in-plane charge carrier mobility of PEDOT:Tos derivatives is also

increasing with the amount of edge-on crystallites of the material.[6] However, both reports focused on the properties of conventional PEDOT materials.

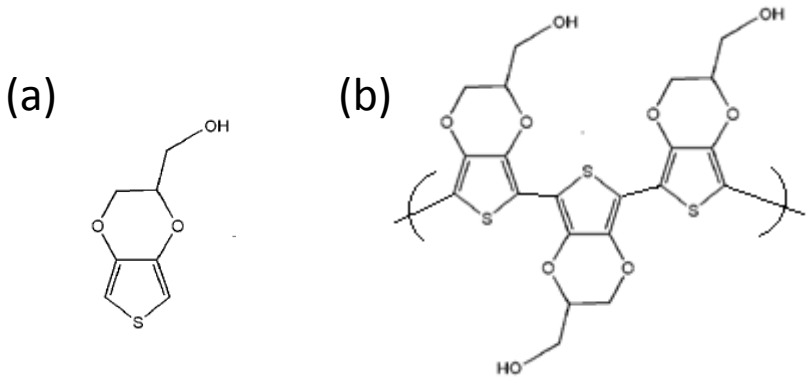

Figure 1: (a) The hydroxymethylated derivative of EDOT, (b) the P(HOM-EDOT) structure.

Another conducting polymer derivated from the EDOT monomers is the hydroxymethyl-PEDOT, P(HOM-EDOT) (**Figure 1**). As reported by Ha *et al.*,[9] P(HOM-EDOT) is a perspective candidate for efficient conductive electrode materials exhibiting high electrical conductivity (σ > 100 S/cm). Additionally, the hydroxymethyl moieties of the units can be further functionalized for sensor applications.[1] However, the addition of the hydroxymethyl group to the PEDOT unit will modifiy the polymer chain packing, and thus the distance between the π-stacked chains in thin film conformation. The aim of this study was to investigate the electrical and structural properties of this PEDOT derivative, as a means to elucidate the effect of π-distance to the electrical properties of conducting polymers.

C.2.2 Results and Discussion

All samples were in-situ polymerized using a procedure reported elsewhere[9-11] for synthesis of PEDOT:Tos. The synthesized P(HOM-EDOT):Tos films exhibited an electrical conductivity, σ, of 150±30 S/cm, lower than the respective PEDOT:Tos derivative, 230±10 S/cm. However, σ is defined as the product between charge carrier concentration, N, and the charge carrier mobility μ. Thus, this difference in the electrical behavior of the two materials can originate either from a different N or μ or both. Charge carrier concentration is related to the oxidation levels of those conducting polymers, as the holes of the oxidized chain units are the charge carriers of the material. Hence, qualitative information on the charge carrier concentration can be extracted from the oxidation levels of the material.

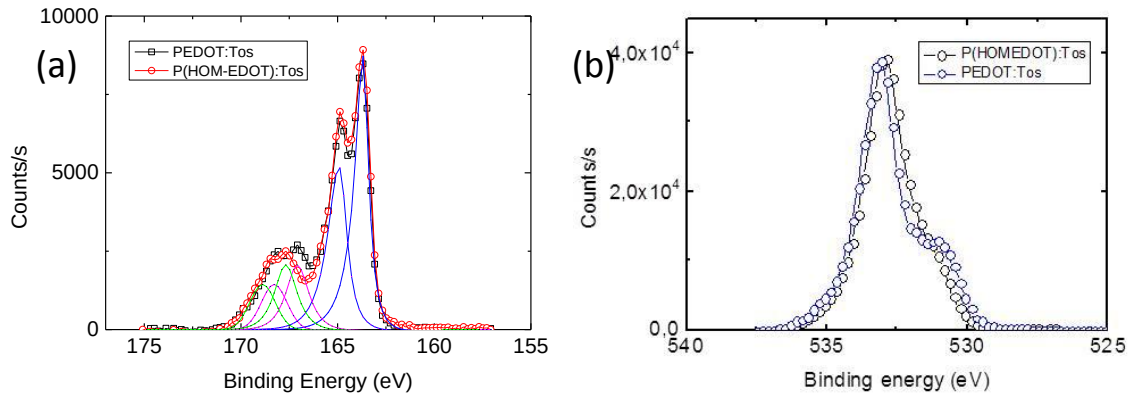

Figure 2: (a) The S(2p) XPS spectra of the PEDOT:Tos (black) and P(HOM-EDOT):Tos (red). With blue are presented the fitted doublets for the Sulfur of the thiophene ring and with green and magenta are the fitted doublets of the Sulfur of the Tos in the P(HOM-EDOT):Tos and PEDOT:Tos respectively.(b) The O(1s) XPS spectra for the P(HOMEDOT):Tos (black) and PEDOT:Tos (blue) thin films.

The oxidation levels of these conducting polymers were calculated from the S(2p) spectra recorded from X-ray Photoelectron Spectroscopy (XPS). In the XPS spectra for PEDOT:Tos and P(HOM-EDOT):Tos (**Figure 2a**), four distinct signals are observed which are characteristic of the doublets of the Sulfur of the thiophene unit (163-166 eV) and of the p-toluenesulfonate counter-ion (167-170 eV). However, the Tos S(2p) signal of the P(HOM-EDOT) derivative is shifted by 0.6 eV towards the higher binding energies, as regards to the one of the PEDOT:Tos. This shift originates from the different environment of the Sulfur atoms induced by the presence of the Hydroxymethyl groups on the PEDOT chains. Particularly, the hydrogen of the Hydroxymethyl group can form hydrogen bonds with the Tos Sulfur atoms.[12,13,14] The formation of hydrogen bonds between the Tos moieties and the PEDOT chains were also confirmed through the shift towards lower energy observed on the O(1s) spectra of the P(HOM-EDOT):Tos derivatives (**Figure 2b**). An oxidation level of 33% was further calculated as the ratio between the areas under the lower binding and the higher binding energy signals from the S(2p) spectra, in agreement with values reported in the literature for in-situ polymerized PEDOT derivatives.[6,15]

The identical oxidation levels for both PEDOT:Tos and P(HOM-EDOT):Tos thin films is a strong indication that the charge carrier concentration is also similar. Thus, the observed differences in electrical conuctivity have to be related to the thin film structure.[6] In order to elucidate the structural origin of those changes, GIWAXS experiments were performed on those samples. The (q_r, q_z) 2D scattering patterns recorded for the P(HOM-EDOT):Tos films are presented in **Figure 3**.

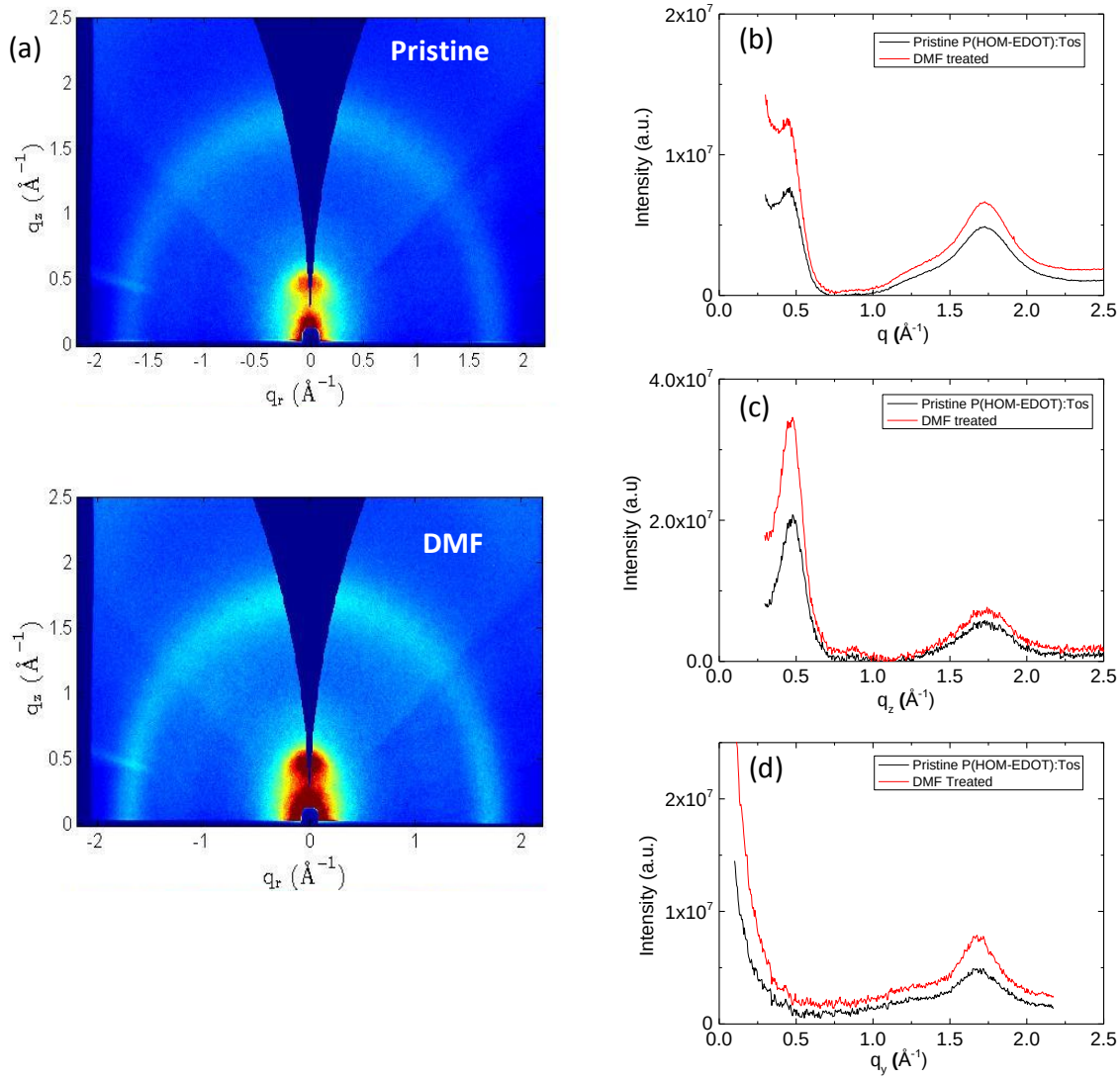

Figure 3: (a) The 2D GIWAXS patterns for the pristine (upper) and the DMF treated P(HOM-EDOT):Tos thin films. (b) The respective radially averaged scattering intensity with regards to the scattering vector *q* , (c) near-out-of-plane and (d) in-plane intensity line-cuts.

An anisotropic scattering is observed in both films with the majority of the scattering intensity along the near-out-of-plane axis that is perpendicular to the substrate. This feature is a strong indication of a preferential orientation of the crystallites in the P(HOM-EDOT):Tos films. In **Figure 3b**, the radially averaged scattered intensity is plotted with respect to the scattering

vector *q*. The two first peaks at 0.44 $Å^{-1}$ and 0.88 $Å^{-1}$ are attributed to the (100) and (200) reflections, corresponding to a repeat distance of 14.28 Å, and are in agreement to the work of Aasmundtveit *et al*.[16,27] for PEDOT:Tos materials. The unit cell proposed by Aasmundtveit *et al*. is presented in **Figure 4**, where the (h00) is along the *a* axis that is the unit monomer direction, perpendicular to the polymer chain axis *c*. It should be noted though, that the low intensity of the (200) peaks is indicative of a limited long-range order along the *a*-axis, which is a typical feature for paracrystalline distortions.

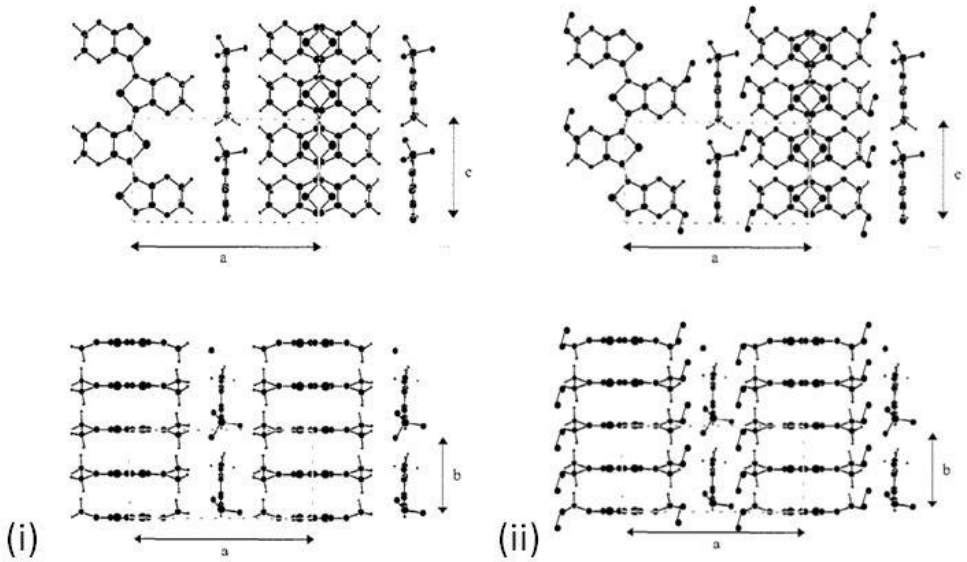

Figure 4 : The structural model proposed by Aasmundsveit *et al,* with the three directions on the unit cell for PEDOT:Tos [16] (i) and for P(HOM-EDOT):Tos (ii).

A third broad and intense peak at 1.68 $Å^{-1}$ is assigned to the respective (020) reflection; the direction of axis b (π-stacking) of the unit model (**Figure 4**). It is observed, that this peak is shifted with respect the one for PEDOT:Tos (see Chapter 2). Consequently, the π-distance for the hydroxymethyl derivative of PEDOT is 3.7 instead of 3.4 Å for PEDOT. An increase of the distance of the chains in the π-stacking can explain the lower electronic properties of for P(HOM-EDOT):Tos thin films, as the intermolecular hopping distance is

increased. Structural anisotropy was also evident in **Figure 3c-3d** and a main edge-on orientation is as well retrieved for the P(HOM-EDOT):Tos films.

Name	T_b (°C)	σ(S/cm)	S(μV/K)	PF (μW/mK^2)
Pristine	--	150±30	32±2	15±3
Acetonitrile	82	210±21	--	--
Toluene	110,6	195±10	--	--
Chlorobenzene	137	191±10	--	--
DMF	153	450±20	38±5	64±9
DMAC	165	410±10	--	--
DMSO	189	430±20	--	--
Ethylene Glycol	197,3	254±10	--	--
Propylene Carbonate	242	249±22	--	--

Table 1: The various solvent additives used in the present study with their respective boiling points and the electrical conductivity, Seebeck coefficient and Power Factor of the synthesized P(HOMEDOT):Tos films.

In order to further enhance the electrical conductivity of the polymer thin film, a high boiling point solvent additive like DMF was added in the oxidant solution.[6] Such additives favors the crystallization of the PEDOT chains, resulting in polymer of higher electrical and electronic properties (see **Table 1**). As observed in **Figure 5**, the electrical conductivity of the P(HOM-EDOT):Tos films is following a similar trend to the one of PEDOT:Tos (Chapter 2). It is noteworthy, that for both systems, the highest electrical conductivity was measured for the films formulated with DMF or DMSO (450±30 S/cm).

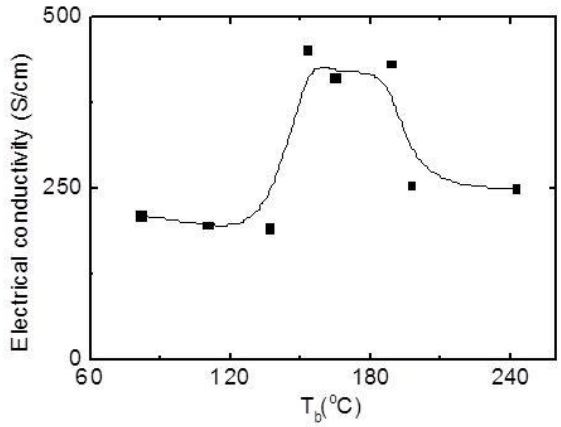

Figure 5: The electrical conductivity of the P(HOMEDOT):Tos thin films plotted against the boiling temperature of the various solvent additives, used in the synthesis.

Subsequently, the Seebeck coefficient was measured for the pristine and DMF treated P(HOM-EDOT):Tos films (**Table 1**). Both values are quite close to the ones reported for the respective PEDOT:Tos films (see Chapter 2). Hence, with this treatment the Power Factor of P(HOM-EDOT):Tos is enhanced from 15 to 64 $\mu W/mK^2$. Nevertheless the Power Factors of the P(HOMEDOT):Tos samples (pristine and DMF treated) are lower than the respective ones for the PEDOT:Tos films, which originates from the lower electrical conductivity of the films. This behavior is inherent to the increased π-distance in the P(HOM-EDOT).

In Chapter 2 is presented that such additives would not affect the oxidation levels of the PEDOT material [6]. A similar behavior is apparent for the new system studied herein, as the XPS spectra of the pristine P(HOM-EDOT):Tos and the DMF treated are overlapping (**Figure 6)**. As a result, the increased electrical behavior of the polymer should have a structural origin.[6-8]Consequently, the 2D GIWAXS patterns are presented for the DMF treated P(HOM-EDOT) (**Figure 3**). Similarly to the pristine film, an anisotropic scattering is observed in the directions along and perpendicular to the substrate. In **Figure 3b** is presented

the radially averaged scattering intensity plot vs the scattering vector for this new material. The (100), (200) and (020) reflections are still apparent, indicating that the unit cell has not changed. The area under the (100) peak acts as a crystallinity quantifier, allowing to compare the degree of crystallinity of the two systems. Hence, an increase in the degree of the thin film crystallinity is observed, as the area under (100) for the DMF treated sample is increased with respect to the pristine one. So, this finding justifies the observed increase in the electrical conductivity of the system. However, this increased degree of crystallinity should benefit the charge carrier mobility of the system,

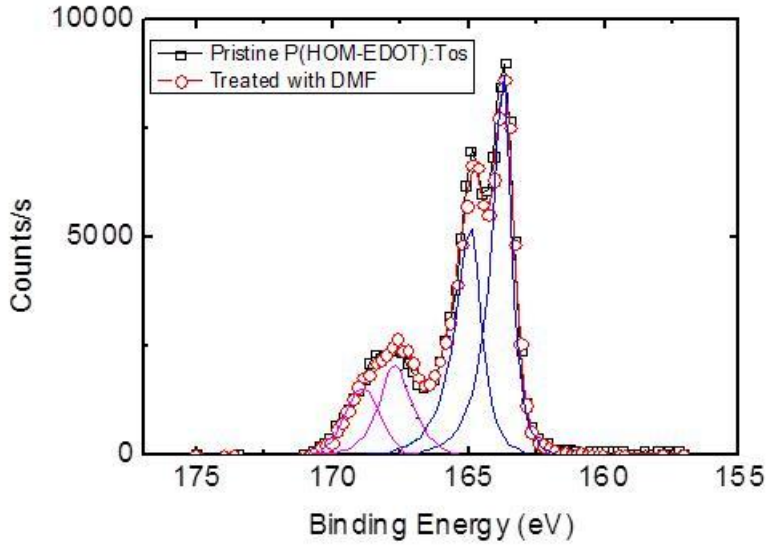

Figure 6: the S(2p) XPS spectra for the Pristine (black) and the DMF treated (red) P(HOM-EDOT):Tos thin films. With blue and magenta are the fitted doublets that correspond to the Sulfur of the thiophene unit and the Tos counter ions.

Subsequently, electrolyte gated transistors were fabricated with the pristine and DMF treated P(HOM-EDOT):Tos thin films (see **Appendix B** for the fabrication of the transistors) in order to calculate the charge carrier mobility of the P(HOMEDOT):Tos derivatives.[6,17] The

output and transfer curves are presented in **Figure 6a-b** and **6c-d**, respectively. As observed from **Figure 6a**, the transistors of the DMF treated sample are turning "off" faster than the devices of the pristine material; a feature inherent to a higher charge carrier mobility. The calculated mobilities obtained from the transfer curves are presented in **Table 2**. From the values of μ and σ, the charge carrier concentration, N, is calculated for the P(HOMEDOT):Tos samples (similarly to Chapters 2-3), as equal to 6.9×10^{24} carriers/cm^3, which in the same order of magnitude to the one of PEDOT:Tos samples. It should be noted that the charge carrier mobilities of both P(HOMEDOT):Tos samples are lower than the respective values for the PEDOT:Tos samples (**Table 2**) which is in accordance with the increased π-π stacking distance.

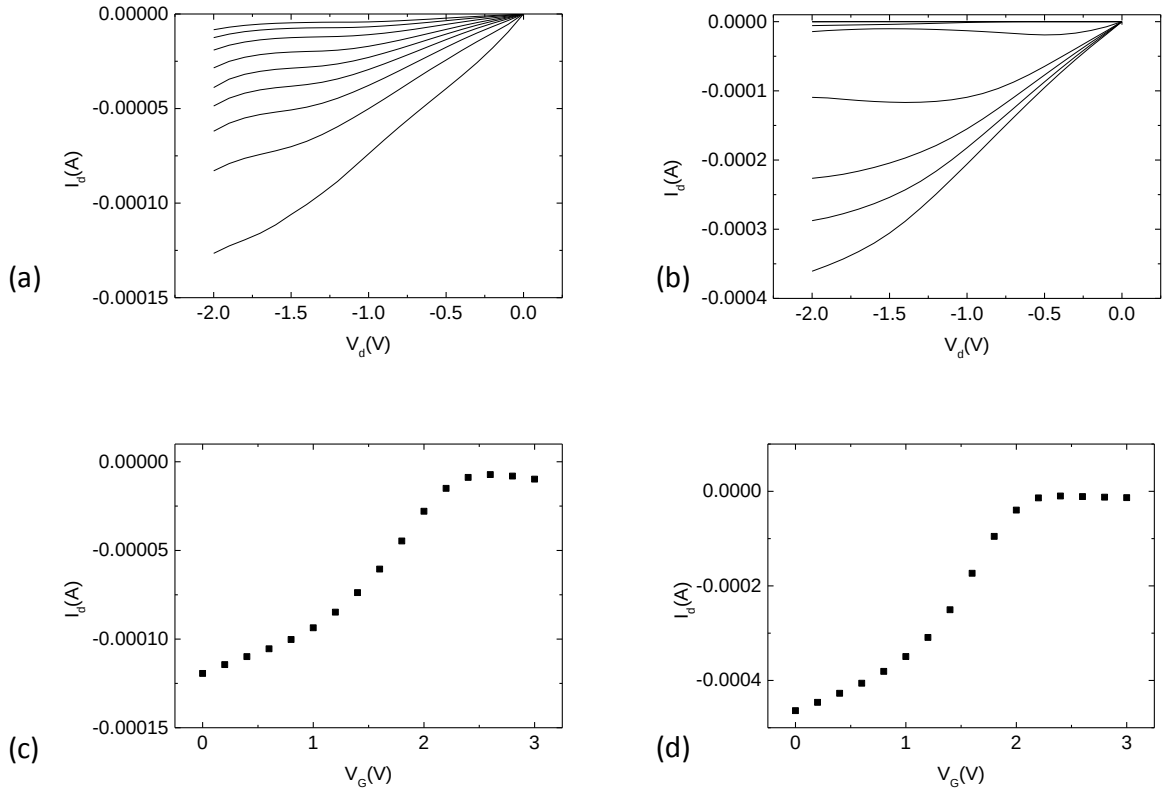

Figure 6: (a)-(b) the output characteristics from the electrolyte gated transistors synthesized from the pristine and DMF treated P(HOMEDOT):Tos samples. **(c)-(d)** the respective transfer curves for these devices.

	σ (S/cm)	μ x10^{-4}(cm^2/Vs)
PEDOT:Tos	230±10	2.4±0.1
DMF treated PEDOT:Tos	640±10	6.6±0.4
P(HOMEDOT):Tos	150±30	1.4±0.2
DMF treated P(HOMEDOT):Tos	450±20	4.0±0.3

Table 2: The electrical conductivity and charge carrier mobility values for the PEDOT:Tos and P(HOMEDOT):Tos samples

C.2.3 Conclusions:

As an alternative to the PEDOT:Tos material, P(HOM-EDOT) was synthesized with in-situ oxidative polymerization. The resulted films had an electrical conductivity of 150 S/cm, lower than the PEDOT:Tos equivalent. This difference in the material properties is inherent to the structural characteristics of the films, as the oxidation levels are equal for the two materials. A shift in the S(2p) XPS spectra of the Tos counter-ions of the P(HOM-EDOT):Tos was observed and was attributed to hydrogen bonding between the Sulfur atoms of the Tos units and the Hydroxymethyl group of the thiophene unit. An increased π-π distance (from 3.4 to 3.6 Å) was also observed by GIWAXS for the P(HOM-EDOT):Tos. The electrical conductivity of the films was increased to 450 S/cm by adding DMF in the formulation which was also inherent to an increase of the degree of crystallinity resulting in a higher charge carrier mobility. The charge carrier mobilities of the P(HOMEDOT):Tos films were nevertheless lower than the respective values obtained for PEDOT:Tos films, a feature that is related to the comparatively higher π-distance for the P(HOM-EDOT):Tos films.

C.2.4 References:

1 Persson, K. M. *et al.* Electronic Control over Detachment of a Self-Doped Water-Soluble Conjugated Polyelectrolyte. *Langmuir* **30**, 6257-6266, doi:10.1021/la500693d (2014).

2 Lindell, L. *et al.* Transparent, Plastic, Low-Work-Function Poly(3,4-ethylenedioxythiophene) Electrodes. *Chemistry of Materials* **18**, 4246-4252, doi:10.1021/cm061081m (2006).

3 Bubnova, O. & Crispin, X. Towards polymer-based organic thermoelectric generators. *Energy & Environmental Science* **5**, 9345, doi:10.1039/c2ee22777k (2012).

4 Kaiser, A. B. & Skakalova, V. Electronic conduction in polymers, carbon nanotubes and graphene. *Chem Soc Rev* **40**, 3786-3801, doi:10.1039/c0cs00103a (2011).

5 Sirringhaus, H. *et al.* Two-dimensional charge transport in self-organized, high-mobility conjugated polymers. *Nature* **401**, 685-688 (1999).

6 Petsagkourakis, I. *et al.* Structurally-driven Enhancement of Thermoelectric Properties within Poly(3,4-ethylenedioxythiophene) thin Films. *Scientific Reports* **6**, 30501, doi:10.1038/srep30501

http://www.nature.com/articles/srep30501#supplementary-information (2016).

7 Palumbiny, C. M. *et al.* The Crystallization of PEDOT:PSS Polymeric Electrodes Probed In Situ during Printing. *Adv Mater* **27**, 3391-3397, doi:10.1002/adma.201500315 (2015).

8 Palumbiny, C. M. *et al.* Molecular Reorientation and Structural Changes in Cosolvent-Treated Highly Conductive PEDOT:PSS Electrodes for Flexible Indium Tin Oxide-Free Organic Electronics. *The Journal of Physical Chemistry C* **118**, 13598-13606, doi:10.1021/jp501540y (2014).

9 Ha, Y. H. *et al.* Towards a Transparent, Highly Conductive Poly(3,4-ethylenedioxythiophene). *Advanced Functional Materials* **14**, 615-622, doi:10.1002/adfm.200305059 (2004).

10 Elschner, A., Kirchmeyer, S., Lovenich, W., Merker, U. & Reuter, K. *PEDOT: Principles and Applications of an Intrinsically Conductive Polymer*. (CRC Press, 2010).

11 Lövenich, W. PEDOT-properties and applications. *Polymer Science Series C* **56**, 135-143, doi:10.1134/s1811238214010068 (2014).

12 Krepps, M. K., Parkin, S. & Atwood, D. A. Hydrogen Bonding with Sulfur. *Crystal Growth & Design* **1**, 291-297, doi:10.1021/cg015505v (2001).

13 Porté-Durrieu, M. C. *et al.* Cyclo-(DfKRG) peptide grafting onto Ti–6Al–4V: physical characterization and interest towards human osteoprogenitor cells adhesion. *Biomaterials* **25**, 4837-4846, doi:http://dx.doi.org/10.1016/j.biomaterials.2003.11.037 (2004).

14 Porté-Durrieu, M. C. *et al.* Development of RGD peptides grafted onto silica surfaces: XPS characterization and human endothelial cell interactions. *Journal of Biomedical Materials Research* **46**, 368-375, doi:10.1002/(SICI)1097-4636(19990905)46:3<368::AID-JBM9>3.0.CO;2-8 (1999).

15 Bubnova, O. *et al.* Optimization of the thermoelectric figure of merit in the conducting polymer poly(3,4-ethylenedioxythiophene). *Nat Mater* **10**, 429-433, doi:10.1038/nmat3012 (2011).

16 Aasmundtveit, K. E. *et al.* Structure of thin films of poly(3,4-ethylenedioxythiophene). *Synthetic Metals* **101**, 561-564, doi:http://dx.doi.org/10.1016/S0379-6779(98)00315-4 (1999).

17 Boudouris, B. W. *et al.* Real-Time Observation of Poly(3-alkylthiophene) Crystallization and Correlation with Transient Optoelectronic Properties. *Macromolecules* **44**, 6653-6658, doi:10.1021/ma201316a (2011).

Title : High Performance Polymer and Polymer/Inorganic Thermoelectric Materials

Abstract :

Conducting polymers (CPs) have recently gained the attention of the scientific community due to their prospective use in thermoelectric applications [1,2]. Particularly, it has been proven that an important parameter for tuning the thermoelectric properties and the charge transport behavior of the CP is the shape of the DOS in the band edge, where a more steep band edge would be translated in a semi-metallic behavior for the system, with higher thermoelectric efficiencies. In the present study the correlation between material structure, electronic structure and electronic/ thermoelectric properties, is investigated through careful material design, towards an efficient thermoelectric polymer material. Additionally, the hybrid devices were fabricated as an alternative means to further enhance the thermoelectric efficiency of the material.

Keywords : Polymer, Conducting, Thermoelectric

Title : High Performance Polymer and Polymer/Inorganic Thermoelectric Materials

Resume :

Les polymères conducteurs ont attiré l'attention de la communauté scientifique en raison de leur utilisation potentielle dans les applications thermoélectriques [1, 2]. En particulier, il a été prouvé qu'un paramètre important pour accorder les propriétés thermoélectriques et le comportement de transport de charge du polymères, est la forme du DOS dans le bord de bande. Dans la présente étude, la corrélation entre la structure du matériau, la structure électronique et les propriétés électroniques / thermoélectriques, est étudiée par une conception soigneuse et rigoureux du matériau, vers un matériau polymère, thermoélectrique efficace. En outre, les dispositifs hybrides ont été fabriqués comme un moyen alternatif pour améliorer encore l'efficacité thermoélectrique du matériau.

Mots de clé : Polymères, Conducteur, Thermoélectricité

[1] Bubnova, O. *et al.* Optimization of the thermoelectric figure of merit in the conducting polymer poly(3,4-ethylenedioxythiophene). *Nat. Mater.* **10,** 429–433 (2011).

[2] Petsagkourakis, I. *et al.*Structurally-driven Enhancement of the Thermoelectric Properties within Poly(3,4-ethylenedioxythiophene) Thin Films. *Scientific Reports* **6**, 30501 (2016)